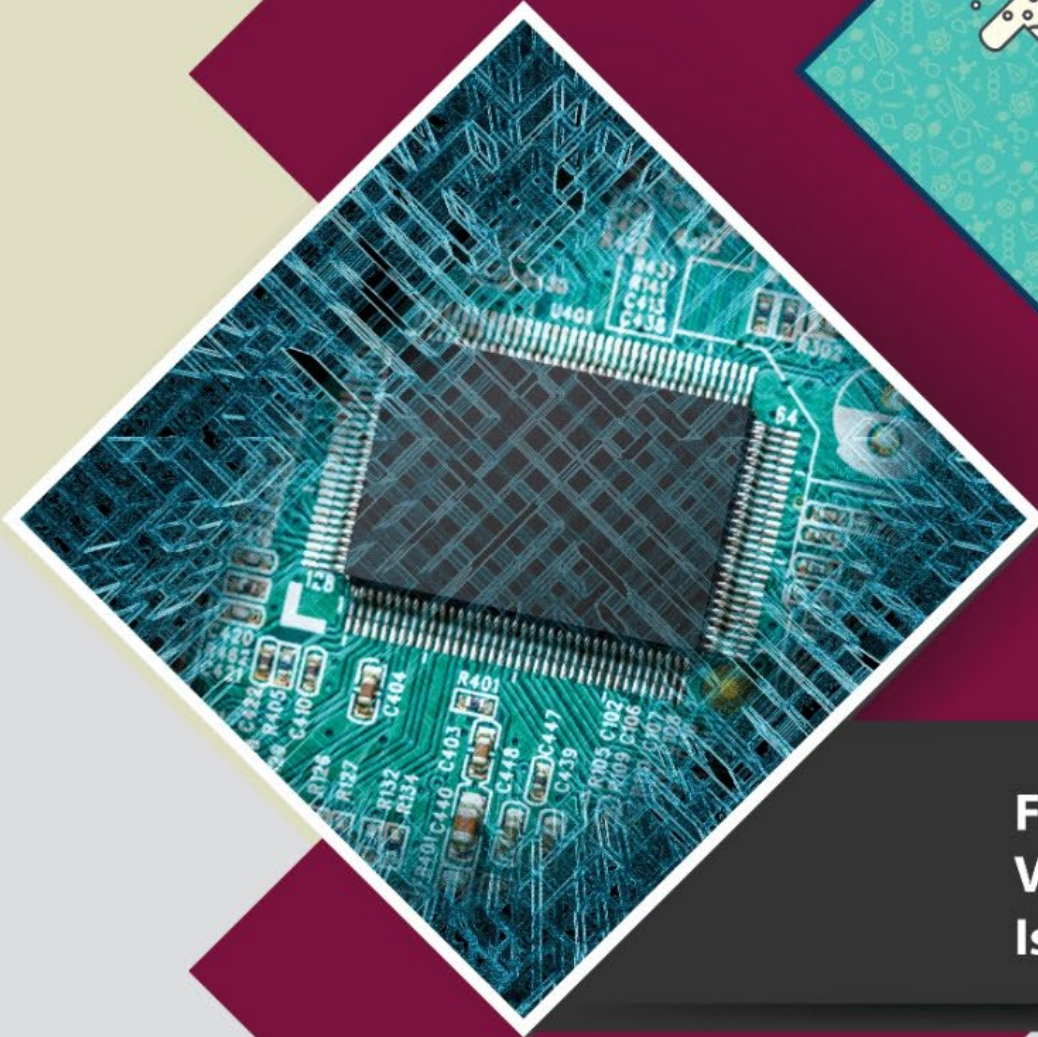


e-ISSN: 2822-2881



# FUJECE

Firat University Journal of Experimental and Computational Engineering



**Feb: 2024**  
**Volume: 3**  
**Issue:1**



<https://dergipark.org.tr/tr/pub/fujece>

**Owner**

On Behalf of Firat University

**Rector**

Prof. Dr. Fahrettin GÖKTAŞ

**Editor-in-Chief**

Prof. Dr. Mehmet YILMAZ, Firat University, Turkey

**Vice Editor-in-Chief**

Prof. Dr. Ebru AKPINAR, Firat University, Turkey

Prof. Dr. Ragıp İNCE, Firat University, Turkey

Prof. Dr. Mete Onur KAMAN, Firat University, Turkey

Assoc. Prof. Dr. Erkut YALÇIN, Firat University, Turkey

**Editorial Advisory Board**

Prof. Dr. Yakup DEMİR, Firat University, Turkey

Prof. Dr. Levent TAŞÇI, Firat University, Turkey

Prof. Dr. Abdussamet ARSLAN, Gazi University, Turkey

Prof. Dr. Ahmet ŞAŞMAZ, Firat University, Turkey

Prof. Dr. Abdulkadir Cuneyt AYDIN, Atatürk University, Turkey

Prof. Dr. Fatih CETİŞLİ, Pamukkale University, Turkey

Prof. Dr. Bilal ALATAŞ, Firat University, Turkey

Prof. Dr. Erhan AKIN, Firat University, Turkey

Prof. Dr. Erkan KÖSE, Nuh Naci Yazgan University, Turkey

Prof. Dr. Filiz KAR, Firat University, Turkey

Prof. Dr. Hasan SOFUOĞLU, Karadeniz Technical University, Turkey

Prof. Dr. Özge Kaya HANAY, Firat University, Turkey

Prof. Dr. Yusuf AYVAZ, Yıldız Technical University, Turkey

Prof. Dr. M. Şaban TANYILDIZI, Firat University, Turkey

Doç. Dr. Tacettin GEÇKİL, İnönü University, Turkey

Doç. Dr. José NORAMBUENA-CONTRERAS, Bio Bio University, Chile

Res. Assist. Dr. Ulaş Baran BALOĞLU, University of Bristol, England

### Editorial Board

Prof. Dr. Mehmet YILMAZ (Editor-in-Chief)	Civil Engineering
Prof. Dr. Ebru AKPINAR (Vice Editor-in-Chief)	Mechanical Engineering
Prof. Dr. Ragıp İNCE (Vice Editor-in-Chief)	Civil Engineering
Prof. Dr. Mete Onur KAMAN (Vice Editor-in-Chief)	Mechanical Engineering
Assoc. Prof. Dr. Erkut YALÇIN (Vice Editor-in-Chief)	Civil Engineering
Prof. Dr. Ali TOPAL	Civil Engineering
Prof. Dr. Ali YAZICI	Software Engineering
Prof. Dr. Ayşe Vildan BEŞE	Chemical Engineering
Prof. Dr. Bilge Hilal CADIRCI EFELİ	Bioengineering
Prof. Dr. Kadir TURAN	Mechanical Engineering
Prof. Dr. H. Soner ALTUNDOĞAN	Bioengineering
Prof. Dr. Mehmet Deniz TURAN	Metallurgy and Materials Engineering
Prof. Dr. Mustafa YANALAK	Geodesy and Photog. Engineering
Prof. Dr. Nuno MENDES	Mechanical Engineering
Prof. Dr. Rashid NADİROV	Chemical
Prof. Dr. Serdar Ethem HAMAMCI	Electrical-Electronics Engineering
Prof. Dr. Selçuk ALEMDAĞ	Geological Engineering
Prof. Dr. Mehmet KARAKÖSE	Computer Engineering
Prof. Dr. Alvaro Garcia HERNANDEZ	Civil Engineering
Prof. Dr. Ömür GÖKKUŞ	Environmental Engineering
Assoc. Prof. Dr. Fatih DEMİR	Software Engineering
Lecturer Batuhan SELVİ (Language Editor)	English Language Teaching
Mustafa Gani GENÇER (Language Editor)	English Language Teaching
Res. Assist. Dr. Özge Erdoğan YAMAÇ (Secretariat)	Civil Engineering
Res. Assist. Beyza Furtana YALÇIN (Pub. Coordinators)	Civil Engineering

### Composition

Hakan YURDAKUL

### Correspondence Address

Firat University Faculty of Engineering Journal of Experimental and Computational Engineering Publishing

Coordinatorship

23119 Elazığ/TÜRKİYE

E-mail: [fujece@firat.edu.tr](mailto:fujece@firat.edu.tr)

Web page: <http://fujece.firat.edu.tr/>

Firat University Journal of Experimental and Computational Engineering a peer-reviewed journal.

## CONTENTS

---

A HOG Feature Extractor and KNN-Based Method for Underwater Image Classification (Research Article) Su Altı Görüntü Sınıflandırma için HOG Özellik Çıkarıcı ve KNN Tabanlı Bir Yöntem (Araştırma Makalesi) <b>Kübra Demir, Orhan YAMAN</b>	<b>1</b>
Numerical Investigation of the Effect of Geocell-Reinforced Cushion on Load Distribution and Settlement Reduction in Unconnected Piled Raft Foundations (Research Article) Temassız Kazıklı Radye Temellerde Geohücre ile Güçlendirilmiş Yastıkların Yük Dağılımı ve Oturmanın Azaltılmasına Etkisinin Nümerik Olarak İncelenmesi (Araştırma Makalesi) <b>Mojtaba Pourgholamali, Farzin Asghapour</b>	<b>11</b>
Farklı İçeriklerde PVC Atığı ile Hazırlanan Sönmüş Kireç İçeren Bitümlü Karışımların Suya Bağlı Bozulmalara Karşı Direncinin Belirlenmesi (Research Article) Determination of Resistance to Water-Induced Damage of Bituminous Mixtures Containing Hydrated Lime Prepared with Different Contents of PVC Waste (Araştırma Makalesi) <b>İsmail Çağrı GÖRKEM, Salih Serkan ARTAGAN, F Bekir Tuna KAYAALP, Cem SAYKAN, İmer Arda ÖZDEMİR</b>	<b>28</b>
Investigation of The Effect of Phase Angle on The Aerodynamic Performance of Three-Bladed Helical Savonius Wind Turbines Using Computational Fluid Dynamics Method (Research Article) Hesaplamalı Akışkanlar Dinamiği Yöntemi Kullanarak Üç Kanatlı Helisel Savonius Rüzgâr Türbinlerinin Aerodinamik Performansına Faz Açısı Etkisinin Araştırılması (Araştırma Makalesi) <b>Mernuş GÜL, Muhammed Safa KAMER, Erdem ALIÇ</b>	<b>52</b>
Evaluation of Susurluk Basin Flows Using Trend Analysis Methods (Research Article) Susurluk Havzası Akımlarının Trend Analiz Yöntemleri Kullanılarak Değerlendirilmesi (Araştırma Makalesi) <b>Ramazan ACAR</b>	<b>65</b>

---



## Su Altı Görüntü Sınıflandırma için HOG Özellik Çıkarıcı ve KNN Tabanlı Bir Yöntem

Kübra DEMİR<sup>1\*</sup>, Orhan YAMAN<sup>2</sup>

<sup>1,2</sup>Adli Bilişim Mühendisliği, Teknoloji Fakültesi, Fırat Üniversitesi, Elazığ, Türkiye.

<sup>1</sup>1202141107@firat.edu.tr, <sup>2</sup>orhanyaman@firat.edu.tr

Geliş Tarihi: 26.05.2023  
Kabul Tarihi: 13.11.2023

Düzeltilme Tarihi: 06.06.2023

doi: 10.62520/fujece.1443818  
Araştırma Makalesi

Alıntı: K. Demir ve O. Yaman, "Su altı görüntü sınıflandırma için HOG özellik çıkarıcı ve KNN tabanlı bir yöntem", Fırat Univ. Jour.of Exper. and Comp. Eng., vol. 3, no 1, pp. 1-10, Şubat 2024.

### Öz

Su altındaki çöpler deniz canlılarının yaşamı ve tüm ekosistemi etkilemektedir. Su altındaki çöplerin tespit edilmesi önemli bir araştırma alanıdır. Bu çalışmada su altındaki çöplerin tespit edilebilmesi için bir yöntem önerilmiştir. Önerilen yöntemin uygulanması için erişime açık Trash-ICRA19 veri seti kullanılmıştır. Veri seti kırpma işlemi uygulanmış ve toplamda 11060 görüntüden oluşan bir veri seti elde edilmiştir. Bu görüntüler ön işleme kullanılarak 200×200 piksele dönüştürülmüştür. Yönlü Gradyan Histogramı (HOG) algoritması uygulanarak, 11060×900 öznitelik vektörleri elde edilmiştir. Elde edilen öznitelik vektörleri daha sonra KNN (K En Yakın Komşu Algoritması), DT (Karar Ağacı), LD (Linear Discriminant), NB (Naive Bayes) ve SVM (Destek Vektör Makinesi) sınıflandırıcıları kullanılarak sonuçlar hesaplanmıştır. Elde edilen sonuçlar KNN sınıflandırıcının bu yöntemde kullanılması durumunda %97.78 doğruluk elde edilmiştir. Önerilen yöntemde sadece özellik çıkarıcı ve sınıflandırıcı kullanılması, yöntemin hafiflik olduğunu göstermektedir. Literatürdeki mevcut çalışmalara kıyasla düşük hesapsal karmaşıklığa sahiptir. Ayrıca performans sonuçlarına göre literatürdeki yöntemlerden başarılıdır.

**Anahtar kelimeler:** Su altı görüntüleri, HOG algoritması, KNN sınıflandırma, Çöp tespiti

\*Yazışılan yazar



## A HOG Feature Extractor and KNN-Based Method for Underwater Image Classification

Kübra DEMİR<sup>1\*</sup> , Orhan YAMAN<sup>2</sup> 

<sup>1,2</sup>Department of Forensic Engineering, Faculty of Technology, Firat University, Elazig, Turkey.

<sup>1</sup>[1202141107@firat.edu.tr](mailto:1202141107@firat.edu.tr), <sup>2</sup>[orhanyaman@firat.edu.tr](mailto:orhanyaman@firat.edu.tr)

Received: 26.05.2023

Accepted: 13.11.2023

Revision: 06.06.2023

doi: 10.62520/fujece.1443818

Research Article

Citation: K. Demir and O. Yaman, "A HOG feature extractor and KNN-based method for underwater image classification", *Firat Univ. Jour. of Exper. and Comp. Eng.*, vol. 3, no 1, pp. 1-10, February 2024.

### Abstract

Underwater garbage affects the life of marine creatures and the entire ecosystem. Detecting underwater garbage is an important research area. In this study, a method is proposed to detect underwater garbage. The open-access Trash-ICRA19 dataset was used to implement the proposed method. The data set cropping process was applied and a data set consisting of 11060 images in total was obtained. These images were converted to 200×200 pixels using preprocessing. By applying the Directed Gradient Histogram (HOG) algorithm, 11060×900 feature vectors were obtained. The resulting feature vectors were then calculated using KNN (K Nearest Neighbor Algorithm), DT (Decision Tree), LD (Linear Discriminant), NB (Naive Bayes), and SVM (Support Vector Machine) classifiers. The results obtained showed that 97.78% accuracy was obtained when the KNN classifier was used in this method. The use of only feature extractors and classifiers in the proposed method shows that the method is lightweight. It has low computational complexity compared to existing studies in the literature. Moreover, according to its performance results, it is more successful than the methods in the literature.

**Keywords:** Underwater images, Hog algorithm, KNN classification, Garbage detection

---

\*Corresponding author

## 1. Introduction

The developments in the exploration process of the underwater world; underwater objects, underwater object detection, and classification have become important. There is hardly any place on earth that is not polluted by marine debris. The main source of plastic waste is land, the second source is the seas and oceans. Marine plastics pose a major threat due to their adverse effects on the marine ecosystem and human health. There are many types of garbage found in the seas. However, plastics, one of the most common and harmful marine garbage in every aspect of our lives, are our focus. Disposable plastics (plastic bottles, plastic cups, bags, etc.) are used vulgarly because they are convenient and cost-effective. 1 plastic bag disappears in nature after approximately 1000 years. Despite this, it is estimated that 1-5 trillion plastic bags are used in the world every year. As plastic wastes stay on the seabed, they turn into very small pieces, namely micro-plastics, after passing through various factors. These microplastics cause the death and extinction of living creatures living underwater. This situation not only affects underwater creatures but also affects people quite a lot. Underwater images contain more difficult problems than the land environment. Underwater objects make images blurry and distorted due to problems such as distortion of their shape, color loss, light weakening, and background noise due to prolonged exposure to water. Therefore, these images are more difficult to detect, classify, and obtain a success rate. These difficulties negatively affect the number of scientific studies in these areas due to the high cost of expenses and the wide variety of objects considered sea wrecks. However, recently, developing technology and increasing underwater pollution have increased such studies. Current studies on garbage and sea creatures in the literature are summarized in Table 1.

**Table 1.** Summary of studies in the literature

Author	Year	Class	Number of Images	Method	Accuracy (%)
Fulton et al. [1]	2019	Tash, bio, and Rov	5720	Faster RCNN	%81
Han et al. [2]	2020	Sea cucumber, sea urchin, and scallop	30000	Faster RCNN	%90
Li et al. [3]	2020	Bottle, bag, and Styrofoam	1505	YoloV3	%91.43
Tata et al. [4]	2021	Plastic	3200	YoloV5	%85
Rosli et al. [5]	2021	Jellyfish, big fish, small fish, crab, shrimp, and starfish	14518	YoloV4	%97.96
Wu et al. [6]	2022	Garbage, living, and underwater robot	7.684	YoloV5	%97.5
Li et al. [7]	2022	Jellyfish, big fish, small fish, crab, shrimp, and starfish	25612	YoloV4	%75
Moorton et al. [8]	2022	Jellyfish, fish, starfish, shell, net, mask, cardboard, plastic, bag, and plastic sheet	1744	CNN	%89
Demir et al. [9]	2022	Small size plastic bottles, large plastic bottles, glass bottles, and packaging	720	YoloV4	%88.7

When current studies are examined, artificial intelligence-based methods have been developed for underwater images and classification has been made. Generally, Yolo [3] and CNN [2] based methods are preferred. Underwater robot [5] technology is used for underwater imaging. Detection of sea creatures and garbage detection were made by using an underwater robot. As sea creatures; Vivid images of sea cucumbers, sea urchins, scallops, jellyfish, big fish, small fish, crabs, shrimp, and starfish were used. In the garbage category, images consisting of metal, plastic, cardboard, and glass objects were used. When the studies in the literature are examined, studies have generally been carried out for the detection of sea creatures [8] or garbage objects [9]. Han et al. [2] proposed a CNN-based method for detecting sea creatures (sea cucumber, sea urchin, and scallop) in underwater images. In the proposed method, only sea creature images were taken into account. No results were obtained for garbage images. Tata et al. [4] presented a method based on YoloV5 by obtaining plastic images with an underwater robot. 3200 images were used and plastic images were examined. Rosli et al. [5] proposed a yoloV4-based method for detecting jellyfish, big fish, small fish, crabs, shrimp, and starfish using an underwater robot. Rosli et al. [5] In the data set they used, many classes

of sea creatures can be detected, but there is no garbage object in the data set. There are only images of sea creatures.

In this study, a Trash-ICRA19 hybrid (garbage, sea creature, and rov) dataset is used, which is designed to find all plastic debris with a large dataset of underwater images and to separate the remains from biological assets and intentionally placed man-made objects [1].

In the literature, the most commonly used image enhancement techniques are histogram equalization [10] and contrast spreading [11]. In addition, the improvement algorithm based on Empirical Mode Decomposition (AKA) and wavelet noise removal method [12], adaptive smoothing techniques, and some filtering methods such as anisotropic filtering and homomorphic filtering [13] are also suggested. In this study, the histogram equalization method was used. 11060×900 feature vectors were obtained. These features are classified by the KNN algorithm. Our motivation is to propose a new inference model to achieve a high rate of classification and detection.

## 2. Materials and Methods

This application is developed on the MATLAB 2020a programming language platform. The steps of the application developed in this section are given below step by step. The general steps of the proposed model are:

Step 0: Crop the Trash-ICRA19 images.

Step 1: Preprocess the cropped images.

Step 2: Obtain feature vectors with the Hog Algorithm.

Step 3: Classify features using a decision tree, support vector machine, linear discriminant, naive Bayes, and k nearest neighbor algorithms.

The flow diagram of the model is shown in Figure 1.

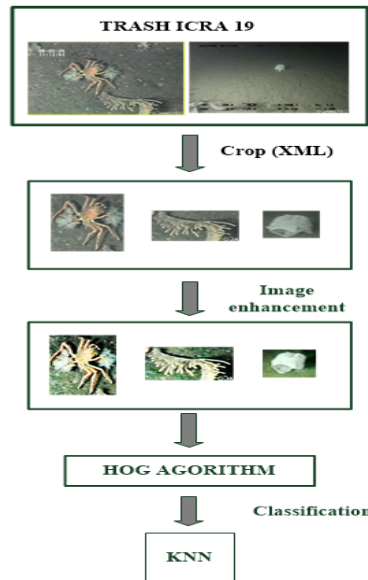


Figure 1. Graphical summary of the proposed method

### 2.1. Dataset preparation

The trash-ICRA19 dataset was used in this study. This data set; includes three parts: training (75%), testing (15%), and validation (10%). The Trash-ICRA19 dataset has a resolution of  $480 \times 360$  pixels. This dataset has 7684 images; It consists of 3 different classes: bio (all natural biological materials including fish), plastic (marine waste, all plastic materials), and rov (remote-controlled underwater vehicle). An object in each image was obtained by extracting the coordinates of the objects from the XML files of the Trash-ICRA19 dataset and cropping it. Thus, a new data set with different dimensions, with the number of images increased to

11060, was created. The class names of the Trash-ICRA19 data set and the number of objects belonging to each class are shown in Table 2.

**Table 2.** Class names and number of objects belonging to each class

Class Name	Number of Objects
Bio	2417
Plastic	6339
Rov	2274
Aggregate	11060

## 2.2. Preprocessing

The second stage of the proposed model is preprocessing. Image enhancement should be done to improve image quality, compensate for attenuation effects, adjust color, reduce noise and blur, and high accuracy. Using the image histogram, the histogram equalization method, which is an image enhancement method, has been applied to the images whose color values are not uniformly distributed. The image needs resizing to avoid any later problems. The image can be any size. The image needs to be set to a constant width and height ratio. Images with different sizes were resized to  $200 \times 200$ . Example image enhancement images are shown in Figure 2.

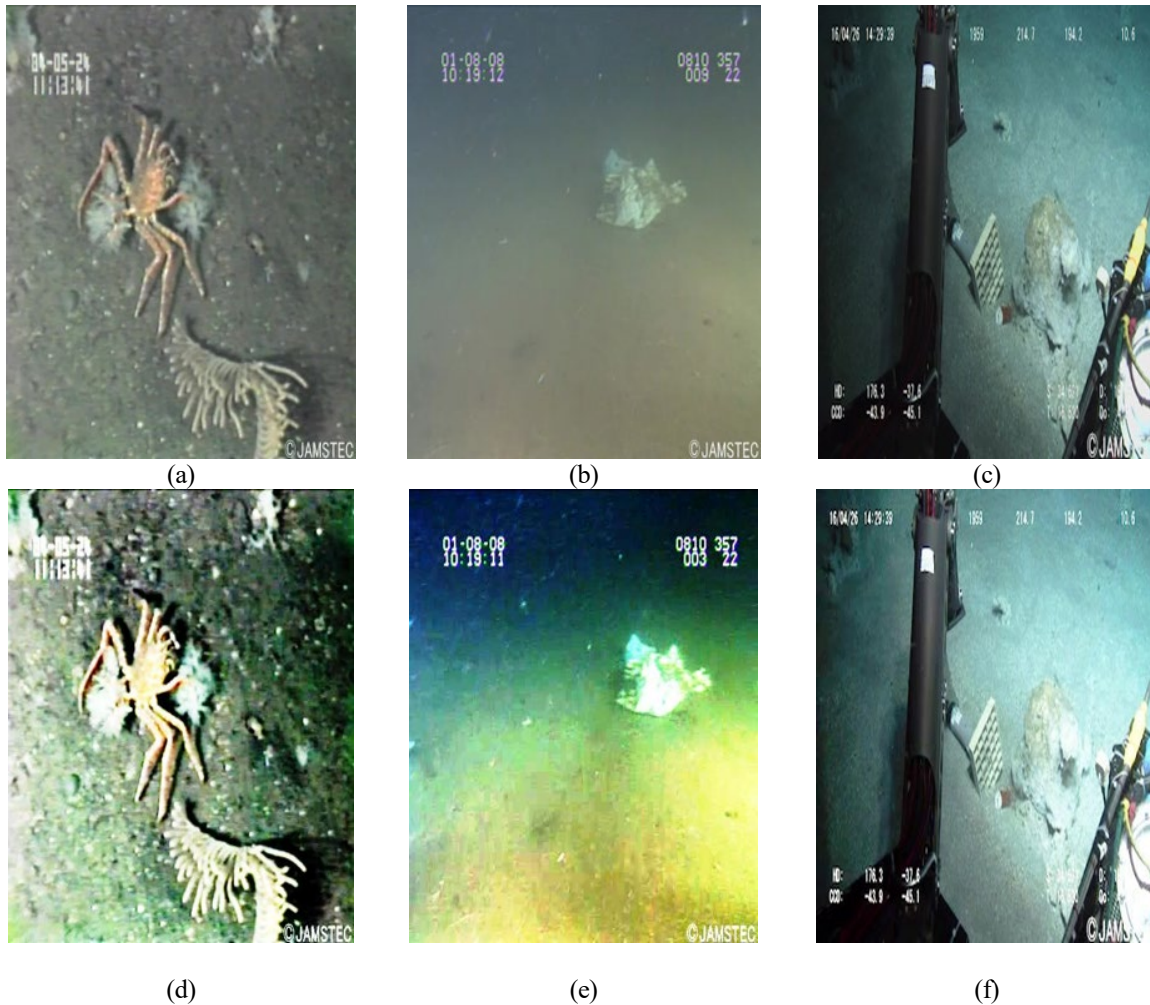


**Figure 2.** Image preprocessing of sample underwater images. (a,b,c) Sample images from TrashIcra dataset, (d,e,f) Images obtained using image preprocessing

Average pooling is one of the pooling techniques generally used in CNN models. The pooling layer is mostly applied to feature matrices. In Figure 3, if a 4x4 feature matrix is applied and a 2x2 average pooling is applied, the 2x2 matrix on the right is formed. For this reason, it includes the calculation of the average for each section with the Average pooling method. The purpose of the pooling method is to reduce dimensionality. Thus, both the required processing power is reduced and the unnecessary features are ignored and the most important features are focused on. In this study, images are reduced to 200×200 pixels and 50×50 pixels with the average polling process.

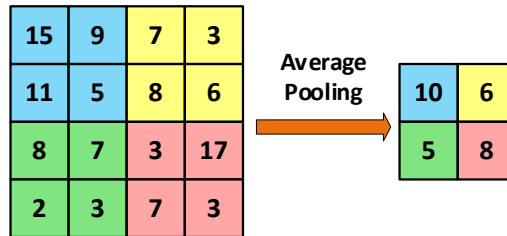


Figure 3. Average pooling process

### 2.3.HOG feature extractor

The use of HOG was first suggested by Shashua [14] and Dalal [15]. The main goal of the HOG method is to define the image as a group of local histograms. These groups are histograms in which the magnitudes of the gradients are summed. To extract the HOG values of an image, firstly, the horizontal and vertical Sobel filters of the image are applied, and the edges,  $I_x$  and  $I_y$ , are determined. It then calculates the gradient and their orientation angles using  $I_x$  and  $I_y$  with the Sobel filter applied. The block diagram of the HOG algorithm is shown in Figure 4.

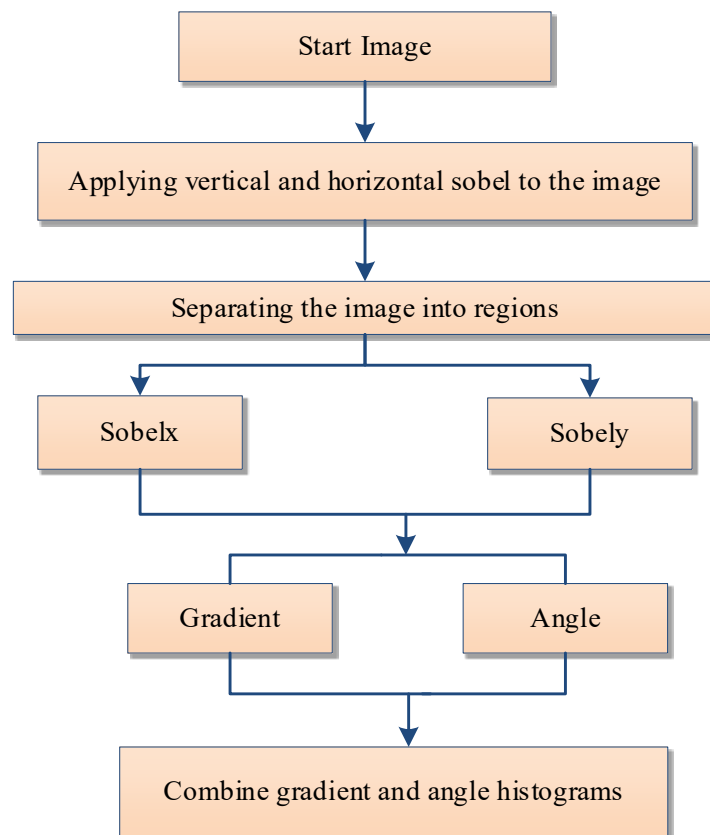


Figure 4. HOG algorithm flowchart

11060×900 feature vectors were obtained by applying the Directional Gradient Histogram (HOG) algorithm, which is one of the methods sensitive to image texture.

## 2.4. Classification

The features obtained as a result of feature selection algorithms are classified by Decision Tree, Linear Discriminant, Naïve Bayes, Support Vector Machine, and KNN algorithms. KNN is one of the simplest Machine Learning algorithms based on the Supervised Learning technique. It is used to solve classification and regression problems. In the KNN algorithm, the training set is first created. Then the K value and a distance function are selected. When new data is encountered, the distance of this data to the data in the training set is calculated one by one using the selected distance algorithm [16] KNN runs the distance formulas to calculate the distance between each data point and the test data. The parameters of the KNN algorithm used in the proposed method are shown in Table 3.

**Table 3.** Parameters of the KNN algorithm used in the proposed method

Parameters	Values
Number of neighbors	1
Distance metric	City block

## 3. Experimental Results

The experiments presented in this section were conducted on a computer equipped with a 64-bit Windows® 10 operating system, a 16-core Intel i7-7200U processor with 64 GB of RAM, and a clock speed of 2.8 GHz. Accuracy, precision, and recall were selected to comprehensively calculate performance. These performance metrics were calculated using the number of true positives (TP), false positives (FP), true negatives (TN), and false negatives (FN). The mathematical expressions of the performance measures used are shown in equations 1-3. [17]-[18].

$$\text{Accuracy} = \frac{TP+TN}{TP+TN+FP+FN} \quad (1)$$

$$\text{Precision} = \frac{TP}{TP+FP} \quad (2)$$

$$\text{Recall} = \frac{TP}{TP+FN} \quad (3)$$

DT, KNN, SVM, NB, and LD classification algorithms were used to classify the selected features. Classification results were obtained using the MATLAB Classification Learner Toolbox. 10-fold cross-validation was chosen as a validation technique to obtain the best results. A comparison of accuracy results with other classifiers (DT: Decision Tree, LD: Linear Discriminant, NB: Naïve Bayes, SVM: Support Vector Machine, KNN: K Nearest Neighbor Algorithm) is shown in Figure 5.

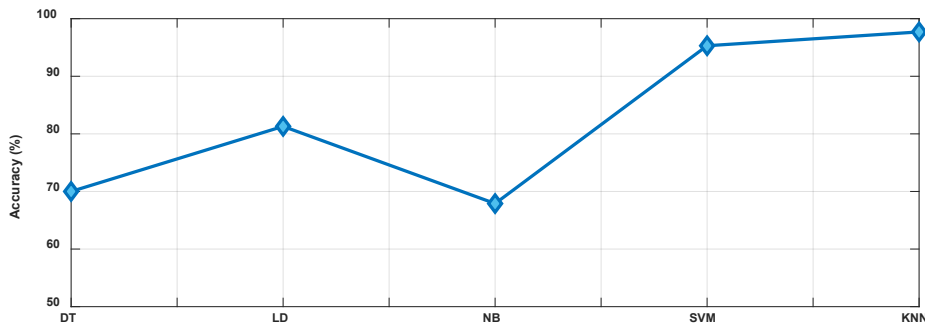


**Figure 5.** Comparison of accuracy results with other classifiers (DT: Decision Tree, LD: Linear Discriminant, NB: Naïve Bayes, SVM: Support Vector Machine, KNN: K Nearest Neighbor Algorithm)

In the proposed method, the confusion matrix values are calculated by running 100 iterations for the KNN classifier. The confusion matrix results are shown in Figure 6.

		Predicted Class		
		Bio	Plastic	ROV
True Class	Bio	2349	60	8
	Plastic	42	6263	49
	ROV	31	55	2188

**Figure 6.** The result of the confusion matrix calculated with 100 iterations of the proposed method

The accuracy, precision, and recall results of the KNN classifier used for 100 iterations are tabulated in Table 4.

**Table 4.** Performance results of the proposed KNN classifier

	Accuracy (%)	Precision (%)	Recall (%)
Maximum	97.78	97.54	97.34
Minimum	97.56	97.23	97.06
Average	97.67	97.40	97.22
Standard Deviation	0.049	0.062	0.065

The class-based accuracy results of the proposed method are shown in Figure 7.

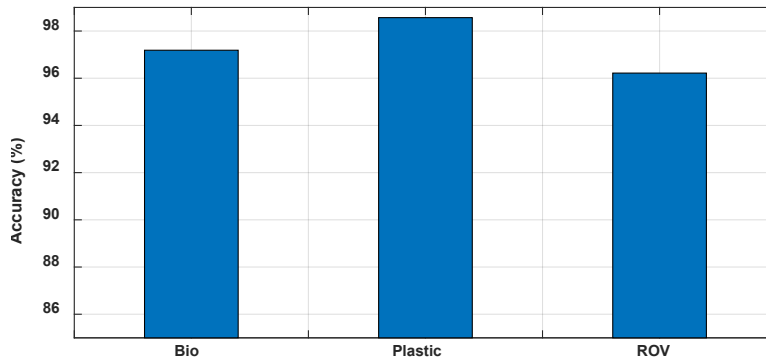


**Figure 7.** Class-based accuracy results of the proposed method

When the studies are examined, there are very few studies in the literature with a mixed (sea creature and garbage) data set. Moorton et al. [11] tested only sea creatures (sea cucumber, sea urchin, and scallop) considering the dataset. Iron et al. [9] examined only garbage (plastic bottles, glass bottles, and packaging) images in the data set they used. In this section, a comparison is made with our study based on ICRA19-Trash datasets. The proposed method was applied to the ICRA19-Trash dataset and obtained high classification accuracy. To demonstrate our high classification ability, our results were compared with other methods, and the results are listed in Table 5. The results of the existing literature studies can be summarized in Table 5.

**Table 5.** Summary of comparison with other state-of-the-art methods using the Trash-ICRA19 dataset.

	Dataset	Number of Images	mAP	Accuracy (%)	Precision (%)	Recall(%)	Geometric Mean (%)	F-Score(%)
Fulton et al. [1]	Trash-ICRA19	5720	81.0	-	-	-	-	-
Wu et al. [6]	Trash-ICRA19	7684	97.5	-	-	-	-	-
Our method	Trash-ICRA19	11060	-	97.78	97.54	97.34	97.34	97.44

Fulton et al. [1] used the Trash-ICRA19 dataset, which consists of garbage, sea creatures, and rov objects. They achieved an 81% success rate with the Faster RCNN method of 5720 images. Wu et al. [6] used 7684 images for the Trash-ICRA19 dataset. For suggested methods, see Fulton et al. [1] 81.0% Wu et al. [6] calculated an accuracy of 97.5%. In the literature, the classification success for Trash-ICRA19 datasets has been calculated as over 80%. Our proposed method KNN model has 97.78% higher accuracy.

#### 4. Conclusions

In this study, the KNN algorithm was applied to classify underwater objects, their analyses were made and the results were recorded. In our study, training was carried out using the Trash-ICRA19 dataset, which is a publicly available dataset. Our study has shown good results using classification algorithms. When we compare the accuracy results with other classifiers, it is seen that the KNN classifier gives the best results for this study. Our recommendation calculated 97.78% classification accuracy. These results and comparisons show that it is successful in classifying underwater image types. The classification of our study with high accuracy constitutes the main motivation. The reason why the Trash-ICRA19 dataset is used instead of other datasets in the literature is that the dataset consists of a large dataset consisting of 11060 images. Another reason is that it consists of two classes that are very important for marine ecosystems, namely sea creatures and garbage images. While the size of the data set makes it easier for us to detect and classify objects, the fact that the number of classes is more than one makes our work more difficult. Despite this disadvantage, a high success rate has been achieved with KNN classification. In future studies, it is envisaged to detect real-time garbage and living things using underwater robots. Also, our method can be tested on larger datasets with more classes.

#### 5. Acknowledgments

This study was supported by the Scientific Technology and Research Council of Turkey (TÜBİTAK) 2210/C Domestic Priority Areas Graduate Scholarship Program with project number 1649B022204832 and project number 1649B022204832. This thesis was supported by the Firat University Scientific Research Projects Coordination Unit (FÜBAP) with the protocol number TEKF.22.01.

#### 6. Author Contribution Statement

In the study, Kübra Demir contributed to the creation of the idea, design, and literature review; Orhan Yaman contributed to the analysis of the results, the provision of materials, and the review of the results.

#### 7. Ethics Committee Approval and Conflict of Interest

There is no need for an ethics committee approval in the prepared article. There is no conflict of interest with any person/institution in the prepared article.

## 8. References

- [1] M. Fulton, J. Hong, M. J. Islam and J. Sattar, "Robotic detection of marine litter using deep visual detection models", *Proc. IEEE Int. Conf. Robot. Autom.*, ss. 5752-5758, May 2019.
- [2] F. Han, J. Yao, H. Zhu and C. Wang, "Underwater image processing and object detection based on deep CNN method", *J. Sens.*, vol. 2020, pp. 20, May 2020.
- [3] X. Li, M. Tian, S. Kong, L. Wu and J. Yu, "A modified YOLOv3 detection method for vision-based water surface garbage capture robot", *Int. J. Adv. Robot. Syst.*, vol. 17, no 3, pp. 1-11, 2020.
- [4] G. Tata, S.-J. Royer, O. Poirion and J. Lowe, "A Robotic Approach towards quantifying epipelagic bound plastic using deep visual models", ss. 1-8, 2021.
- [5] M. S. A. Bin Rosli, I. S. Isa, M. I. F. Maruzuki, S. N. Sulaiman and I. Ahmad, "Underwater Animal Detection Using YOLOV4", *Proc. - 2021 11th IEEE Int. Conf. Control Syst. Comput. Eng. ICCSCE 2021*, sy August, ss. 158-163, (2021).
- [6] C. M. Wu, Y. Q. Sun, T. J. Wang and Y. L. Liu, "Underwater trash detection algorithm based on improved YOLOv5s", *J. Real-Time Image Process.*, vol. 19, no. 5, pp. 911-920, 2022.
- [7] A. Li, L. Yu and S. Tian, "Underwater biological detection based on YOLOv4 combined with channel attention", *J. Mar. Sci. Eng.*, vol. 10, no. 4, 2022.
- [8] Z. Moorton, Z. Kurt and W. L. Woo, "Is the use of deep learning an appropriate means to locate debris in the ocean without harming aquatic wildlife?", *Mar. Pollut. Bull.*, vol. 181, pp. 1-17, 2022.
- [9] K. Demir and O. Yaman, "International informatics congress (IIC2022) 17-19 February 2022, Batman, Turkey Su Altı Çöp Tespiti İçin YOLOv4 Tabanlı Bir Yöntem", vol. February, pp. 17-19, (2022).
- [10] V. S. Thakur and S. Forensic, "On The way towards efficient enhancement of multi-channel underwater images", vol. September, 2015.
- [11] K. Iqbal, R. A. Salam, A. Osman and A. Z. Talib, "Underwater image enhancement using an integrated colour model", vol. November, 2007.
- [12] E. E. Kılınc and S. Metlek, "Su altı görüntülerinden nesne tespiti", *Eur. J. Sci. Technol.*, vol. 23, pp. 368-375, 2021.
- [13] I. Quidu, L. Jaulin and J. Malkasse, "Automatic underwater image pre-processing St ' To cite this version ", 2010.
- [14] A. Shashua, Y. Gdalyahu and G. Hayun, "Pedestrian detection for driving assistance systems: Single-frame classification and system level performance", *IEEE Intell. Veh. Symp. Proc.*, vol. June, pp. 1-6, 2004.
- [15] N. Dalal and B. Triggs, "Histograms of oriented gradients for human detection", *Proc. - 2005 IEEE Comput. Soc. Conf. Comput. Vis. Pattern Recognit. CVPR 2005*, vol. I, pp. 886-893, 2005.
- [16] O. Kaynar, H. Arslan, Y. Görmez and Y. E. Işık, "Makine öğrenmesi ve öznelik seçim yöntemleriyle saldırı tespiti", *Bilişim Teknol. Derg.*, pp 175-185, 2018.
- [17] C. Iwendi, G. Srivastava, S. Khan and P. K. R. Maddikunta, "Cyberbullying detection solutions based on deep learning architectures", *Multimed. Syst.*, 2020.
- [18] M. Baygin, O. Yaman, T. Tuncer, S. Dogan, P. D. Barua and U. R. Acharya, "Automated accurate schizophrenia detection system using Collatz pattern technique with EEG signals", *Biomed. Signal Process. Control*, vol. 70, no. May, pp. 102936, 2021.



## Temassız Kazıklı Radye Temelerde Geohücre ile Güçlendirilmiş Yastıkların Yük Dağılımı ve Oturmanın Azaltılmasına Etkisinin Nümerik Olarak İncelenmesi

Mojtaba Pourgholamali<sup>1</sup> , Farzin Asghapour<sup>2,3\*</sup>

<sup>1</sup>İslamik Azad Üniversitesi, Necefabad Şubesi, İnşaat Mühendisliği Bölümü, Tahran, İran.

<sup>2</sup>Doğu Akdeniz Üniversitesi, Mühendislik Fakültesi, İnşaat Mühendisliği Bölümü, Gazimağusa, Kuzey Kıbrıs.

<sup>3</sup>Doğu Akdeniz Üniversitesi, Tıp Fakültesi, Gazimağusa, Kuzey Kıbrıs.

<sup>1</sup>mojtabapourgholamali@sci.iaun.ac.ir, <sup>2,3</sup>farzin.asghapour@emu.edu.tr

Geliş Tarihi: 04.12.2023

Kabul Tarihi: 09.02.2024

Düzeltilme Tarihi: 02.01.2024

doi: 10.62520/fujece.1399814

Araştırma Makalesi

Alıntı: M. Pourgholamali ve F. Asghapour, "Temassız kazıklı radye temelerde geohücre ile güçlendirilmiş yastıkların yük dağılımı ve oturmanın azaltılmasına etkisinin nümerik olarak incelenmesi", Fırat Univ. Jour. of Exper. and Comp. Eng., vol. 3, no 1, pp. 11-27, Şubat 2024.

### Öz

Temassız kazıklı radye temelerde geohücre ile güçlendirilmiş yastıkların yük dağılımına ve oturmaların azaltılmasına etkisi araştırılmıştır. Abaqus yazılımı kullanılarak çeşitli durumların modellenmesi ve analizi gerçekleştirilmiştir. Bu çalışmada bir temassız, üç temassız ve takviyesiz, beş temassız ve geohücre ile güçlendirilmiş durumlar olmak üzere toplamda dokuz model incelenmiştir. Kalınlıkları temel kalınlığının yarısı, eşit ve temel kalınlığının iki katı kadar olan yastık modelleri kullanılmıştır. Sonuçlar, yük dağıtım verimliliği ve oturmanın en aza indirilmesi açısından en iyi sonuçların, yastığın rijitliği temelin rijitliğinin yarısı kadar olduğu modellerde elde edildiğini göstermiştir. Elde edilen sonuçlar, temassız kazıklı radye temelerin performansını artırma noktasında geohücre takviyesinin olumlu etkisini göstermektedir. Geohücrenin modellere eklenmesi zeminin rijitliğini ve kazık yük oranının artmasını sağlamakta ve dolayısıyla güçlendirilmemiş modellere kıyasla kazıklı radye temelin yük taşıma kapasitesini arttırmaktadır. Çalışmanın bulguları, geohücrelerin inşaat mühendisliği uygulamalarında özellikle yüksek yük taşıma kapasitesi ve minimum temel oturmasını gerektiren durumlarda daha etkin bir şekilde kullanılması için uygun zemini hazırlamaktadır.

**Anahtar kelimeler:** Kazıklar, Radye, Yastık, Temassız kazıklı temeller

\*Yazışılan yazar

İntihal Kontrol: Evet – Turnitin

Şikayet: [fujece@firat.edu.tr](mailto:fujece@firat.edu.tr)

Telif Hakkı ve Lisans: Dergide yayın yapan yazarlar, CC BY-NC 4.0 kapsamında lisanslanan çalışmalarının telif hakkını saklı tutar



## Numerical Investigation of the Effect of Geocell-Reinforced Cushion on Load Distribution and Settlement Reduction in Unconnected Piled Raft Foundations

Mojtaba Pourgholamali<sup>1</sup> , Farzin Asghapour<sup>2,3\*</sup> 

<sup>1</sup>Department of Civil Engineering, Najafabad Branch, Islamic Azad University, Teheran, Iran.

<sup>2</sup>Civil Engineering Department, Faculty of Engineering, Eastern Mediterranean University, Famagusta, North Cyprus.

<sup>3</sup>Faculty of Medicine, Eastern Mediterranean University, Famagusta, North Cyprus.

<sup>1</sup>mojtabapourgholamali@sci.iaun.ac.ir, <sup>2,3</sup>farzin.asgharpour@emu.edu.tr

Received: 04.12.2023

Accepted: 09.02.2024

Revision: 02.01.2024

doi: 10.62520/fujece.1399814

Research Article

Citation: M. Pourgholamali and F. Asghapour, "Numerical investigation of the effect of geocell-reinforced cushion on load distribution and settlement reduction in unconnected piled raft foundations", *Firat Univ. Jour. of Exper. and Comp. Eng.*, vol. 3, no 1, pp. 11-27, February 2024.

### Abstract

The effect of geocell-reinforced cushion on load distribution and settlement reduction in unconnected piled raft foundations was investigated. Modeling and analysis of various scenarios were carried out using Abaqus software. In this research, a total of nine models, including one connected, three unconnected and unreinforced, and five unconnected and reinforced with geocell, were analyzed. Cushions with thicknesses half of, equal to, and twice that of the foundation were used. The results have shown that optimal outcomes in terms of load distribution efficiency and settlement reduction are achieved when the cushion's stiffness is set at half that of the foundation. The obtained results demonstrate the positive effect of geocell reinforcement in enhancing the performance of unconnected piled raft foundations. The introduction of geocells into the models increases soil stiffness and pile load ratio, consequently enhancing the load-bearing capacity of the piled raft foundation compared to the unreinforced models. The study's findings pave the way for a more effective use of geocells in civil engineering applications, particularly in scenarios demanding high load-bearing capacity and minimal foundation settlement.

**Keywords:** Piles, Raft, Cushion, Unconnected piles raft

---

\*Corresponding author

## **1. Introduction**

In the realm of civil engineering, enhancing soil-bearing capacity and mitigating settlement issues are pivotal challenges that have long captivated the attention of researchers and practitioners alike. The quest for effective foundation solutions has led to the exploration of diverse techniques, among which piled raft foundations have stood out for their exceptional ability to efficiently distribute loads across a spectrum of challenging soil conditions. Historically, these foundations have been a cornerstone in the development of strategies aimed at overcoming geotechnical obstacles, earning a revered place within the engineering community for their versatility and effectiveness [1].

Recently, the engineering discourse has shifted towards an innovative iteration of these systems: unconnected piled raft foundations (UCPR). This evolution represents a significant departure from traditional methods, emphasizing a novel approach to soil reinforcement. Unlike their predecessors, UCPR systems strategically forego the direct connection between piles and rafts, instead utilizing a cushion layer of compacted sand and gravel mixtures [2]. This adaptation not only enhances the load capacity of the subsoil but also intricately modifies the interaction dynamics between the piles and the imposed loads [3-6], marking a pivotal advancement in foundation engineering practices.

The introduction of a cushion layer has been identified as a critical innovation in this context, serving a dual function: it amplifies the subsoil's load-bearing capabilities and fundamentally alters the load transfer mechanisms from the superstructure to the foundation [7]. The efficacy of this layer, particularly under seismic loads, has been a focal point of rigorous investigation. Studies have delved into its role in absorbing seismic waves and its influence on the resistance moments and pile displacement under dynamic loading conditions [8-13]. This body of research has underscored the robust response of UCPR systems to earthquake-induced loads, highlighting their potential to significantly improve the resilience of infrastructure against seismic activities.

Parallel to the advancements in piled raft foundations, geocell reinforcement (GR) has emerged as a groundbreaking solution to the perennial challenges of soil instability [14-15]. Characterized by their distinctive three-dimensional honeycomb structure, geocells have demonstrated a remarkable capacity to enhance the strength and modulus of non-cohesive soils, such as sand and gravel. This method of confinement leads to pronounced improvements in soil strength, presenting a compelling case for its integration into foundation designs. Despite the clear benefits of GR, including its contribution to increased stability and reduced soil deformation under varying conditions, the adoption of this technology has been tempered by the absence of comprehensive design methodologies [16-17].

Addressing this gap, the present study embarks on a thorough investigation into the impacts of integrating geocell reinforcement within the cushion layer of unconnected piled raft foundations [18]. It aims to unravel the effects of geocells on subsidence, load distribution to piles and foundations, and to assess the performance of various configurations of piled raft foundations—both connected and unconnected when enhanced with geocell technology [19-22]. Through this exploration, the study seeks to not only contribute to the body of knowledge on foundation engineering but also to pave the way for the development of robust design methodologies that can fully leverage the potential of geocell reinforcement in improving foundation performance.

## **2. Numerical Modelling**

Three-dimensional numerical models were constructed using commercially available finite element software [23]. The parametric model represents a 10×10 m pile raft foundation under two conditions: connected and unconnected to the piles. In the unconnected condition, a reinforced cushion with GEOCELL was considered, along with a version without GEOCELL. The cushion, in this context, refers to the layer beneath the raft, designed to enhance load-bearing capacity and mitigate settlement. Concrete piles, measuring 60 cm in diameter and 12 m in length, were positioned beneath both cushion types. These elements were situated within a soil region measuring 60×60 m with a height of 35 m.

The GEOCELL, a geosynthetic material resembling a three-dimensional honeycomb structure, had dimensions of 287 mm in width and 320 mm in length, with a pocket depth of 150 mm. It was placed within the cushion layer. A vertical pressure of 600 kPa was applied uniformly to the raft as a distributed load.

For a visual representation of this configuration, please refer to Fig. 1 below:

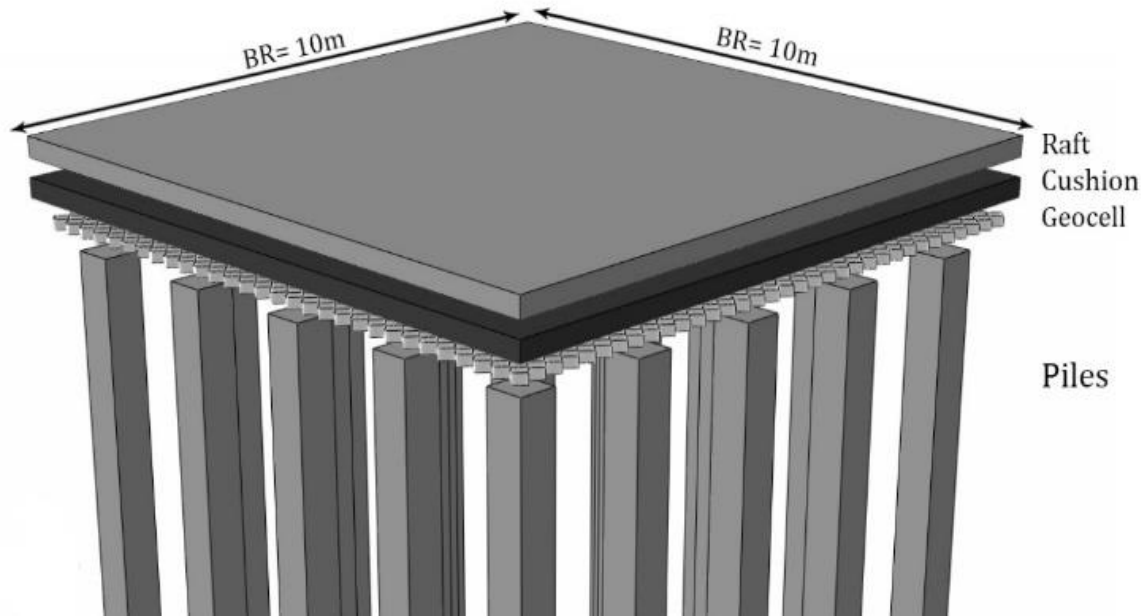


**Figure 1.** Schematic of unconnected reinforced piled-raft foundation

This numerical model allows us to simulate and analyze the behavior of the foundation system under different conditions, including the presence or absence of GEOCELL reinforcement. Subsequent sections of this paper will discuss the results and implications of these simulations.

## 2.1. Materials

The soil used in the model represents medium sand, characterized by an elastic ideal plastic constitutive model. The raft is defined as a linear elastic material, consistent with typical foundation materials. Concrete piles are modeled similarly. The cushion layer, crucial for load distribution, follows the Mohr-Coulomb yield criterion. The geocell material, essential for this study, is represented as an elastic material to simplify computational processes.

### 2.1.1. Soil

The soil in the model represents medium sand and is characterized using the elastic ideal plastic constitutive model based on the Mohr-Coulomb yield criterion. To ensure numerical stability and mitigate modeling challenges, a small cohesion value of 1 Pa was assigned to the sand.

### 2.1.2. Raft

The raft, which serves as the foundation of the system, is defined as a linear elastic material [19].

### 2.1.3. Piles

The concrete piles supporting the foundation are also modeled as linear elastic materials.

### 2.1.4. Cushion

The cushion layer beneath the raft plays a significant role in load distribution and subsoil interaction. It is characterized using the Mohr–Coulomb yield criterion.

### 2.1.5. Geocell

The geocell material properties, sourced from [14], are represented as elastic materials in the model. This simplification is made to reduce computational costs and alleviate numerical complexities.

**Table 1.** Material properties used in Modeling

Material model	Sand Mohr-col.	Raft Elastic	Pile Elastic	Cushion Mohr-col.	Geocell Elastic
Poisson Ratio	0.30	0.20	0.20	0.25	0.35
$\gamma_{sat}$ (kN/m <sup>3</sup> )	17.00	25	25	20	9.61
E (kN/m <sup>2</sup> )	40,000	$3.4 \times 10^7$	$2.1 \times 10^7$	40,000	380,000
C (kPa)	0	–	–	0	–
$\phi$	35	–	–	30	–

These material properties are fundamental to the accurate representation of the foundation system in the numerical model, enabling the simulation of its response under various conditions.

## 2.2. Mesh and boundary

For computational efficiency, a quarter model with symmetric boundary conditions was used. Piles, the foundation, the cushion, and the soil were meshed using C3D8R elements, suitable for solid structures. The GEOCELL, a critical element in our study, was modeled using M3D4R elements to reflect its unique honeycomb structure.

### 2.2.1. Mesh

Piles, the foundation, the cushion, and the soil will be meshed using C3D8R elements, chosen for their suitability in capturing the behavior of solid structures. GEOCELL will be modeled using shell elements with membrane conditions and meshed using M3D4R elements, aligning with the nature of its geometry and behavior.

### 2.2.2. Boundary conditions

To minimize the influence of boundaries on stress distribution, we will define boundaries in the following manner:

1. The boundary for the y-z plane will be designated as XSIMM, indicating symmetry about the x-plane.
2. The x-z plane will be designated as YSIMM, signifying symmetry about the y-plane.

The horizontal boundary will extend to six times the width of the raft (6BR), and the vertical boundary will span three times the width of the raft (3BR) in addition to one-third of the pile's length (L/3) [24]. These dimensions are selected to minimize boundary effects while ensuring computational efficiency.

### 2.2.3. Mesh sizes

For a visual representation of the finite element mesh sizes and boundary designations, please refer to Fig. 2.

#### **2.2.4. Contact modeling**

Interfaces between piles-soil and geocell-cushion will be represented using the penalty friction algorithm. This algorithm incorporates hard normal contact and utilizes a friction coefficient of  $2/3 \tan \phi$  [25-26].

#### **2.3. Modeling verification**

Verification of a numerical model is a crucial step to ensure its accuracy and reliability. In this section, we present our approach to model validation and verification, which involves comparing our numerical simulations with established laboratory and numerical models.

##### **2.3.1. Validation models**

To validate our numerical models, we selected two reference models from prior research:

1. Piled Foundation Model by Elwakil et al. [26]: This model represents a piled foundation with dimensions of 15×15 cm, featuring steel piles measuring 40 cm in height. The entire configuration is placed within a soil box measuring 75×75 cm and with a height of 60 cm.
2. Numerical Model by Alaa et al. (Pokharel et al. [19]): This numerical model replicates a scenario with unconnected piles and a cushion, closely resembling the configuration under investigation in our study.

##### **2.3.2. Validation criteria**

Our primary focus during the validation process was on settlement, a critical parameter for our study. We meticulously compared the settlement values obtained from our numerical simulations with those observed in laboratory tests.

##### **2.3.3. Comparison methodology**

To ensure a robust validation process, we conducted thorough analyses and employed specific methodologies. These methodologies included a systematic examination of settlement data, alongside other relevant factors, to facilitate a comprehensive comparison between our numerical models and the reference models.

##### **2.3.4. Validation findings and correlation**

Our validation efforts produced highly satisfactory results. Notably, the settlement values obtained from our numerical simulations closely mirrored those observed in the laboratory experiments conducted by Elwakil et al. [8]. This remarkable correlation validates the precision and reliability of our numerical models, particularly under similar loading conditions.

##### **2.3.5. Relevance to our study**

The successful validation of our numerical models against established laboratory and numerical models significantly enhances our confidence in the accuracy of our simulations. This assurance underpins the robustness of our study, enabling us to draw dependable conclusions and insights from our numerical analyses.

#### **2.4. Parametric models**

In pursuit of this objective, a series of parametric models were developed to explore different scenarios and conditions. These models are summarized in Table 2 and visually represented in Fig. 3.

**Table 2.** Parametric models

Parametric Study	Raft Thickness (m)	Cushion Thickness (H)	Reinforcement Conditions
connected	0.3	0	non
C-0.5h	0.3	0.5h	non
C-h	0.3	1h	non
C-2h	0.3	2h	non
GRC-0.5h	0.3	0.5	Reinforced with 1 layer of geocell
GRC-hb	0.3	1h	Reinforced with 1 layers of geocell below the cushion
GRC-ha	0.3	1h	Reinforced with 1 layers of geocell above the cushion
GRC-2hb	0.3	2h	Reinforced with 1 layers of geocell below the cushion
GRC-2ha	0.3	2h	Reinforced with 1 layers of geocell above the cushion

These parametric models have been meticulously designed to encompass a range of variables, including raft thickness, cushion thickness, and specific reinforcement conditions. They form the basis for our comprehensive analysis of the impact of these parameters on the behavior of the piled-raft foundation system.

### 3. Results and Discussion

This section presents the key findings of our research, focusing on critical outcomes such as the maximum settlement of the unconnected piled raft foundation, differential settlement within the raft foundation, axial load distribution along the pile length, and the pivotal parameter known as the pile load ratio  $\alpha_{PR}$ . We give particular emphasis to the investigation of the pile load ratio and its implications. The pile load ratio, denoted as  $\alpha_{PR}$ , holds a central role in the design of piled raft foundations. It is defined by the following equation:

$$\alpha_{PR} = \frac{\sum P_{pile}}{P_{total}} \quad (1)$$

In this equation,  $\sum P_{pile}$  represents the sum of loads at the pile head, while  $P_{total}$  signifies the total applied loads. Together, these parameters determine the equitable distribution of loads between the piles and the raft.

#### 3.1. Impact of cushion thickness

The effect of cushion thickness on the behavior of the piled raft foundation is a critical aspect of our study. In this section, we discuss our findings in relation to the variation in cushion thickness and its impact on the pile load ratio and settlement patterns.

As depicted in Fig. 4, the graph illustrates the variation in the pile load ratio. It becomes evident that an increase in cushion thickness corresponds to a proportional reduction in the bearing capacity of the piles. This observation holds significant implications for the load distribution within the foundation system.

Fig. 5 provides insights into the settlement patterns across the raft, extending from its center to its periphery. Notably, it is evident that an increase in cushion thickness is accompanied by a notable increase in the maximum settlement of the unconnected piled raft. This increase in settlement is particularly concentrated in the central region of the foundation. Understanding these settlement patterns is crucial for assessing the structural performance and stability of piled raft foundations with varying cushion thicknesses.

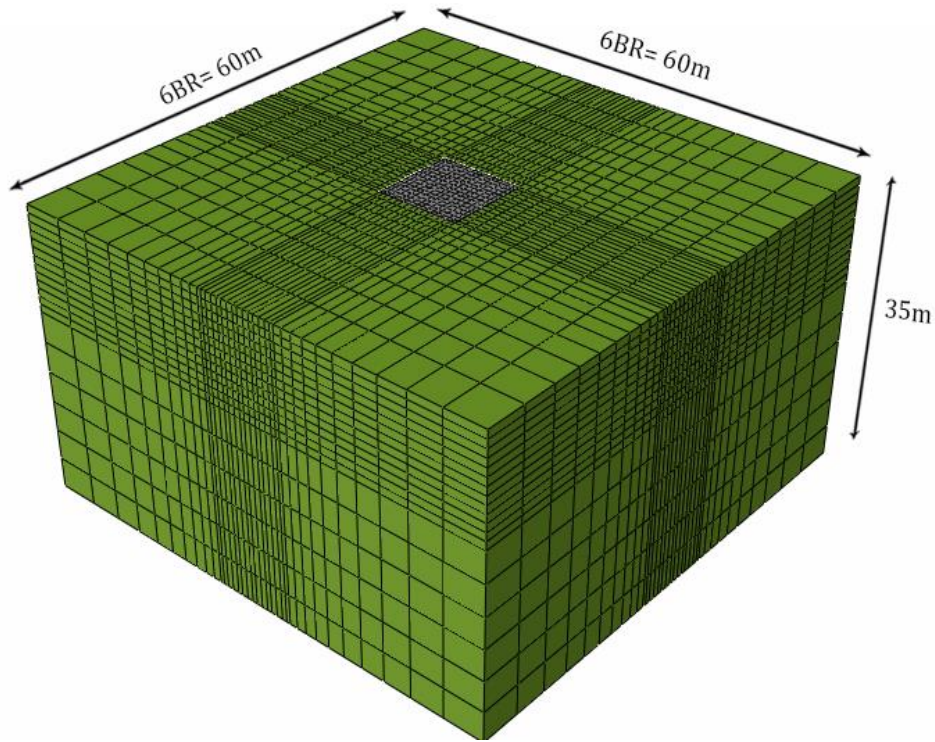


**Figure 2.** Parametric models meshing

### 3.2. Effect of reinforcement of the cushion with Geocell

The integration of geocells for soil improvement plays a pivotal role in enhancing soil stiffness and overall bearing capacity. In this section, we delve into the impact of incorporating geocells within the cushion and examine the resulting changes in the pile load ratio.

As illustrated in Fig. 4, the introduction of geocells into the cushion amplifies the pile load ratio, leading to a more substantial load transmission to the piles across all scenarios. This enhancement in load-bearing capacity surpasses the conditions without reinforcement, emphasizing the beneficial effects of geocell incorporation.

Fig. 6 offers a comparative analysis of the pile load ratio among three key models: the c-2h model (unreinforced), the GRC-2ha model, and the GRC-2hb model. This comparison highlights that when the cushion's thickness is twice that of the foundation and the geocell is positioned beneath the upper cushion region (GRC-2ha model), the pile load ratio exhibits a notable increase. Conversely, placing the geocell at the top of the cushion (GRC-2hb model) yields lower pile load ratios, indicating that the piles can effectively withstand greater loads. Similarly, for a cushion thickness equivalent to that of the foundation, optimal load transfer occurs when the geocell is located at the bottom of the cushion (Fig. 7).

As demonstrated in Fig. 4, the highest pile load ratio is achieved when the cushion's thickness matches half that of the foundation, augmented by geocell reinforcement (GRC-0.5h model). Correspondingly, as depicted in Fig. 5, this model exhibits the lowest degree of settlement, emphasizing its structural stability. Fig. 8 further illustrates the distribution of axial load on the middle pile, highlighting that when connected to the foundation, the pile can endure higher axial loads on its cap. However, as the depth increases, the axial load distribution becomes more uniform between the scenarios. These findings collectively underscore the significance of geocell integration for augmenting load-bearing capacity and optimizing the overall performance of the foundation system.

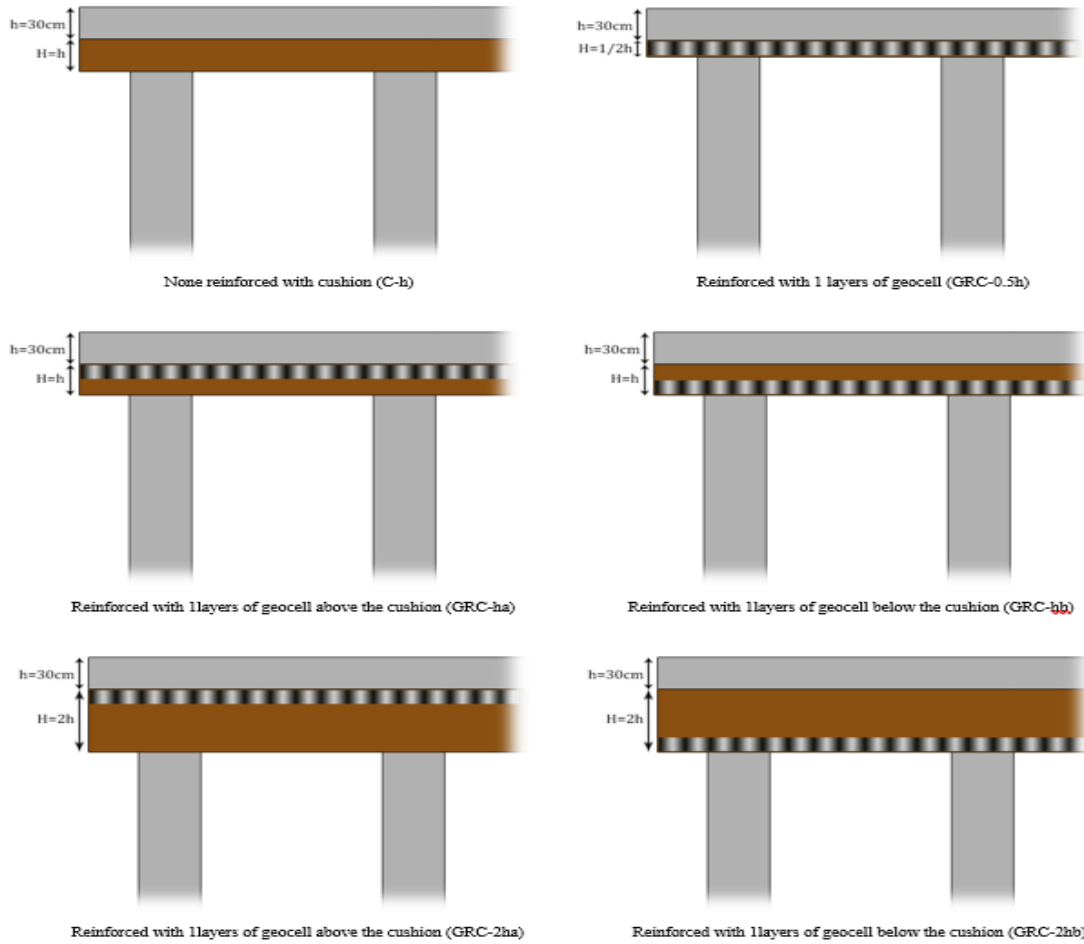


Figure 3. Parametric study

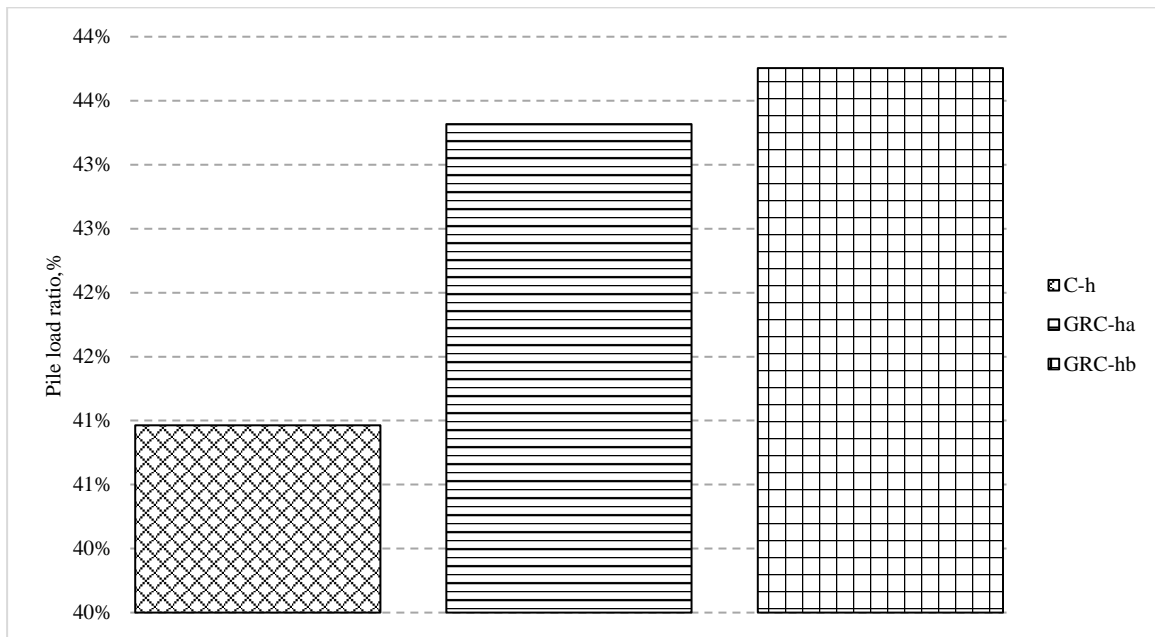


Figure 4. Pile load ratio

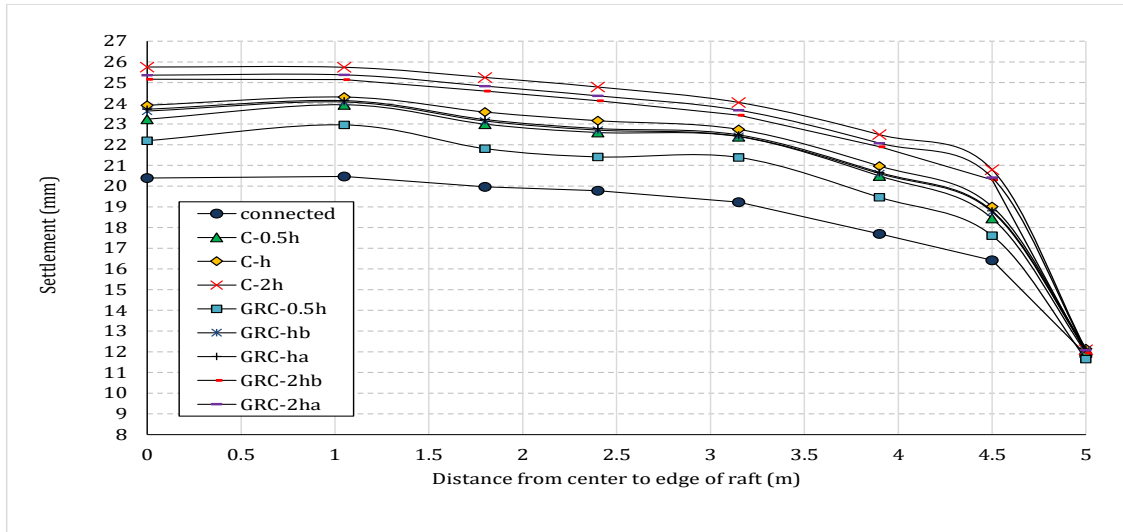


Figure 5. Maximum settlement of the raft

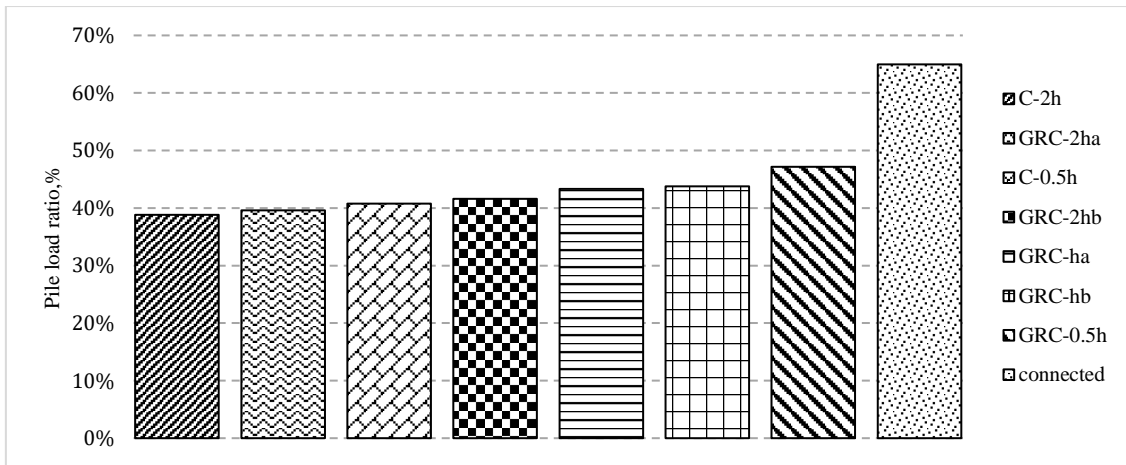


Figure 6. Pile load ratio

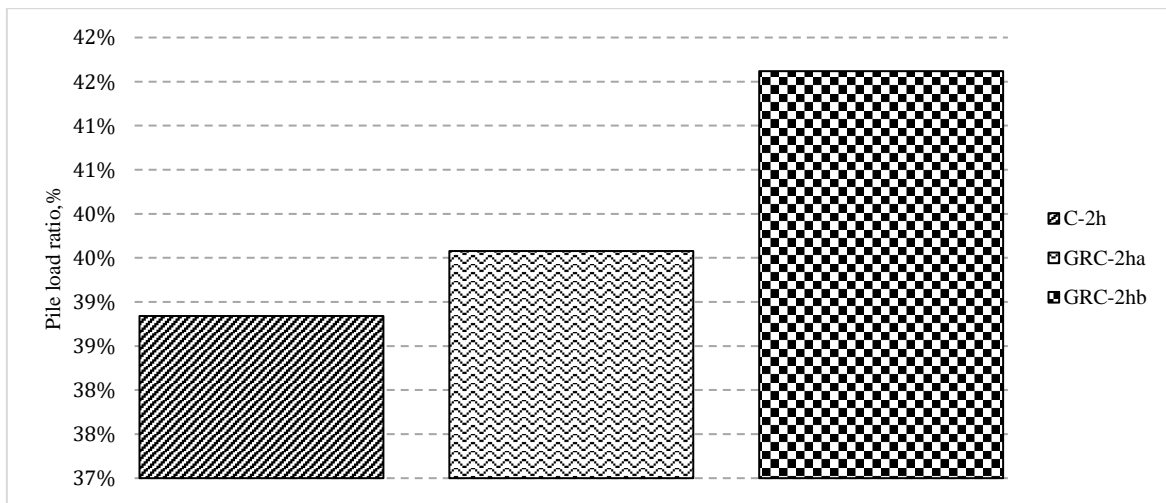
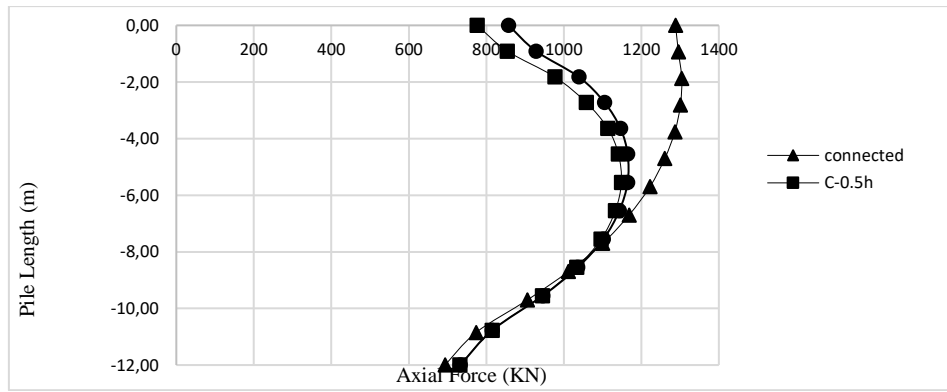
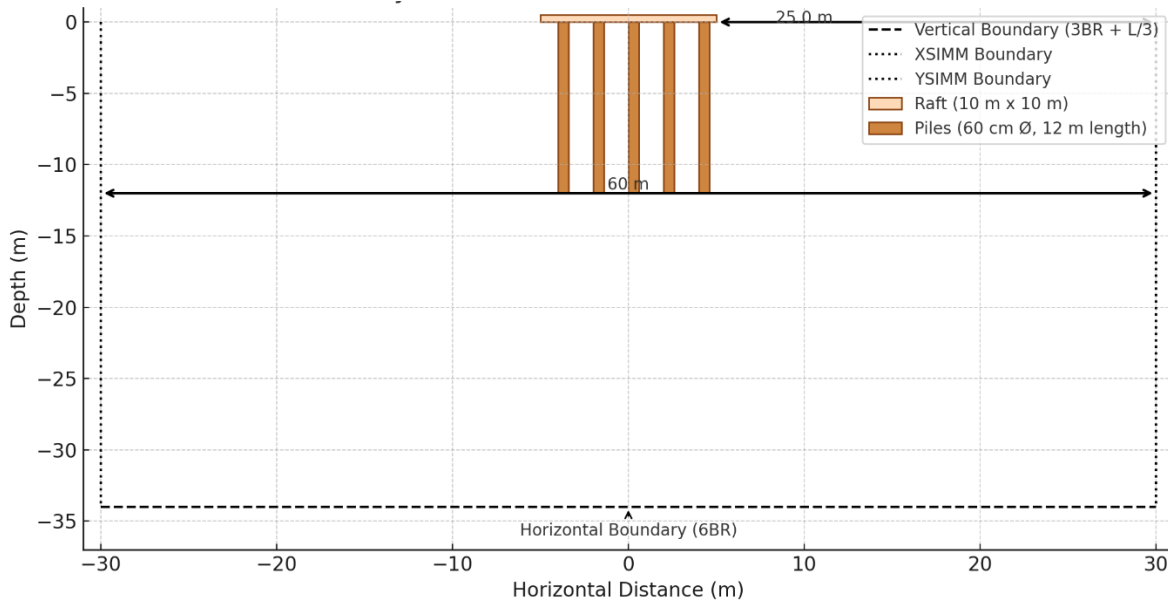


Figure 7. Pile load ratio



**Figure 8.** Axial forces acting on the central pile

In the figure below, Figure 9 represents the model with clear indications of the boundary conditions. Based on these, the details are presented as follows:



**Figure 9.** Boundary conditions

The figure presents a comprehensive view of a 10x10 m raft foundation situated at the top, supported by evenly spaced concrete piles that are 60 cm in diameter and 12 m in length. Directly beneath the raft lies a cushion layer, which is distinctly marked to emphasize the inclusion of GEOCELL, indicating its crucial role in the foundation's structural integrity. Surrounding the foundation, the soil is extended outwards, with its dimensions meticulously specified to illustrate the overall simulation boundary. This detailed representation is complemented by clearly labeled boundary conditions along the figure's periphery. These labels include symmetry conditions (XSIMM/YZIMM) and provide a detailed account of the horizontal and vertical boundaries' extents relative to the size of the raft and the length of the piles. This arrangement not only aids in understanding the structural dynamics of the foundation system but also underscores the importance of precise boundary conditions in the simulation's accuracy.

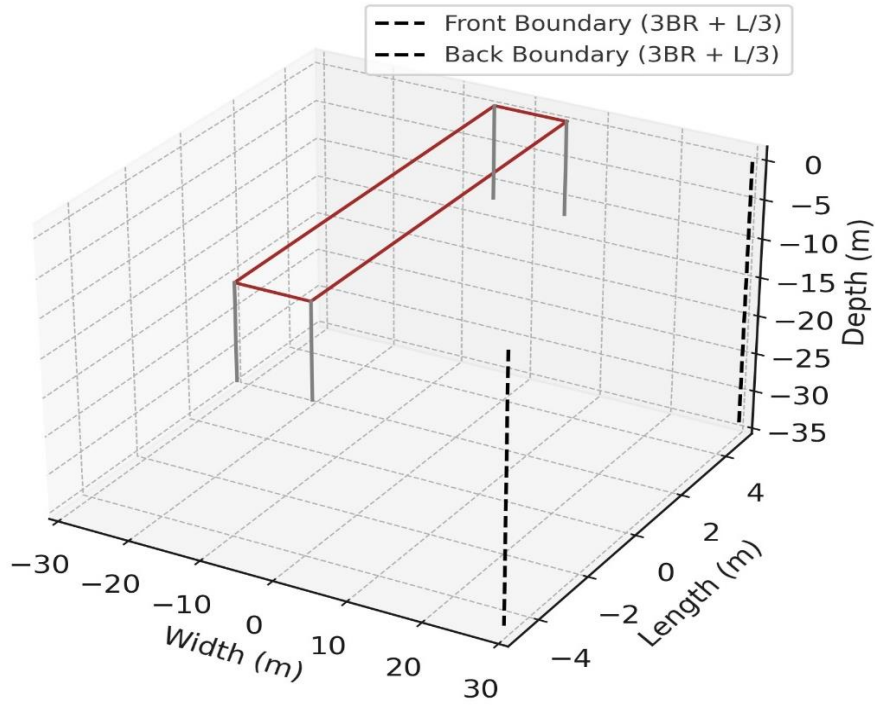


**Figure 10.** 3D Boundary conditions representation

According to Figure 10, a 3D-like representation offers a detailed view of the boundary conditions for a piled-raft foundation model. At the heart of the model, a 10x10 m raft is positioned at the origin, clearly depicted by a brown line at the top. Extending downward from each corner of the raft are concrete piles, illustrated as grey lines, each 60 cm in diameter and 12 m in length, anchoring the structure firmly into the ground. The model further delineates the front and back vertical boundaries with dashed lines, these extend horizontally to six times the raft's width ( $6BR$ ) and vertically to three times the raft's width plus one-third of the pile's length ( $3BR + L/3$ ), providing a comprehensive understanding of the spatial limitations and interactions at play. Additionally, the z-axis indicates the soil depth, reaching down to 35 m, which further contributes to a full appreciation of the model's subsurface context and the engineering challenges addressed

This schematic provides a clear view of the physical dimensions and symmetry conditions (XSIMM/YZIMM) applied to the model. This visualization aids in understanding how the boundary conditions are defined around the piled-raft foundation to minimize external influences on the stress distribution within the model.

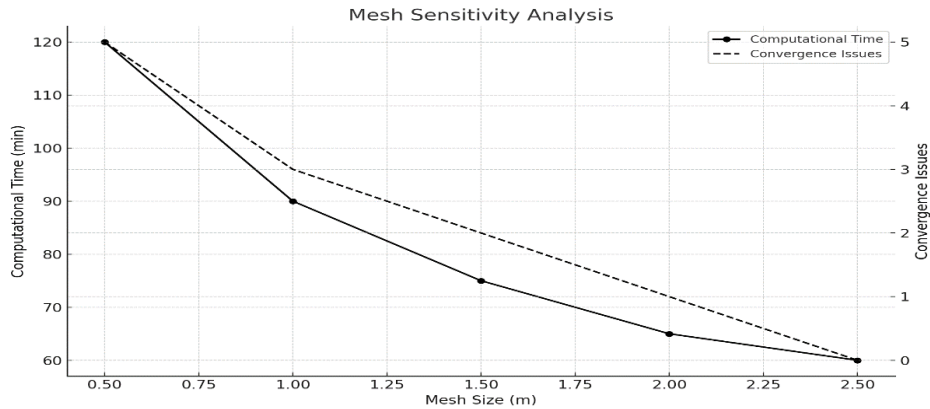


**Figure 11.** Mesh sensitivity analysis

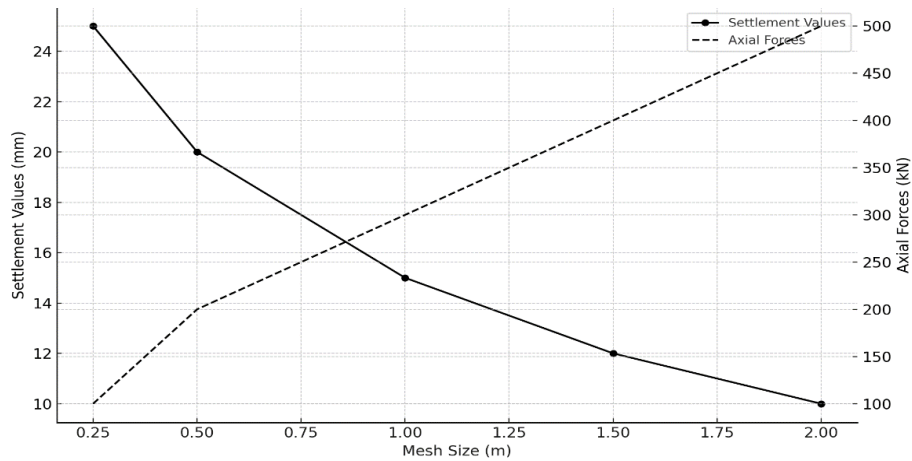


**Figure 12.** Mesh sensitivity analysis: settlement and axial forces

Figures 11 and 12 present a mesh sensitivity analysis crucial for assessing the numerical model's robustness and reliability. This analysis is instrumental in determining the optimal mesh size that balances computational efficiency and the accuracy of settlement predictions.

The bar chart in Figure 1, illustrates a comparative analysis of settlement values, a critical parameter in geotechnical engineering that reflects the vertical displacement experienced by a structure under load. The settlement is measured in millimeters (mm), providing a direct indication of the foundation's performance under stress.

The data showcased in the figure are drawn from both historical and current research, with the blue bar representing findings from Elwakil et al. [8], the green bar drawing from Alaa et al. [19], and the red bar depicting results from the current numerical model discussed in the manuscript. The proximity of settlement values across the different models—with Elwakil et al. at 10 mm, Alaa et al. at 12 mm, and the current numerical model at 11 mm—demonstrates a high degree of consistency. Such minor variations in the data suggest that the current numerical model exhibits behavior similar to that of the reference models. This consistency indicates the model's capability to forecast settlement with accuracy comparable to that of established models, reinforcing the validity of the current simulations.

The mesh sensitivity analysis thus not only informs the choice of mesh size for the current study but also substantiates the model's predictive power in simulating real-world scenarios, lending confidence to its application in practical geotechnical engineering problems.

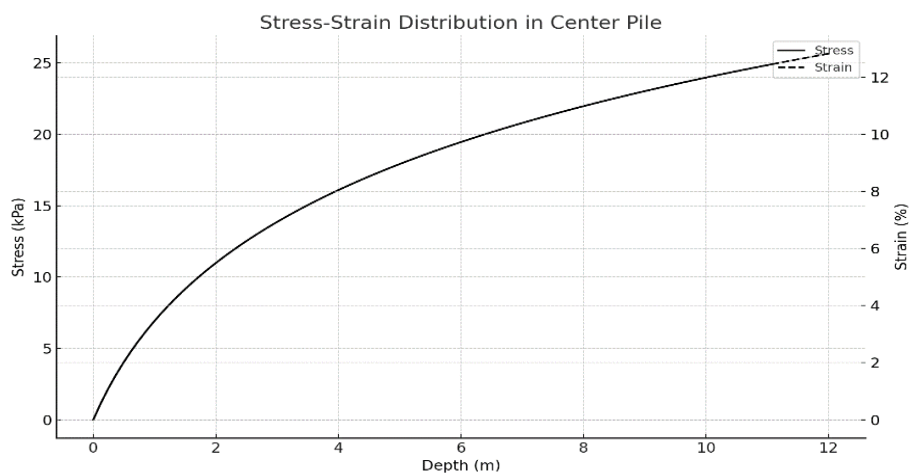


**Figure 13.** Stress-strain distribution in the center pile

Figure 13 illustrates the relationship between stress and strain along the length of a center pile used in a piled-raft foundation. This type of distribution is pivotal for understanding the behavior of the pile under axial loads and for assessing the pile's performance in terms of its elasticity and strength characteristics.

In the figure, the vertical axis represents both stress (in kilopascals, kPa) and strain (as a percentage), while the horizontal axis signifies the depth (in meters) from the top of the pile. The solid black line denotes the variation of stress with depth, indicating an increase in stress as the pile penetrates deeper into the soil. This trend is consistent with the expectation that stress within a pile will increase due to the accumulation of soil pressure and the effect of overburden as depth increases.

Conversely, the dashed black line represents the strain experienced by the pile. The strain also increases with depth, reflecting the deformation of the pile material under the growing stress. The relationship between stress and strain showcased here is essential for determining the point at which the pile material will yield or fail, which is crucial for the safe design of pile foundations.

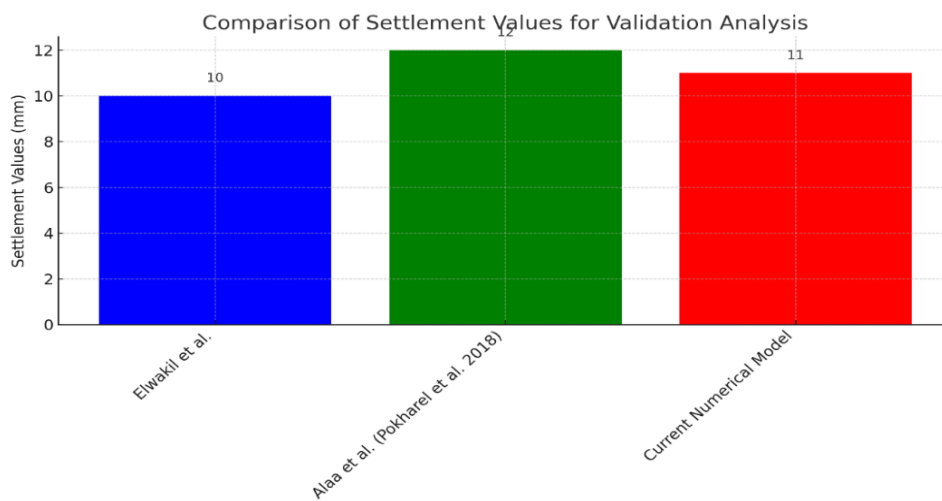


**Figure 14.** Comparison of settlement values

Figure 14 provides a comparative analysis of settlement values from different models, including two reference models and the current numerical model being presented in the manuscript. Settlement, often measured in millimeters (mm), is a critical parameter in geotechnical engineering, indicating the amount of vertical displacement or sinking that a structure undergoes when subjected to loading.

In the bar chart, each bar represents the settlement value associated with a particular model. The blue bar corresponds to the data from Elwakil et al., the green bar represents Alaa et al. and the red bar corresponds to the current numerical model that the manuscript focuses on.

The figure shows that the settlement values for the models are relatively close, with the Elwakil et al. model showing a settlement of 10 mm, Alaa et al. (Pokharel et al. [19]) showing a slightly higher value of 12 mm, and the current numerical model showing a settlement of 11 mm. The minor differences between these values may suggest that the current numerical model behaves similarly to the reference models, indicating that the model can potentially be used to predict settlement with a comparable level of accuracy as the established reference models.

This type of validation is essential to ensure that the new or current numerical model is reliable. It provides confidence to both the modelers and the readers that the numerical predictions are grounded in previously verified results. The closeness in settlement values also serves as a quality check against the model's ability to simulate real-world behavior, which is particularly important for any engineering application that relies on precise numerical modeling to predict structural behavior under various loading conditions.

## **4. Conclusion**

This investigation delved into the potential enhancements of unconnected piled raft foundations through geocell reinforcement, spurred by the noticeable lack of comprehensive design strategies despite their established advantages. Employing sophisticated numerical modeling and examining diverse setups under varying conditions, our study has shed light on the considerable benefits of geocell reinforcement for improving load distribution and reducing settlement in these foundations.

Our research consistently found that adjusting the cushion's stiffness to half that of the foundation maximizes load distribution and minimizes settlement, a key factor in preserving structural integrity across various loading scenarios. These insights offer a ground-breaking approach to tackling the longstanding issues of soil instability and enhancing load-bearing capacities in unconnected piled raft foundation systems.

The evidence from this study strongly supports the integration of geocell reinforcement into piled raft foundation systems, underlining its role in fortifying soil strength, stability, and load distribution. Based on our findings, we advocate for the creation and implementation of comprehensive design methodologies that:

1. Tailor cushion stiffness to foundation characteristics, specifically recommending cushions with half the stiffness of the foundation for superior performance.
2. Standardize the use of geocell reinforcement in unconnected piled raft foundations to markedly bolster soil mechanics and overall foundation efficacy.
3. Strategically position geocells within the cushion layer to capitalize on their benefits in load capacity enhancement and settlement reduction, guided by our research insights.

The implications of our work suggest a significant leap forward in civil engineering, particularly for projects requiring enhanced load support and minimal foundation settlement. Incorporating our recommendations into practice could revolutionize foundation engineering, steering it towards more robust, efficient, and eco-friendly methods.

To sum up, the adoption of geocell technology in unconnected piled raft foundations offers a viable solution to the intricate demands of contemporary foundation engineering. We are optimistic that our study will not only enrich the academic discourse but also encourage the broader application and development of geocell reinforcement in foundation engineering, leading to the emergence of more sophisticated, dependable, and innovative foundation systems.

## **5. Author Contribution Statement**

Mojtaba Pourgholamali: Conceptualization, Methodology, Software, Data curation, Writing-Original draft preparation, Software, Validation; Farzin Asgharpour: Visualization, Investigation, Writing-Reviewing and Editing

## **6. Ethics Committee Approval and Conflict of Interest**

“There is no conflict of interest with any person/institution in the prepared article”

## 7. References

- [1] A. Ata, E. Badrawi and M. Nabil, "Numerical analysis of unconnected piled raft with cushion," *Ain Shams Engineering Journal*, vol. 6, no. 2, pp. 421–428, Jun. 2015.
- [2] M. M. Biabani, N. T. Ngo and B. Indraratna, "Performance evaluation of railway subballast stabilised with geocell based on pull-out testing," *Geotextiles and Geomembranes*, vol. 44, no. 4, pp. 579–591, Aug. 2016.
- [3] B. Das, R. Saha and S. Haldar, "Effect of in-situ variability of soil on seismic design of piled raft supported structure incorporating dynamic soil-structure-interaction," *Soil Dynamics and Earthquake Engineering*, vol. 84, pp. 251–268, May 2016.
- [4] P. Deb and S. K. Pal, "Numerical analysis of piled raft foundation under combined vertical and lateral loading," *Ocean Engineering*, vol. 190, p. 106431, Oct. 2019.
- [5] A. M. J. Alhassani and A. N. Aljorany, "Parametric Study on Unconnected Piled Raft Foundation Using Numerical Modelling," *Journal of Engineering*, vol. 26, no. 5, pp. 156–171, May 2020.
- [6] W. El Kamash, H. El Naggar, M. Nabil, and A. Ata, "Optimizing the Unconnected Piled Raft Foundation for Soft Clay Soils: Numerical Study," *KSCE Journal of Civil Engineering*, vol. 24, no. 4, pp. 1095–1102, Apr. 2020.
- [7] X. D. Cao, I. H. Wong, and M.-F. Chang, "Behavior of Model Rafts Resting on Pile-Reinforced Sand," *Journal of Geotechnical and Geoenvironmental Engineering*, vol. 130, no. 2, pp. 129–138, Feb. 2004.
- [8] A. Z. Elwakil and W. R. Azzam, "Experimental and numerical study of piled raft system," *Alexandria Engineering Journal*, vol. 55, no. 1, pp. 547–560, Mar. 2016.
- [9] J. Han, X. M. Yang, D. Leshchinsky, R. L. Parsons, and A. Rosen, "Numerical Analysis for Mechanisms of a Geocell-Reinforced Base Under a Vertical Load," in *Geosynthetics in Civil and Environmental Engineering*, Berlin, Heidelberg: Springer Berlin Heidelberg, pp. 741–746.
- [10] X. Han, Y. Li, J. Ji, J. Ying, W. Li, and B. Dai, "Numerical simulation on the seismic absorption effect of the cushion in rigid-pile composite foundation," *Earthquake Engineering and Engineering Vibration*, vol. 15, no. 2, pp. 369–378, Jun. 2016.
- [11] A. Hegde, "Geocell reinforced foundation beds-past findings, present trends and future prospects: A state-of-the-art review," *Constr Build Mater*, vol. 154, pp. 658–674, Nov. 2017.
- [12] H. Bolouri Bazaz, A. Akhtarpour, and A. Karamodin, "A study on the effects of piled-raft foundations on the seismic response of a high rise building resting on clayey soil," *Soil Dynamics and Earthquake Engineering*, vol. 145, p. 106712, Jun. 2021.
- [13] H.-J. Park et al., "Centrifuge modeling of disconnected piled raft using vertical pushover tests," *Acta Geotech*, vol. 15, no. 9, pp. 2637–2648, Sep. 2020.
- [14] A. Hegde and T. G. Sitharam, "3-Dimensional numerical modelling of geocell reinforced sand beds," *Geotextiles and Geomembranes*, vol. 43, no. 2, pp. 171–181, Apr. 2015.
- [15] A. Kumar, D. Choudhury, and R. Katzenbach, "Effect of Earthquake on Combined Pile–Raft Foundation," *International Journal of Geomechanics*, vol. 16, no. 5, Oct. 2016.
- [16] B. Leshchinsky and H. I. Ling, "Numerical modeling of behavior of railway ballasted structure with geocell confinement," *Geotextiles and Geomembranes*, vol. 36, pp. 33–43, Feb. 2013.
- [17] F. Y. Liang, L. Z. Chen, and X. G. Shi, "Numerical analysis of composite piled raft with cushion subjected to vertical load," *Comput Geotech*, vol. 30, no. 6, pp. 443–453, Sep. 2003.
- [18] H. Pincus, R. Bathurst, and R. Karpurapu, "Large-Scale Triaxial Compression Testing of Geocell-Reinforced Granular Soils," *Geotechnical Testing Journal*, vol. 16, no. 3, p. 296, 1993.
- [19] S. K. Pokharel, J. Han, D. Leshchinsky, and R. L. Parsons, "Experimental evaluation of geocell-reinforced bases under repeated loading," *International Journal of Pavement Research and Technology*, vol. 11, no. 2, pp. 114–127, Mar. 2018.
- [20] M. Saadatinezhad, A. Lakirouhani, and S. Jabini Asli, "Seismic response of non-connected piled raft foundations," *International Journal of Geotechnical Engineering*, vol. 15, no. 1, pp. 66–80, Jan. 2021.
- [21] S. R. Satyal, B. Leshchinsky, J. Han, and M. Neupane, "Use of cellular confinement for improved railway performance on soft subgrades," *Geotextiles and Geomembranes*, vol. 46, no. 2, pp. 190–205, Apr. 2018.
- [22] Simulia, CAE. 2014.

- [23] J. K. Thakur, J. Han, and R. L. Parsons, “Factors Influencing Deformations of Geocell-Reinforced Recycled Asphalt Pavement Bases under Cyclic Loading,” *Journal of Materials in Civil Engineering*, vol. 29, no. 3, Mar. 2017.
- [24] F. Tradigo, F. Pisanò, C. di Prisco, and A. Mussi, “Non-linear soil–structure interaction in disconnected piled raft foundations,” *Comput Geotech*, vol. 63, pp. 121–134, Jan. 2015.
- [25] I. H. Wong, M. F. Chang, and X. D. Cao, “17. Raft foundations with disconnected settlement-reducing piles,” in *Design applications of raft foundations*, Thomas Telford Publishing, 2000, pp. 469–486.
- [26] L. Zhang, S. H. Goh, and H. Liu, “Seismic response of pile-raft-clay system subjected to a long-duration earthquake: centrifuge test and finite element analysis,” *Soil Dynamics and Earthquake Engineering*, vol. 92, pp. 488–502.



## Farklı İçeriklerde PVC Atığı ile Hazırlanan Sönmüş Kireç İçeren Bitümlü Karışımların Suya Bağlı Bozulmalara Karşı Direncinin Belirlenmesi

İsmail Çağrı GÖRKEM<sup>1\*</sup>, Salih Serkan ARTAGAN<sup>2</sup>, Bekir Tuna KAYAALP<sup>3</sup>,  
Cem SAYKAN<sup>4</sup>, İmer Arda ÖZDEMİR<sup>5</sup>

<sup>1</sup>İnşaat Mühendisliği Bölümü, Mühendislik Fakültesi, Muğla Sıtkı Koçman Üniversitesi, Muğla, Türkiye.

<sup>2</sup>Ulaştırma Hizmetleri Bölümü, Ulaştırma Meslek Yüksek Okulu, Eskişehir Teknik Üniversitesi, Eskişehir, Türkiye.

<sup>3</sup>İnşaat Mühendisliği Bölümü, Mühendislik Fakültesi, Eskişehir Teknik Üniversitesi, Eskişehir, Türkiye.

<sup>4,5</sup>İnşaat Mühendisliği ABD, Fen Bilimleri Enstitüsü, Muğla Sıtkı Koçman Üniversitesi, Muğla, Türkiye.

<sup>1</sup>cagriorkem@mu.edu.tr, <sup>2</sup>ssartagan@eskisehir.edu.tr, <sup>3</sup>bt@eskisehir.edu.tr, <sup>4</sup>cemsaykan33@gmail.com, <sup>5</sup>imrzdmr@gmail.com

Geliş Tarihi: 18.12.2023

Kabul Tarihi: 05.02.2024

Düzeltilme Tarihi: 02.01.2024

doi: 10.62520/fujece.1406206

Araştırma Makalesi

Alıntı: İ. Ç. Görkem, S. S. Artagan, B. T. Kayaalp, C. Saykan ve İ. A. Özdemir, "Farklı içeriklerde PVC atığı ile hazırlanan sönmüş kireç içeren bitümlü karışımların suya bağlı bozulmalara karşı direncinin belirlenmesi", Fırat Üni. Deny. ve Hes. Müh. Derg., vol. 3, no 1, pp. 28-51, Şubat 2024.

### Öz

Dünya genelinde artan ticari hareketlilik yollara olan ihtiyacı artırmış ve bunun sonucunda yeni yol ağları ortaya çıkmıştır. Ülkemizde inşa edilen karayollarının üstü yapısı önemli ölçüde esnek kaplamalardan oluşmaktadır. Ağır taşıt sayısı, tekrarlanan yükler, çevre ve iklim koşulları gibi parametreler esnek kaplamalar üzerinde farklı deformasyonlara neden olmaktadır. Bu deformasyonlardan biri de su kaynaklı hasarlardır. Özellikle değişen iklim koşulları bazı bölgelerin yıl boyunca alması gereken yağışları çok kısa sürelerde yoğun olarak almasına neden olmaktadır. Bunun sonucunda esnek kaplamalar hasar görmekte ve hizmet ömürleri beklenenden daha kısa olmaktadır. Artan çevre bilinciyle birlikte, bazı atık malzemelerin bitümlü karışımlarda kullanılması son derece önemli bir konu haline gelmiştir. Bu çalışmada, farklı Polivinil Klorür (PVC) içerikleri ile modifiye edilmiş bitümlü malzemeler uygun gradasyonlu agregalar ile karıştırılmış ve su kaynaklı hasarlara karşı direnci değerlendirilmiştir. Ayrıca, sönmüş kireç ilavesinin numunelerin su kaynaklı hasara karşı direnci üzerindeki etkisini değerlendirmek için çeşitli performans testleri gerçekleştirilmiştir. Bu kapsamda, modifiye edilmiş bitüm ve agregaların özellikleri, geleneksel bitüm ve agrega testleri yapılarak belirlenmiştir. Çalışmanın son hedefi olarak, bitümlü malzemelere PVC ilavesinin su kaynaklı hasara karşı dirence etkisini belirlemek amacıyla karışımlara Modifiye Lottman (AASHTO T 283) Deneyi uygulanmıştır.

**Anahtar kelimeler:** PVC atığı, Bitümlü karışımlar, Bitüm modifikasyonu, Suya bağlı bozulmalar, Modifiye Lottman deneyi

\*Yazışılan yazar



## Determination of Resistance to Water-Induced Damage of Bituminous Mixtures Containing Hydrated Lime Prepared with Different Contents of PVC Waste

İsmail Çağrı GÖRKEM<sup>1\*</sup>, Salih Serkan ARTAGAN<sup>2</sup>, Bekir Tuna KAYAALP<sup>3</sup>,  
Cem SAYKAN<sup>4</sup>, İmer Arda ÖZDEMİR<sup>5</sup>

<sup>1</sup>Department of Civil Engineering, Faculty of Engineering, Muğla Sıtkı Koçman University, Muğla, Turkey.

<sup>2</sup>Department of Transportation Services, Vocational School of Transportation, Eskisehir Technical University, Eskişehir, Turkey.

<sup>3</sup>Department of Civil Engineering, Faculty of Engineering, Eskisehir Technical University, Eskişehir, Turkey.

<sup>4,5</sup>Department of Civil Engineering, Graduate School of Natural and Applied Sciences, Muğla Sıtkı Koçman University, Muğla, Turkey.

<sup>1</sup>cagrigorkem@mu.edu.tr, <sup>2</sup>ssartagan@eskisehir.edu.tr, <sup>3</sup>btk@eskisehir.edu.tr, <sup>4</sup>cemsaykan33@gmail.com, <sup>5</sup>imrzdmr@gmail.com

Received: 18.12.2023

Accepted: 05.02.2024

Revision: 02.01.2024

doi: 10.62520/fujece.1406206

Research Article

Citation: İ. Ç. Görkem, S. S. Artagan, B. T. Kayaalp, C. Saykan and İ. A. Özdemir, "Determination of resistance to water-induced damage of bituminous mixtures containing hydrated lime prepared with different contents of PVC waste", *Firat Univ. Jour. of Exper. and Comp. Eng.*, vol. 3, no 1, pp. 28-51, February 2024.

### Abstract

Increasing commercial mobility throughout the world has increased the need for roads and as a result, new road networks have emerged. The pavement type of the highways constructed in our country consists of flexible pavements to a significant extent. Parameters such as the number of heavy vehicles, repeated loads as well as environmental and climatic conditions cause different deformations on flexible pavements. One of these deformations is water-induced damage. In particular, changing climatic conditions cause some regions to experience intense precipitation in a very short period of time, which they should receive throughout the year. As a result, flexible pavements are damaged and their service life becomes shorter than expected. With increasing environmental awareness, the use of some waste materials in bituminous mixtures has become an extremely important issue. In this study, bituminous materials modified with different Polyvinyl Chloride (PVC) contents were mixed with properly graded aggregates and their resistance to water-induced damage has been evaluated. In addition, several performance tests were carried out to evaluate the effect of hydrated lime addition on the resistance of the samples to water-induced damage. In this context, the properties of the modified bitumen and aggregates were determined by performing conventional bitumen and aggregate tests. As the final objective of the study, Modified Lottman Test (AASHTO T 283) was performed on the mixtures to determine the effect of PVC addition to bituminous materials on resistance to water-induced damage.

**Keywords:** PVC waste, Bituminous mixtures, Bitumen modification, Water induced damage, Modified Lottman test

\*Corresponding author

## **1. Introduction**

The durability of bituminous mixtures is greatly affected by environmental factors such as temperature, air and water. The use of good quality bituminous materials and aggregates during the construction of flexible pavements at mild climatic conditions generally results in deformations such as fatigue cracking and rutting caused by stresses due to traffic loads [1]. When tough climatic conditions are taken into consideration, stresses due to traffic loads increase as a result of inadequate material quality and the service life of flexible pavements decreases. Because water or moisture in the environment is relatively neutral in the acid-basic balance, it interferes with the ability of the bituminous material to bond to the aggregate. This causes a type of deformation known as “stripping” in flexible pavements [2]. Because the mixture no longer acts as a coherent structural unit and strength is compromised. The cohesive resistance of the interstitial bitumen body is rendered useless by the loss of adhesion. Water can penetrate the interface by diffusion through the bituminous films and can enter directly into the particulate-coated aggregate [3]. There are five different mechanisms by which water can cause stripping, including detachment, displacement, spontaneous emulsification, pore pressure, and hydraulic scour [1].

Bituminous materials and crushed stone aggregates are the main constituents used in flexible pavements. Due to the limited availability of these materials in nature, the use of recycled materials has become a necessary issue to consider [4]. Therefore, many countries are actively researching and developing methods to minimize their impact on the environment by reusing waste materials [5]. This increasing trend towards the use of waste materials in flexible pavements aims to (I) reduce the use of limited natural resources, (II) minimize environmental degradation and problems caused by waste disposal, (III) increase production efficiency, and (IV) reduce material costs [4, 6]. The waste materials that can be incorporated into bituminous mixtures can be classified into three main categories: (I) industrial waste, which includes cellulose waste, wood lignins, slags, bottom ash, and fly ash; (II) municipal/domestic waste, which encompasses incinerator residue, scrap rubber, waste glass, and roofing shingles; and (III) mining waste, specifically coal mine refuse [7].

Polymer Modified Bitumens (PMB), one of the new asphalt materials developed in recent years to improve the mechanical properties of pavements, make the pavement more resistant to fatigue cracking, rutting and thermal effects [8]. However, despite these advantages, the average market price of PMB material is high, resulting in a 30-40% cost increase in asphalt mixtures [8, 9]. Therefore, the use of recovered/waste polymers as an alternative to reduce the cost of PMB material to be used in pavements has become an approach of interest [9]. In this context, in this study, waste Polyvinyl Chloride (PVC), a polymer from the thermoplastic elastomer class, will be used as a binder modifier. By adding thermoplastics to bitumen, bituminous materials are made harder and bituminous mixtures can withstand heavy loads without flexing too much. Some thermoplastics used in bitumen modification are polyethylene (PE), polypropylene (PP), polyvinyl chloride (PVC), polystyrene (PS) and ethylene vinyl acetate (EVA). When mixed with bituminous materials, they increase the viscosity and stiffness of bitumen at service temperatures [10]. PVC accounts for 10.1% of European plastic production and is used in the manufacture of window frames, profiles, cable insulation and garden hoses [9]. Waste PVC material to be used as bitumen modifying agent can be pipes [11, 12], window frames or cables [13]. The usability of PVC waste in bituminous materials has been demonstrated in many studies. The use of PVC particles in the paving industry has been shown to protect the environment, reduce pavement production and maintenance costs, and improve the mechanical properties of asphalt mixtures [14]. The addition of PVC waste to bituminous materials results in an improvement in phase angle and complex modulus values and an increase in indirect tensile strength (ITS) values. However, the rutting values were significantly reduced by the use of waste PVC in the asphalt mix [15]. It was studied the effects of different PVC wastes including blinds, window wastes and cable wastes, PVC based on bitumen. The results showed that the addition of PVC blinds and window waste in the range of 1-3% improved the performance of the bitumen modified at high temperatures. Also, 5% of cable waste causes bitumen to perform better at low temperatures [14]. The ductility, penetration and solubility values of bituminous mixtures decrease with increasing addition of PVC waste to bituminous mixtures [16]. Salman et al. studied the physical properties of bitumen mixed with PVC waste at different percentages ranging from 2.5% to 15% by weight of the bituminous material. According to the results obtained, the penetration decreased significantly with the addition of PVC waste additive, the ductility also reduced and the softening point increased as the PVC

percentage increased [17]. Ezzat et al. evaluated the aging values of bituminous materials by FTIR test. The addition of PVC waste to bitumen has a positive effect on the aging resistance of bituminous materials, according to the results obtained [18].

Durability of bituminous mixtures can be significantly affected by environmental factors such as temperature, weather and water [19]. Especially in regions exposed to heavy rainfall and high groundwater levels, bituminous mixtures often suffer early water-related damage and their performance under load is reduced [20]. The presence of water on the asphalt surface, combined with other environmental factors such as freeze-thaw cycles, can have negative consequences [21]. Moisture-induced damage is a complex form of deterioration that results in a reduction in the stiffness and strength of bituminous mixtures, ultimately leading to costly maintenance of the entire pavement structure [22]. Moisture-induced damage can be managed or reduced through a variety of methods, such as selecting appropriate materials, designing appropriate mixtures, increasing asphalt film thickness, using additives, implementing an effective surface design, ensuring proper compaction, and developing drainage systems [23]. Among these, the use of anti-stripping additives to improve the adhesion between bitumen and aggregate has become attractive over the years to limit or control moisture-related damage on bituminous mixtures [26]. Although a wide variety of anti-stripping additives have been used recently, hydrated lime is reported to be the most commonly used [19, 22, 25].

In light of the literature review, one of the most economical methods of reducing moisture sensitivity in bituminous mixtures is the addition of hydrated lime. The relatively high silica content in limestone aggregate makes it difficult for the aggregate to bond with bitumen in highly moisturized environmental conditions. When added to the bituminous mixture, hydrated lime reacts with the aggregate, strengthening the bitumen/aggregate interphase. When dry hydrated lime is added to a wet aggregate, the additive completely covers the aggregate and reduces the silica content of the aggregate. Thus, by strengthening the bond between the bituminous material and the aggregate, it reduces the moisture sensitivity of flexible pavements and reduces water-induced damages [19, 26]. Considering these advantages, hydrated lime was used in the experiments to evaluate the effect of different contents of PVC waste on the resistance to moisture-induced deterioration of bituminous mixtures conditioned and unconditioned with this anti-stripping agent.

When hydrated lime is added to the bituminous mixture, it reacts with the aggregate and increases the bond between the bitumen and aggregate phase. Lime reacts with highly polar molecules to inhibit the formation of soluble soaps that promote stripping. When these molecules react with lime, they form salts that are not affected by water. The ability of hydrated lime to make an asphalt mixture harder, more durable and resistant to rutting is a reflection of its superior performance as an active mineral filler [27].

There are five methods for introducing hydrated lime into bituminous mixtures. These are: (I) lime slurry to dry or wet aggregate, (II) dry lime to wet aggregate, (III) dry lime to dry aggregate (IV) dry lime to bitumen, and (V) quicklime slurry to dry or wet aggregate [28, 29].

The addition of hydrated lime to wet aggregate is generally a better method and provides good mixing, coating and processing, especially with weak materials. It is also best suited for application under laboratory conditions [28-29].

Furthermore, recent research has shown that hydrated lime has additional effects on bituminous mixtures that can act as active fillers, an antioxidant and an additive that interacts with fine clay grains in bituminous mixtures [30]. Several studies have highlighted the use of hydrated lime as a means of increasing resistance to moisture damage in bituminous mixtures, as well as providing other advantages such as increased stiffness and better resistance to rutting [31].

## 2. Materials and Methods

### 2.1. Aggregate

The aggregate materials used in the study were obtained from 2<sup>nd</sup> Region and 26<sup>th</sup> Branch of General Directorate of Highways. Aggregate properties were determined by standard aggregate tests, where specified in the General Directorate of Highways, Highways Technical Specification (KTŞ), such as specific gravity, Los Angeles abrasion, flatness index, and Sodium soundness test. The results are given in Table 1. After the tests on the utilization of aggregate properties in bituminous mixtures were performed, Sieve Analysis Test was applied according to the Type-1 gradation limits specified in the Highways Technical Specifications for wearing courses.

**Table 1.** Properties of limestone aggregate

Test	Specification	Results	Spec. Limit
Sieve No	ASTM C 136		
¾"		100	100
½"		92	88-100
⅜"		80	72-90
No 4		47.3	42-52
No 10		33	25-35
No 40		13	10-20
No 80		9	7-14
No 200		5.3	3-8
Specific Gravity (Coarse Agg.)	ASTM C 127		
Bulk		2.645	-
SSD		2.666	-
Apparent		2.713	-
Specific Gravity (Fine Agg.)	ASTM C 128		
Bulk		2.643	-
SSD		2.672	-
Apparent		2.722	-
Specific Gravity (Filler)		2.686	-
Los Angeles Abrasion (%)	TS EN 1097-2	27.4	Max. 27
Flatness Index (%)	BS 812	5	Max. 10
Freeze-thaw resistance (MgSO <sub>4</sub> ) (%)	TS EN 1367-2	4.154	Max. 6

### 2.2. Bitumen

50/70 penetration grade bitumen obtained from İzmir Refinery of Turkish Petroleum Refineries Inc. (TÜPRAŞ) was used as bituminous material. Penetration, softening point, viscosity and etc. tests were performed on base bitumen to determine the properties of the binder. The test results are given in Table 2.

**Table 2.** Properties of base bitumen

Test	Specification	Results	Spec. Limits
Penetration (25 °C;0,1 mm)	ASTM D5 TS EN 1426	55	50-70
Softening Point (°C)	ASTM D36 TS EN 1427	49	46-54
Viscosity at (135°C)-Pa.s	ASTM D4402	412.5	-
Thin Film Oven Test (TFOT) (163°C, 5 hr.) Loss on Mass (%)	TS EN 12607-1	0.04	0.5 (Max.)
Thin Film Oven Test (TFOT) (163°C, 5 hr.) Penetration after TFOT (%)	ASTM D5 TS EN 1426	75	50 (Min.)
Softening Point after TFOT (°C)	ASTM D36 TS EN 1427	6	9 (Max.)
Ductility (25°C), cm	ASTM D113	100	-
Specific Gravity	ASTM D92	1.03	-
Flash Point (°C)	EN 22592	260	230 (Min.)

## 2.2. Hydrated lime

The hydrated lime admixture used in the experimental studies, which contains a high percentage of calcium hydroxide (Ca(OH)<sub>2</sub>), was obtained locally in Muğla, Türkiye. The properties of the hydrated lime admixture used are given in Table 3. The usage characteristics of hydrated lime are described in the previous section. Since the main focus of the study was on the proportions of PVC content, hydrated lime was used at 1.5% as recommended in previous studies [19].

**Table 3.** Properties of hydrated lime layer

Components after analysis			Components after calculation		
Name	Formula	%	Name	Formula	%
Silicon dioxide	SiO <sub>2</sub>	0.40	Calcium carbonate	CaCO <sub>3</sub>	3.95
Ferrous oxide+	Fe <sub>2</sub> O <sub>3</sub> +	0.12	Calcium hydroxide	Ca(OH) <sub>2</sub>	95.03
Aluminum oxide	Al <sub>2</sub> O <sub>3</sub>	0.10	Magnesium carbonate	MgCO <sub>3</sub>	–
Calcium oxide	CaO	–	Magnesium hydroxide	Mg(OH) <sub>2</sub>	–
Magnesium oxide	MgO	–	Calcium sulfate	CaSO <sub>4</sub>	–
Sulphur trioxide	SO <sub>3</sub>	–	Sulphur	S	–
Loss on heating	CO <sub>2</sub>	–			
Surface moisture	H <sub>2</sub> O	0.40	Sieve number		
Relative humidity	H <sub>2</sub> O	–	Sieve size: 25 μ		
Insoluble materials		–	% Passing: 99.74		

## 2.4. Test applied on aggregates

The limestone aggregate used in the study was subjected to standard aggregate testing. Sieve analysis (ASTM C 136), specific gravity determination for coarse/fine/filler materials (ASTM C 127, ASTM C 128), Los Angeles abrasion (TS EN 1097-2), flatness index (TS EN 933-3) and soundness test (TS EN 1367-2) were performed on aggregate samples.

### 2.4.1. Sieve analysis test (ASTM C 136)

This test method involves determining the grain size distribution of coarse and fine aggregates by sieving. To determine the particle size distribution, the aggregate sample of known dry weight is sieved through progressively smaller apertures. This method is especially used to determine the gradation of the materials to be used as aggregate. The results provide the necessary data for verifying the conformity of the particle size distribution to the specifications and the aggregates or aggregate mixtures produced. Figure 1 shows the set used in the sieve analysis.



**Figure 1.** Set used in sieve analysis

#### **2.4.2. Specific gravity determination for coarse/fine/filler materials (ASTM C 127, ASTM C 128)**

The specific gravity of an aggregate is the ratio of the weight per unit volume of that aggregate to the weight of water in the same volume and at 25°C. There are different specific gravity types of particles, depending on the volume definition.

Apparent Specific Gravity is the ratio of the weight in air of the unit volume containing the impermeable voids of the aggregate at a given temperature to the weight of distilled water at the same temperature and in the same volume.

Bulk Specific Gravity is the ratio of the weight in air of the unit volume of the aggregate containing the permeable and non-permeable voids of the aggregate at a given temperature to the weight in air of the same temperature and volume of the same volume of distilled water at the same temperature and volume.

#### **2.4.3. Los Angeles abrasion test (ASTM C131, AASHTO T96, TS EN 1097-2)**

The Los Angeles Abrasion Test determines the wear of aggregate particles due to impact and abrasion. With this test, the abrasion resistance of coarse aggregates with a grain size of less than 75 mm is determined by Los Angeles Abrasion Machine. In the experiment, metal abrasive spheres are placed in the machine, which is in the form of a two-ended closed cylinder, together with the aggregate, and the machine is operated at a certain speed and rotation. As a result, the percentage by weight of the material abraded by the metal spheres falling on it compared to the material taken at the beginning of the experiment is given as abrasion loss. The test apparatus for the Los Angeles abrasion test is given in Figure 2.



**Figure 2.** Device used for the Los Angeles Abrasion Test

#### **2.4.4. Flatness index test (TS EN 933-3)**

It is a method based on the identification of aggregate particles with a thickness less than 0.6 of their nominal size as flat. The flatness index of aggregate samples is expressed as a percentage of the ratio of the weight of flat particles separated using a template with specific openings to the total sample weight. The template for flatness index determination is shown in Figure 3.



**Figure 3.** Flatness Index Determination

#### **2.4.5. Soundness test (TS EN 1367-2)**

This test is a rapid test used to measure the resistance to freezing and thawing of aggregates that have been exposed to weathering for a long time.  $\text{Na}_2\text{SO}_4$  and  $\text{MgSO}_4$  solutions can be used in the test. The test is applied to the aggregate above 4.75 mm for 5 freeze-thaw periods and the percentage loss at the end of these processes is calculated. The effect on the aggregate is equivalent to about 500 freezing and thawing events in nature. The meshed aggregate bucket and the  $\text{Na}_2\text{SO}_4$  and  $\text{MgSO}_4$  solutions used in the experiment are shown in Figure 4.



**Figure 4.** The meshed aggregate bucket and the  $\text{Na}_2\text{SO}_4$  and  $\text{MgSO}_4$  solutions

#### **2.5. Test applied on bitumen**

As part of the study, conventional bitumen tests were performed on the bituminous materials used. Summary information on the tests is provided below as well as bituminous materials containing PVC waste as an additive.

##### **2.5.1. Preparation of bituminous materials containing PVC waste additives**

The PVC waste used in the study was obtained from the chips generated during window production. PVC wastes were added to bituminous materials in powder form (Figure 5).



**Figure 5.** PVC waste additive

The additive rates were 0%, 0.5%, 1% and 1.5% by weight of the bituminous material. PVC waste was slowly added to the bituminous material heated to 150°C in an air circulation oven and mixed at 1500 rpm for 60 minutes while keeping the temperature constant (Figure 6). The PVC-modified bitumen produced was used immediately after production.



**Figure 6.** Production of PVC Waste-Modified Bituminous Material

### **2.5.2. Penetration test (TS EN 1426)**

This method covers the determination of hardness and viscosity of bitumen and bituminous binders. This method is applied for samples with penetration values up to 330\*0.1 mm, while a different method is applied for samples with penetration values between 330\*0.1 mm and 500\*0.1 mm. It is the depth of penetration of a standard needle into a conditioned specimen. The test conditions are 25 °C, 100 grams application load and 5 seconds loading time for penetrations up to 330 x 0.1 mm. For penetrations exceeding 330 x 0.1 mm, the test temperature is reduced to 15 °C but the application load and time remain the same. The needle is slowly

lowered downwards to the zero position on the sample surface. The needle holder is released to allow the needle to penetrate the sample. The first reading is recorded. A clean needle is used for each reading. At least three valid readings are taken at points on the surface of the test sample with three separate needles. The distance from the remaining edges of the measured points and the distance of each point from each other should not be less than 10 mm. Figure 7 shows the setup of the penetration test.



**Figure 7.** Penetration test machine

### **2.5.3. Softening point test (TS EN 1427)**

This method covers the determination of the softening point of bitumen and bituminous binders between 28 °C and 150 °C. The method is also referred to as the Ring & Ball Method. Two horizontally positioned disk-shaped bituminous binder samples, each with a ball on top, cast in brass rings are heated in a controlled manner in a test bath. The softening point is given as the average of the temperatures read from the thermometer when each ball embedded in the disc-shaped bitumen samples falls  $(25.0 \pm 0.4)$  mm into the test bench.

To obtain the initial temperature, the bath is placed in ice water or a thermostatic device and the water is cooled to  $(5 \pm 1)$  °C. This temperature should be maintained for 15 minutes but should not exceed 20 minutes. Using a pair of pliers, one ball is inserted into each ball center guide. The bath liquid is stirred to distribute the temperature evenly and the temperature is increased by 5°C per minute. The thermometer reading is recorded as soon as the bituminous binder on both balls touches the baseplate when using a non-automatic tester, or cuts the light beam when using a semi-automatic or automatic tester.

For modified bitumen, the test is repeated if the measured temperature difference of the two samples exceeds 2 °C either if the ball breaks the thin layer without touching the bottom plate or if partial separation between the ball and bitumen is observed. The apparatus for the softening point experiment is given in Figure 8.

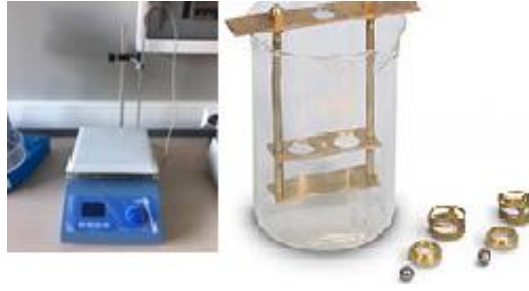


**Figure 8.** Ring and ball test apparatus

#### **2.5.4. Rolling thin film oven test (TS EN 12607-1)**

This method is used to measure the combined effects of air and temperature on a thin film of bitumen or bituminous binder. The method is not applicable to some modified binders or binders with very high viscosity values. The method is also referred to as rolling thin film oven test (RTFOT). A moving film of bituminous binder is heated in an oven at a specified temperature. The effects of air and temperature are determined by changes in mass or changes in properties of the bituminous binder such as penetration, softening point or dynamic viscosity.

Make sure that the oven is in equilibrium. Preheat the oven to the experimental temperature. Weigh at least two empty glass containers separately and pour  $(35 \pm 0.5)$  grams of sample into each container. To determine the percentage change in mass, two containers (designated A and B) containing bituminous binder (empty weights  $M_0$  and  $M'_0$ ) are taken and cooled to room temperature in a desiccator for 1 hour.

The empty containers are filled into the cavities in the carrier system and the lid is closed. The oven is rotated at a speed of  $(15.0 \pm 0.2)$  r/min. The specimens are exposed to air flow at  $(4.0 \pm 0.2)$  l/min. The specimens are kept in the oven and air is blown for  $(75 \pm 1)$  minutes and until the temperature is  $1^\circ\text{C}$  below the test temperature. If the experimental temperature of  $(163 \pm 1)^\circ\text{C}$  is not reached in the first 15 minutes, the experiment is terminated. At the end of the experiment, the containers are removed from the oven. The two containers (A and B) are allowed to cool down to room temperature in a desiccator for 1 hour. The relative masses,  $M_2$  and  $M'_2$ , are found to a precision of 1 mg. For the other containers, the binders are poured into the same collection vessel before it cools and hardens and before the containers are heated. The container is shaken to ensure homogeneity and no air bubbles are formed. Within 72 hours,  $P_2$ , penetration at  $25^\circ\text{C}$  (TS EN 1426);  $T_2$ , Softening Point (TS EN 1427) and  $H_2$ , viscosity at  $60^\circ\text{C}$  (TS EN 12596) of the hardened binder are measured. The RTFOT device is shown in Figure 9.



**Figure 9.** RTFOT Device

#### **2.5.5 Ductility test (ASTM D113)**

This method covers the procedure for measuring the tensile properties and determining the ductility of a bituminous material. Unless otherwise specified, the test is performed at a temperature of  $(25 \pm 0.5)^\circ\text{C}$  and a speed of  $5\text{ cm/min}$  ( $\pm 5.0\%$ ).

The mold is mounted on a brass plate. The surface of the plate and the surfaces a and a' of the mold are covered with a mold release agent. The plate on which the mold is placed must be flat and stable. The sample is heated until it is sufficiently liquid. After complete mixing, the sample is poured into the mold. While filling the mold, care should be taken to ensure that the mold parts do not move so that the sample does not deteriorate. The mold is filled with a little more material than the full level. The filled mold is kept at room temperature for  $35 \pm 5$  minutes. Then it is placed in a water bath at the experimental temperature and kept for  $35 \pm 5$  minutes. The sample is removed from the water bath and the excess material is shaved off with a spatula. The shaved specimen and mold are placed in the water bath for  $90 \pm 5$  minutes. The specimen and the plate are separated with a shearing motion, avoiding to bend of the specimen. The side parts (a and a') are removed without damaging the specimen. The rings at the end of the clamps are attached to the pins or hooks on the ductility device. The two clamps are pulled at the specified constant speed until the specimen breaks or reaches its length limits. When breakage occurs or the final length is reached, the length obtained is measured in centimeters. Figure 10 shows the ductility test device.



Figure 10. Ductility Test Device

#### 2.5.6. Flash point determination test with Cleveland open cup method (TS EN ISO 2592)

This method covers the determination of flash and fire points of bitumen and bituminous binders using the Cleveland Open Cup. The open cup method can be used for bituminous materials with flash points between  $79^{\circ}\text{C}$  -  $400^{\circ}\text{C}$ .

It is the value of the lowest temperature at which a flame source ignites the vapor of the test sample under the specified test conditions, corrected for 101.3 kPa pressure. Knowing the Flash Point of a material is very important to prevent any ignition and fire hazard that may occur when that material is heated during application. The test vessel is filled to a certain level with the test specimen. The temperature of the test specimen is increased at a constant rate, first rapidly and then slowly. At certain temperatures, a small flame is passed over the test vessel. Under the specified test conditions, the lowest temperature at which the vapor of the test sample ignites is taken as the flash temperature. The vapor is allowed to burn for at least 5 seconds to determine the fire temperature. The values obtained are calculated using an equation. Flash And Fire Point Test apparatus is shown in Figure 11.



Figure 11. Cleveland Open Cup Flash and Fire Point Test Apparatus

## **2.6. Performance determination test on bituminous mixtures**

### **2.6.1. Marshall stability and flow test (AASHTO T 245)**

In this study, the use of waste PVC in bitumen modification at 0.5%, 1% and 1.5% by weight and its effects on pavement performance were investigated. Mixture performance was investigated according to American Association of State Highway and Transportation Officials (AASHTO) T245 standard, also known as Marshall Stability and Flow Test. The aggregate mixture is obtained by the method given in AASHTO. The weight of aggregates contained in the samples was determined as 1150 gr. The aggregates were kept in an oven at 160°C for 24 hours before mixing and the bitumen was kept for 3 hours to minimize loss on heating. Control sample sets were prepared with B50-70 bitumen with 0.5% intermediate values between 3% and 7%, three for each ratio, and the optimum bitumen percentage was determined. After determining of the optimum bitumen content, a sufficient amount of bitumen was modified with 0.5%, 1% and 1.5% PVC and viscosity values were determined in accordance with AASHTO T316 standard to obtain the appropriate mixing temperature. The bituminous mixture samples were prepared according to the mixing procedure and compacted to a void percentage in the range of 3%-5% with Marshall Compactor. After resting for 24 hours, the specimens were tested in Marshall Testing Machine and the stability and flow values of the specimens were obtained.

The aggregate sample weighing 1150 g with predetermined gradation is kept for one day (24 hours) and the bitumen is kept for 2-3 hours in an oven set at 160°C. Materials such as molds and aggregate containers to be used during the experiment should be kept in an oven at 160°C to avoid any heat loss during the experiment. The aggregate mixture is removed from the oven. It is placed in the mixer container and a well is made in the center to add the bitumen. A certain amount of bitumen (with respect to optimum bitumen content-OBC) weighed on a scale is poured onto the aggregate. Aggregate and bitumen are mixed in the mixer for 1.5-2 minutes. Meanwhile, the mixer container is placed in the mixer heating device to prevent the temperature of the mixture from dropping. When the mixing of the sample is about to end, the molds are removed from the oven and lubricated to prevent sticking. Place a sheet of greaseproof or impermeable paper cut to the appropriate size on the bottom of the mold. Take the mixture from the mixer and place it into the mold by pre-compressing. Measure the temperature of the mixture at this stage and place greaseproof or impermeable paper on it again. The temperature of the mixture should not fall below 140°C. The sample mold is placed in the Marshall compactor and 75 strokes are applied on each side. The molds are allowed to cool for about 3 hours. The specimens are removed from the cooling mold with the help of a jack, named and marked. The samples are kept at room temperature for one day. Height measurements are taken from the specimens with the help of calipers. For this, a measurement should be taken from 3 different parts of the sample at approximately 120°. The weights of the samples in air and water are measured. The samples are kept in a water bath at 60°C for 30-40 minutes. The samples removed from the water bath are placed in the Marshall device. The device is started and the jaws of the device apply a load to the sample at a speed of 51 mm/min. As a result, the flow and strength values of the specimen are obtained. The results are recorded in terms of height, weight in air and water, Marshall stability and flow values

### **Determination of aggregate mixing ratios and gradation**

The aggregate to be used in the construction of bituminous hot mix layers should consist of a mixture of at least three different grain groups (coarse, medium, fine). In the crusher, the crushing of aggregate groups should be done in such a way as to ensure the gradation of the layer in which the aggregate will be used. In order to determine whether the appropriate mixture gradation will be obtained with the aggregates produced, it is necessary to calculate the aggregate mixture ratios from the day production starts. The proportions required to mix three or more aggregate groups to give the desired specification gradation can be determined by different methods.

### **Determination of optimum bitumen content (OBC)**

Optimum bitumen content (OBC) is used to determine the optimum amount of bitumen to be used in a bituminous mixture in order to mix bituminous material with graded aggregates. OBC is directly dependent

on the type and capillary structure of aggregate. When determining the OBC, aggregates with a certain gradation are mixed with bituminous material at a rate of 0.5% incrementation between 3.0% and 7.0%. Three samples of each percentage of bituminous material should be prepared.

Samples of all contents should be at the appropriate mixing and compaction temperature. The mixed samples are homogeneously placed in the Marshall mold and compressed by 75 strokes on both sides. The compacted bituminous mixtures are removed from the molds after reaching ambient temperature. With the results obtained according to the Marshall Table, "Bitumen ratio-Practical specific gravity", "Bitumen ratio-Marshall strength", "Bitumen ratio-air void ratio" and "Bitumen ratio - Voids filled with asphalt ratio" graphs are drawn. According to these graphs; the bitumen ratio corresponding to the maximum practical specific gravity value, the maximum Marshall strength value, 4% air void ratio value and 70% voids filled with asphalt ratio are determined. The optimum bitumen ratio for the mixture is found by averaging these four bitumen ratios. In order to determine whether the optimum bitumen content found is within the specification limits, the "Bitumen ratio - Flow" graph is drawn. If the optimum bitumen ratio meets the flow limits, it is accepted.

## **2.7. Modified Lottman test (AASHTO T 283)**

Flexible pavement practitioners have been aware since the 1920s that the adhesion between asphalt and aggregate weakens (stripping occurs) when water is present. In addition, the deterioration of cohesion in the asphalt binder with the presence of water has also been observed since that time. Therefore, attempts have been made to develop a reliable laboratory test method that can simulate the sensitivity of asphalt pavement to moisture in the field [32]. Lottman (1978) introduced to the industry a well-established laboratory test method for predicting moisture-induced damage of asphalt concrete [33]. This procedure developed by Lottman was later modified and standardized by AASHTO as Test Procedure T283 [32].

In this study, Modified Lottman (AASHTO T283) tests have been applied to determine the moisture susceptibility of bituminous mixtures. This test (AASHTO T283, TS EN 12697-12), which is applied to determine the resistance of mixtures to water-induced damage, includes the measurement of the indirect tensile strength (ITS) in the diameter plane due to accelerated water effects of compacted bituminous mixtures prepared in the laboratory. The bituminous mixtures prepared using PVC modified and base bitumen with the addition of hydrated lime were placed in an aluminum container and cooled at room temperature for 2 hours (Figure 12).



**Figure 12.** Loose Mixture During The Cooling Process for 2Hours

Then the mixtures were kept in an oven at 60°C for 16 hours for curing. After curing, the mixtures were kept in an oven at 135°C for 2 hours, then kept in an oven at 165°C for another 20 minutes and compressed using a Marshall Compactor at an air void of  $7 \pm 1.0\%$ . Three specimens are designated as dry (i.e. unconditioned) and tested without moisture exposure. In addition to the unconditioned specimens, three additional specimens are selected and subjected to conditioning (moisture conditioning). These samples are placed in a cylindrical metal pycnometer and then water absorption was applied to the sample by adding pure water at 25°C. The

plastic bag containing the sample was placed in a freezer cabinet at -18 °C for 16 hours and then cured in a 60 °C water bath for 24 hours. After this treatment, the samples were placed in a water bath set at 25 °C for 2 hours. The ITS values in the diameter plane of the dry specimens and the conditioned specimens as above were determined. The water-induced damage is determined by the ratio of ITS values of dry to conditioned specimens. This ratio should be minimum 80 % according to the General Directorate of Highways Technical Specifications. The flowchart of this experiment is given in Figure 13.

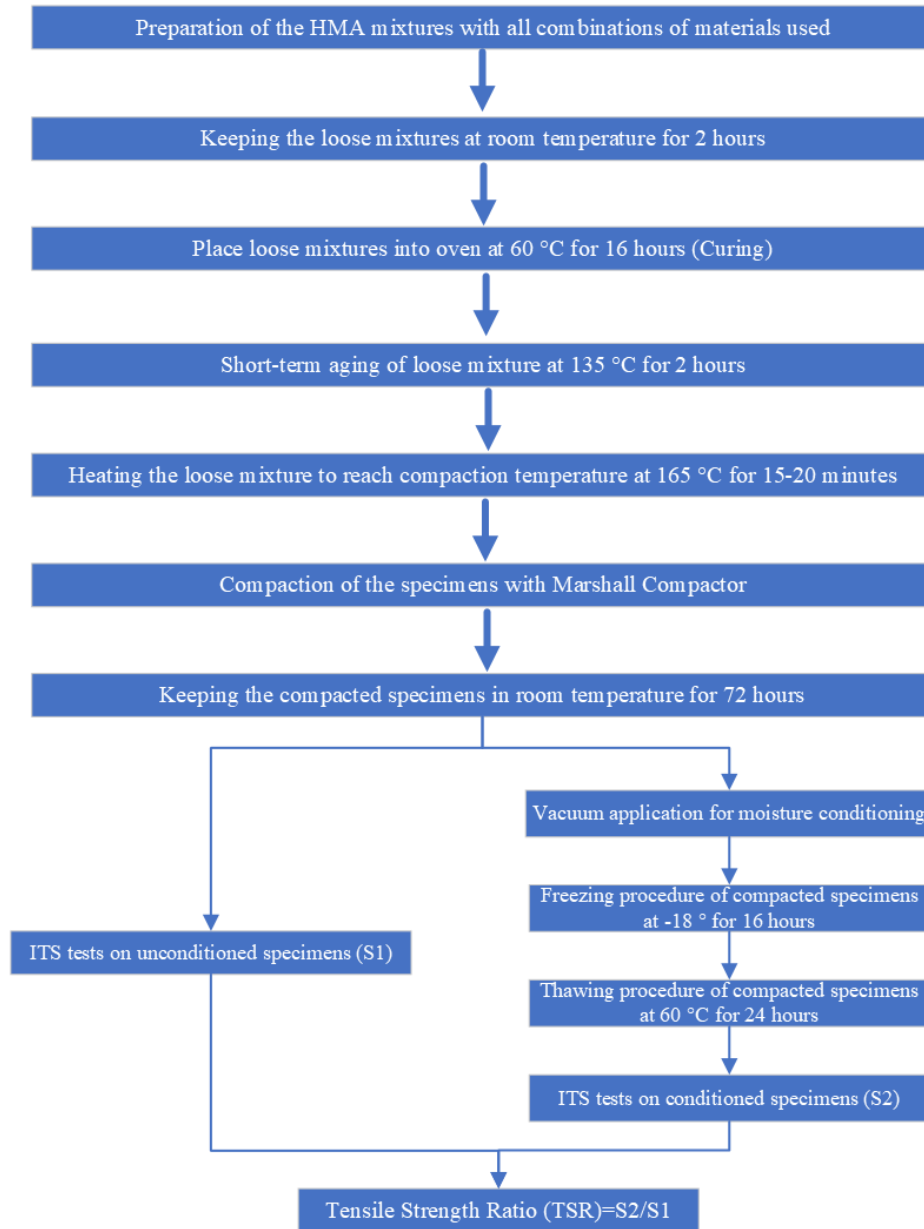


Figure 13. Modified Lottman (AASHTO T283, TS EN 12697-12) Test Flow Chart

### 3. Results and Discussion

With environmental factors, oxidation occurs in bituminous mixtures over time. This oxidation causes aging of bituminous materials, leading to a stiffer and more brittle structure of flexible pavements. Polar molecules in construction materials used in road building react with environmental factors to break down and cause deformation in flexible pavements. Adding hydrated lime to bituminous materials reduces the oxidation and aging rate of the flexible pavement. Since a chemical reaction occurs between the calcium hydroxide and the

highly polar molecules in the bituminous material, the pavement is not affected by environmental conditions. As a result, the bituminous material remains flexible and protected from crack occurrence for many years.

Stripping is caused by the presence of moisture in the bond between the bituminous material and the aggregate. In regions where the moisture in the air or ambient water is high, water entering between the bituminous material and the aggregate causes the binder to separate from the aggregate. Certain types of material, such as aggregates obtained from igneous rocks, are particularly susceptible to stripping. Severe environmental conditions such as heat, heavy rains, freeze/thaw cycles and traffic loads are significant contributors to peeling. Hydrated lime is one of the most effective and economical anti-peel admixtures available.

Hydrated lime reacts with highly polar molecules that can form water-soluble soaps that cause stripping in bituminous mixtures. As a result, they form hydrophobic insoluble salts. Furthermore, the homogeneous distribution of hydrated lime throughout the mix makes the mixture stiffer and more durable, reducing the likelihood of mechanical breakage of the bond between the bituminous material and the aggregate.

In many studies, it has been observed that the addition of 1-1.5% hydrated lime to bituminous mixtures increases the crushing strength by 77%. At low temperatures, the solidification effect of hydrated lime in bituminous mixtures is not significantly higher than that of other additives. The reason for this is that hydrated lime is more effective due to the strong interactions of the components that make up the bituminous mixtures [34].

Within the scope of the study, the reusability of waste Polyvinyl Chloride (PVC) materials as asphalt binder was investigated and it was aimed to improve the mechanical properties of the road pavement material as well as positive results in terms of environmental and economic aspects. In other words, it was aimed to reduce bitumen consumption and recycle waste PVC by mixing PVC waste into bitumen used as a binder in flexible pavements. In this context, the properties of modified bitumen with waste PVC powder were investigated and Marshall specimens were prepared with PVC-modified bitumen. Prepared specimens were subjected to Marshall Stability and Flow tests and stability flow and values were determined.

The performance of PVC addition to bituminous material in heavy rainfall areas was also evaluated. For this purpose, hydrated lime was added directly to aggregates as specified in the Turkish General Directorate of Highways, Highways Technical Specification Type-1 gradation for wearing course at the rate recommended in previous studies and its resistance to water-induced deterioration was determined. At this point, the use of hydrated lime was evaluated on a single-ingredient basis, as the focus was primarily on the performance of PVC in bituminous mixtures.

### **3.1. Test results of bituminous material prepared with PVC wastes with different contents**

Bitumen modification has been made by mixing 0.5%, 1% and 1.5% of waste PVC powder into bitumen. Firstly, the viscosity of pure and modified bitumen was measured with a rotational viscometer to determine the mixing and compaction temperatures. A set of specimens were prepared using asphalt cement at 4.0%, 4.5%, 5.0% and 5.5% then Marshall stability and flow tests were performed on these specimens to determine the optimum bitumen percentage. Using the optimum bitumen percentage of 4.22%, Marshall stability and flow tests were performed on the specimens prepared by using waste PVC powder at varying rates of 0.5%, 1% and 1.5% by weight of bitumen.

The Rotational Viscometer (RV) test is applied to determine the flow properties of bituminous materials at high temperatures. Viscosity values are obtained by the resistance to rotation of a shaft rotating at 20 rpm in the binder (Figure 14).



**Figure 14.** Brookfield Viscosity Test Device

For the experiment, a sample of about 30 grams of binder is taken and heated in an oven with a temperature of less than 150°C. About 11 grams is filled into the sample chamber and placed in a temperature-controlled container kept at a constant temperature. The sample is kept at a constant temperature for 15 minutes and then the experiment is performed. Viscosity readings are taken for temperatures of 135°C and 165°C. In this study, the viscosity of unmodified and modified bitumen was measured using a rotational viscometer. Measured viscosity results are given in Table 4 and the graphs for the determination of mixing and compression temperatures are shown in Figure 15.

**Table 4.** Viscosity values

PVC additive (%)	Viscosity value (cP)	
	135 °C	165 °C
0.0	562.5	87.5
0.5	572.5	150
1.0	550	87.5
1.5	612.5	162.5

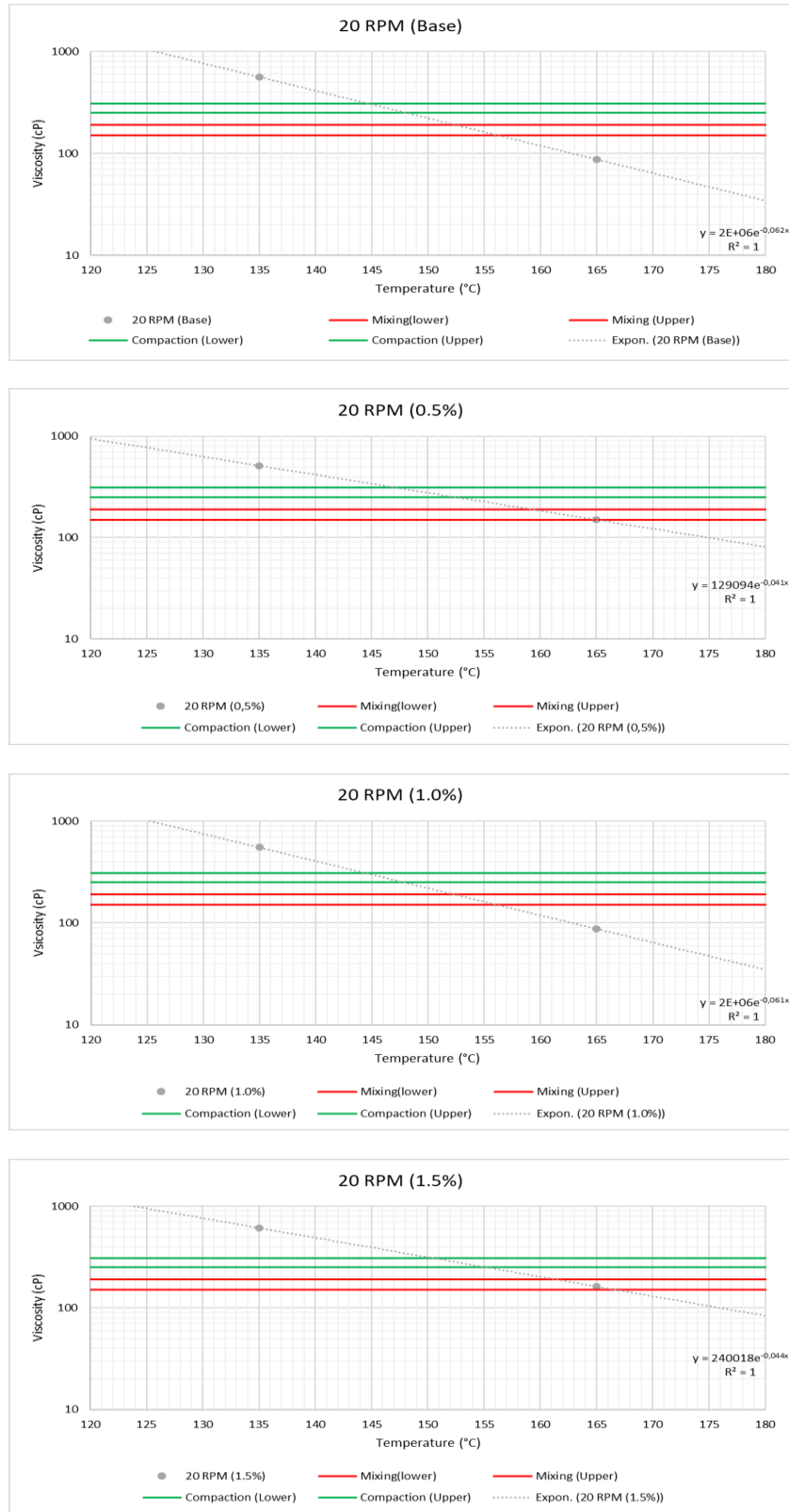


**Figure 15.** Mixing and compaction temperatures

Mixing and compaction temperature ranges determined according to viscosity values are given in Table 5.

**Table 5.** Mixing and compaction temperatures

PVC additive (%)	Mixing temp. (°C)	Compaction temp. (°C)
0	152-156	144-148
0.5	159-165	147-153
1.0	152-156	144-148
1.5	161-167	150-156

### 3.2. Results of the Marshall stability and flow test of bituminous mixtures containing hydrated lime, prepared with different contents of PVC waste

Marshall stability and flow tests were performed on these samples and the optimum bitumen percentage was found to be 4.22%. According to the optimum bitumen percentage, 48.5 grams of bitumen was used for each Marshall sample. The bitumen to be used for the samples was then modified. For each percentage (for 0.5%, 1% and 1.5%), the relevant amount was added to the bitumen and mixed at 1500 rpm at 150°C for 1 hour. The specimens were placed in Marshall molds and compacted by applying 75 strokes on both surfaces of the specimens as specified in the Directorate of Highways Technical Specifications. Marshall samples were then prepared according to the relevant procedure. The prepared samples were allowed to cool and the physical properties of the samples were measured after 24 hours.

The specimens were cured in a water bath at 60°C for 30-40 minutes before conducting the Marshall strength and flow test. Following this curing period, the specimens were placed in Marshall test apparatus. At the end of the test, the stability, ITS and TSR values given in Figure 16 and Figure 17 respectively were obtained. Marshall mix design was performed on bituminous mixtures containing hydrated lime. The reason for this is to evaluate the effect of moisture sensitivity on the mixture in bituminous materials prepared with different contents of waste PVC additives.

According to the Turkish General Directorate of Highways, Highways Technical Specification, the minimum stability value (TS EN 12697-34) for wearing course Type-1 is 900kgf and the flow (TS EN 12697-34) is between 2-4 mm.

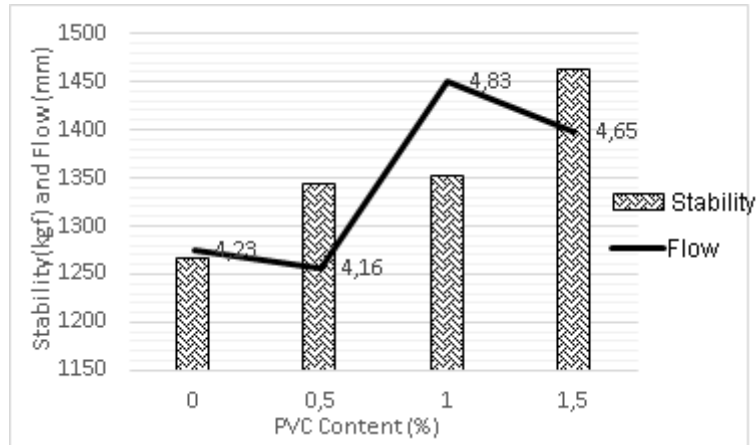


**Figure 16.** Marshall Stability and Flow test results

When Figure 16 is evaluated in terms of stability values, all of the bituminous mixture samples containing hydrated lime and prepared with different contents of PVC waste are well above the minimum value. It is seen that as the content of waste PVC additive to the bituminous mixture samples increases, the stability values of the specimens also increase.

During the production phase of the bituminous mixture, short-term aging occurs in asphalt plants due to bitumen oxidation and loss of the evaporated component. Long-term aging of bituminous materials is caused by the evaporation of the bituminous material in the asphalt mixture during mixing and paving [35].

The main factors in the aging of bituminous materials are parameters such as oxidation, evaporation, aging within the structure (thixotropy), which depend on environmental conditions such as time, temperature and oxygen [36]. It is thought that the bituminous material used in the study may have aged to some extent due to the distance of the source from which the material was brought and the fact that it was repeatedly heated and exposed to excessive temperatures during use. Indeed, when Figure 16 is examined, the flow values obtained from the bituminous mixtures are above the 2-4 mm values specified in the Technical Specifications of Highways. However, the evaluations made in the light of the obtained results were made by taking this situation into consideration and considered proportionally in order to eliminate the error situation.

In this study, Marshall mix designs for the experiments on bituminous mixtures were made with samples containing 1.5% hydrated lime. The results shown in Figure 16 were obtained by mixing dry hydrated lime with wet aggregate gradation and adding different proportions of PVC containing bituminous materials to the aggregate mixtures. At this stage, the proportions of PVC added to the bituminous material were varied from 0% to 1.5%, while the hydrated lime containing 1.5% mixed with the aggregate was kept constant.

When the figure mentioned above is examined, it is understood that the flow values increase up to the samples prepared with 1.5% PVC waste and decrease from this content onwards. The reason for this decrease in the samples containing 1.5% PVC waste is thought to be that the additive used during mixing could not be distributed homogeneously in the bituminous material.

The classification of the samples used in the experimental studies is given in Table 6.

**Table 6.** Contents of the samples in accordance with the specimen nomenclature

Name of Specimen	Type of Aggregate	Type of Additive	Additive Content (%)
LP0HL0	Limestone	Unconditioned	0% for both
LP0HL1.5	Limestone	Hydrated lime	1.5% Hydrated lime
LP0.5HL0	Limestone	PVC	0.5% PVC
LP0.5HL1.5	Limestone	PVC and Hydrated lime	0.5% PVC, 1.5%hydrated lime
LP1HL0	Limestone	PVC	1.0% PVC
LP1HL1.5	Limestone	PVC and Hydrated lime	1.0% PVC, 1.5%hydrated lime
LP1.5HL0	Limestone	PVC	1.5% PVC
LP1.5HL1.5	Limestone	PVC and Hydrated lime	1.5% PVC, 1.5%hydrated lime

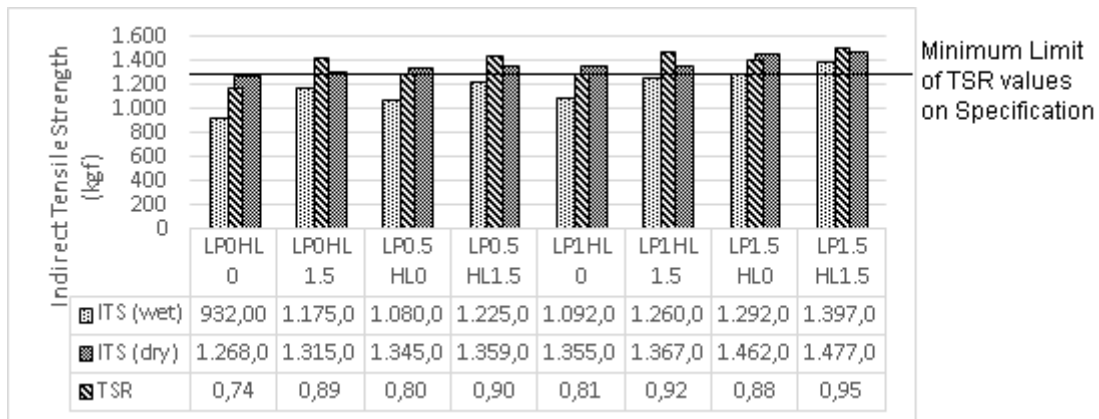


**Figure 17.** Indirect tensile strength (ITS) and tensile strength ratio (TSR) results

PVC waste is a synthetic material made from petroleum and salt that is used industrially to make doors and windows. The PVC used in the study is the material that accumulates as waste around the looms during production.

According to Figure 17, when the hydrated lime additive ratios were kept constant, a slight increase in TSR values was observed with increasing PVC waste content. It can be concluded that the addition of PVC waste to the bituminous material slightly increases the adhesion between bitumen and aggregate. The main increase was observed when 1.5% PVC waste was added to the specimens.

On the other hand, Figure 17 shows that the addition of hydrated lime to the bituminous mixture samples has higher TSR values than the samples prepared with PVC wastes. It can be concluded that the addition of hydrated lime to bituminous mixtures is significantly more effective than the addition of PVC waste in reducing the sensitivity of the mixtures to moisture. The reason why PVC wastes did not have as much effect on the stripping strength as hydrated lime is that PVC did not show sufficient binding properties at the current mixing temperature [37].

In the corresponding figure, the TSR values of bituminous mixtures without any additives were below the minimum value specified in the Highways Technical Specifications. The reason for this may be that the bituminous material used in the study may have aged due to uncontrollable environmental factors during the experimental studies. However, ignoring this possible factor, the use of both PVC waste and hydrated lime admixture in bituminous mixtures reduced the moisture sensitivity of the test specimens.

#### **4. Conclusion**

In the light of the data obtained within the scope of the study, the following conclusions were reached:

The stability of the mixture increased with the increase in the proportion of waste PVC added to the bituminous material. This can be attributed to the homogeneous distribution of polyvinyl chloride (PVC) in the bitumen without melting. In particular, the addition of 1.5% PVC to the bitumen significantly improved the stability values. Additionally, it is considered that the direct addition of PVC waste to bituminous materials with higher contents would have positive results in terms of increasing the strength of bituminous mixtures.

According to the Marshall Stability and Flow Test results, a significant increase in the flow rate was observed in bituminous mixtures with 1% additive content when PVC waste was added directly to the bituminous materials. On the other hand, the flow ratios of the samples prepared with higher additive content showed a tendency to decrease. The reason for this, especially for the flow values, can be attributed to the rigid nature of the PVC waste and its homogeneous distribution within the bituminous material without melting, thereby reducing the lateral flexibility. Although the flow values measured for all ingredients exceeded the upper limit of 4 mm, they are not far beyond the limit values and are at acceptable levels.

When the bituminous mixture samples prepared with all PVC contents were evaluated among themselves, the most significant increase in flow ratio was observed in the samples prepared with 1% PVC content, which showed the best resistance to lateral deflection without deformation. Accordingly, it is thought that the best resistance to lateral deflection without permanent deformation may also contribute positively to the workability of the flexible pavement during paving in the construction area.

Again, according to the results of Marshall stability and flow test, increasing the waste PVC content added to the bituminous materials increased the stability values, while decreasing the flow rates after 1% PVC content. This indicates that bituminous mixtures prepared with higher PVC contents will have limited lateral deflection on roads with high levels of heavy tonnage vehicle traffic, and thus their durability values will be better. According to this, the service life of the flexible pavement will be extended, and the service life will increase.

The effective recycling of PVC waste by using it as a binder modifier in asphalt pavements makes a very positive environmental contribution. In addition, by reducing the amount of bitumen used in asphalt pavements, almost all of which is imported, by approximately 16%, waste PVC will be transformed into an economic value. Thus, while decreasing environmental pollution, it will provide an economic contribution by reducing the amount of used bitumen that is imported.

When the bituminous mixture samples prepared with all PVC additive contents were analyzed, it was found that the addition of hydrated lime significantly reduced the sensitivity to moisture.

As the PVC content increased, it was seen more clearly that hydrated lime reduced the sensitivity to moisture, thus it was determined that the use of hydrated lime improved the water-induced damage of bituminous mixture samples prepared with waste PVC.

The study was conducted to evaluate the moisture sensitivity of adding PVC waste at different percentages to bituminous mixtures containing hydrated lime. The type of aggregate used in the experiments is limestone. Limestone is known to have a low silica content compared to other igneous rocks used in highway construction. The study can be extended to different igneous rocks with particularly high stability values and high moisture susceptibility. In addition, the interactions of different anti-stripping additives with PVC waste should also be evaluated.

## **5. Acknowledgement**

This study was supported by Eskişehir Technical University Scientific Research Projects Commission under grant no: 22ADP028.

## **6. Author Contribution Statement**

All authors contributed equally to this work

## **7. Ethics Committee Approval and Conflict of Interest**

The authors have no conflicts of interest to declare. All co-authors have seen and agree with the contents of the manuscript and there is no financial interest to report. We certify that the submission is original work and is not under review at any other publisher.

## **8. References**

- [1] R. L. Terrel and S. Al-Swailmi “Water sensitivity of asphalt–aggregate mixes: test selection”, Strategic Highway Research Program, SHRP report A-403, National Research Council, 1994.
- [2] H. J. Fromm, “Mechanism of asphalt stripping from aggregate surfaces”, AAPT, vol. 43, pp. 191–223, 1974.
- [3] K. D. Stuart, “Moisture damage in asphalt mixtures: a state of art report”, Research Development and Technology, Turner-Fairbank Highway Research Center, 1990.
- [4] İ. Ç. Görkem and M. Özkan, “Muğla Mermerinin Esnek Üstyapılı Yol Kaplamalarında Kullanımının Performansa Etkisinin Değerlendirilmesi, Suya Bağlı Bozulmalara Karşı Direncinin İncelenmesi”, Gümüşhane Üniversitesi Fen Bilim. Enst. Derg., vol. 2, pp. 385-394, Apr. 2020.
- [5] M. Kardeş and S. Terzi, “Evaluation of marble waste dust in the mixture of asphaltic concrete”, Constr. Build. Mater., vol. 21, no. 3, pp. 616–620, Mar. 2007.
- [6] P. K. Gautam, P. Kalla, A. S. Jethoo, R. Agrawal, and H. Singh, “Sustainable use of waste in flexible pavement: A review”, Constr. Build. Mater., vol. 180, pp. 239–253, Aug. 2018.
- [7] P. Ahmedzade and B. Sengoz, “Evaluation of steel slag coarse aggregate in hot mix asphalt concrete”, J. Hazard. Mater., vol. 165, no. 1–3, pp. 300–305, Jun. 2009.
- [8] F. Moreno-Navarro, M. Sol-Sánchez and M. C. Rubio-Gámez, “Structural analysis of polymer modified bituminous materials in the rehabilitation of light-medium traffic volume roads”, Constr. Build. Mater., vol. 156, pp. 621–631, Dec. 2017.
- [9] L. Brasileiro, F. Moreno-Navarro, R. Tauste-Martínez, J. Matos and M. Rubio-Gámez, “Reclaimed Polymers as Asphalt Binder Modifiers for More Sustainable Roads: A Review”, Sustainability, vol. 11, no. 3, p. 646, Jan. 2019.
- [10] Lu, X., Isacson, U., “Modification of road bitumens with thermoplastic polymers”, Polymer Testing, vol. 20, no. 1, pp. 77-86, September 2000.

- [11] M. A. Abdel-Goad, “Waste polyvinyl chloride-modified bitumen”, *J. Appl. Polym. Sci.*, vol. 101, no. 3, pp. 1501–1505, Aug. 2006.
- [12] A. Behl, G. Sharma, and G. Kumar, “A sustainable approach: Utilization of waste PVC in asphaltting of roads”, *Constr. Build. Mater.*, vol. 54, pp. 113–117, Mar. 2014.
- [13] S. Köfteci, P. Ahmedzade and B. Kultayev, “Performance evaluation of bitumen modified by various types of waste plastics”, *Constr. Build. Mater.*, vol. 73, pp. 592–602, 2014.
- [14] S. Köfteci, P. Ahmedzade and B. Kultayev, “Performance evaluation of bitumen modified by various types of waste plastics”, *Constr. Build. Mater.*, vol. 73, pp. 592–602, 2014.
- [15] A. Behl, G. Sharma, G. Kumar, “A sustainable approach: Utilization of waste PVC in asphaltting of roads”, *Constr. Build. Mater.*, vol. 54, pp. 113–117, March 2014.
- [16] M.N. Rahman, M. Ahmeduzzaman, M.A. Sobhan and T.U. Ahmed, “Performance evaluation of waste polyethylene and PVC on hot asphalt mixtures”, *Am. J. Civ. Eng. Archit.*, vol. 1, no. 5, pp. 97-102, 2013.
- [17] N. Salman and Z. Jaleel, “Effects of waste PVC addition on the properties of (40-50) grade asphalt”, *MATEC Web Conf.*, EDP Sciences, 1046, 2018.
- [18] E.N. Ezzat and A.H. Abed, “Enhancement rheological properties of asphalt binder modified with hybrid polymers according to superpave system”, *Mater. Today Proc.*, vol. 20, pp. 572-578, 2020.
- [19] Ç. Görkem and B. Sengoz, “Predicting stripping and moisture induced damage of asphalt concrete prepared with polymer modified bitumen and hydrated lime”, *Constr. Build. Mater.*, vol. 23, no. 6, pp. 2227–2236, Jun. 2009.
- [20] A. D. Nataadmadja, E. Prahara, O. Setyandito and R. W. Ananditha, “Evaluation of moisture susceptibility of hot mix asphalt”, *International Conference On Science And Applied Science (ICSAS) 2019*, Surakarta, Indonesia, p. 020106, 2019.
- [21] M. Ameri, S. Kouchaki and H. Roshani, “Laboratory evaluation of the effect of nano-organosilane anti-stripping additive on the moisture susceptibility of HMA mixtures under freeze–thaw cycles”, *Constr. Build. Mater.*, vol. 48, pp. 1009–1016, Nov. 2013.
- [22] A. Diab, D. Singh and J. C. Pais, “Moisture susceptibility of asphalt mixtures: A literature review”, *4th Conference of Transportation Research Group of India (CTRG)*, 2017.
- [23] D.-W. Park, W.-J. Seo, J. Kim and H. V. Vo, “Evaluation of moisture susceptibility of asphalt mixture using liquid anti-stripping agents”, *Constr. Build. Mater.*, vol. 144, pp. 399–405, Jul. 2017.
- [24] E. R. Hunter, *Evaluating moisture susceptibility of asphalt mixes*. University of Wyoming, 2001.
- [25] Y.-R. Kim, I. Pinto, and S.-W. Park, “Experimental evaluation of anti-stripping additives in bituminous mixtures through multiple scale laboratory test results”, *Constr. Build. Mater.*, vol. 29, pp. 386–393, Apr. 2012.
- [26] P. V. Peltonen, “Road Aggregate Choice Based on Silicate Quality and Bitumen Adhesion”, *Journal of Transportation Engineering*, vol. 118, no. 1, pp. 50-61, January 1992.
- [27] National Lime Association, “Lime the versatile chemical hydrated lime: a solution for high performance hot mix asphalt”, fact sheet, 2003.
- [28] T. W. Kennedy and N. J. Anagnos, *Lime treatment of asphalt mixtures*, Center for Transportation Research, The University of Texas at Austin, 1983
- [29] D. G. Tunnicliff and R. E. Root, “Introduction of lime into asphalt concrete mixtures”, *Interim guidelines*, The Federal Highway Administration, 1984.
- [30] P. E. Sebaaly, D. N. Little and J. A. Epps, “The benefits of hydrated lime in hot mix asphalt”, *National Lime Association*, 2006.
- [31] M. Nazirizad, A. Kavussi and A. Abdi, “Evaluation of the effects of anti-stripping agents on the performance of asphalt mixtures”, *Constr. Build. Mater.*, vol. 84, pp. 348–353, Jun 2015.
- [32] M. Solaimanian, J. Harvey, M. Tahmoressi and V. Tandon, “Test methods to predict moisture sensitivity of hot-mix asphalt pavements”, *Transportation research board national seminar*, San Diego, California, 77-110, 2003.
- [33] R. P. Lottman, “Predicting Moisture Induced Damage to Asphaltic Concrete”, *Transportation Research Board*, NCHRP Report 48-3, 1978.
- [34] KISAD, URL: [https://kirec.org/haber/sicak\\_asfalt\\_karisimlara\\_kirec\\_katilmasi-h69](https://kirec.org/haber/sicak_asfalt_karisimlara_kirec_katilmasi-h69), Visited on Feb. 27, 2024.

- [35] P. Ahmedzade, M. Yılmaz and M. Yılmaz, “Bitümlü bağlayıcıların yaşlandırılmasında kullanılan deney yöntemlerinin karşılaştırılması”, Erciyes Üni.Fen Bilimleri Enst. Derg., vol. 23, no. 1, pp. 112-126, Feb. 2007.
- [36] R. N. Traxler, “Durability of asphalt cements, proceedings, association of asphalt paving technologists”, vol. 32, pp 44-58, 1963.
- [37] K. B. Akalın, and M. Karacasu. "Çevresel atıklarla modifiye edilmiş sathi kaplamaların performansının agrega-bitüm ilişkisi bağlamında değerlendirilmesi", Fırat Üni. Müh. Bil. Derg., vol. 32, no. 1, pp. 127-36, March 2020.



## Hesaplamalı Akışkanlar Dinamiği Yöntemi Kullanarak Üç Kanatlı Helisel Savonius Rüzgâr Türbinlerinin Aerodinamik Performansına Faz Açısı Etkisinin Araştırılması

Mernuş GÜL<sup>1</sup> , Muhammed Safa KAMER<sup>2</sup> , Erdem ALIÇ<sup>3\*</sup> 

<sup>1</sup>Türk Havacılık ve Uzay Sanayii A.Ş., Ankara, Türkiye.

<sup>2</sup>Makine Mühendisliği Bölümü, Mühendislik Mimarlık Fakültesi, Kahramanmaraş Sütçü İmam Üniversitesi, Kahramanmaraş, Türkiye.

<sup>3</sup>Andırın Meslek Yüksekokulu, Kahramanmaraş Sütçü İmam Üniversitesi, Kahramanmaraş, Türkiye.  
<sup>1</sup>mernusdertlii@gmail.com, <sup>2</sup>msafakamer@ksu.edu.tr, <sup>3</sup>ealic@ksu.edu.tr

Geliş Tarihi: 03.01.2024  
Kabul Tarihi: 12.02.2024

Düzeltilme Tarihi: 09.02.2024

doi: 10.62520/fujece.1414345  
Araştırma Makalesi

Alıntı: M. Gül, M. S. Kamer ve E. Alıç, "Hesaplamalı akışkanlar dinamiği yöntemi kullanarak üç kanatlı helisel savonius rüzgâr türbinlerinin aerodinamik performansına faz açısı etkisinin araştırılması", *Firat Univ. Jour. of Exper. and Comp. Eng.*, vol. 3, no 1, pp. 52-64, Şubat 2024.

### Öz

Bu çalışmada dikey eksenli rüzgâr türbinlerinden üç kanatlı çift kademeli helisel Savonius rüzgâr türbinlerinin (HSRT) kademeler arasındaki yarı dairesel kanatların birbirlerine olan faz açısının aerodinamik performansına olan etkisi hesaplamalı akışkanlar dinamiği (HAD) yöntemiyle incelenmiştir. Savonius rüzgâr türbini sisteminde aerodinamik performans en ciddi katkıyı sürüklenme kuvveti etkisi sağlar. Sürüklenme kuvvetine etki edebilecek performans iyileştirmeleri önemli avantajlar sağlayabilir. Bu amaç için merkezden kaçıklığı  $L/H=1/2$  olan ve kademeler arasındaki yarı dairesel kanatların faz açıları  $\Theta=0^\circ$ ,  $45^\circ$  ve  $90^\circ$  olan üç kanatlı çift kademeli helisel Savonius rotorları tasarlanmıştır. Tasarımlar için Solidworks R2018, analizler için ANSYS-Fluent 18.1 programları kullanılmıştır.  $L/H=1/2$  ve  $\Theta=90^\circ$  olan türbin 3B yazıcıda üretilmiş ve deneysel olarak test edilmiştir. Deneysel T-490 hava tüneline gerçekleştirilmiştir. Elde edilen sonuçlar sayısal analizlere referans olarak kullanılmış ve en ideal türbin modeli belirlenmeye çalışılmıştır. Sayısal analizde 3,83-20,35 m/s arasında değişen 10 farklı hava hızı kullanılmıştır. Sonuç olarak HSRT 1/2'lerde; faz açısının  $0^\circ$ 'den,  $45^\circ$ 'ye değiştirilmesi ile sürüklenme kuvvetinde %11,64 oranında artış görülmüştür. HSRT 1/2'lerde; faz açısının  $0^\circ$ 'den,  $45^\circ$ 'ye değiştirilmesi ile sürüklenme katsayısında %10,77 oranında düşüş olduğu görülmüştür. Sürüklenme kuvvetinde meydana gelen iyileşme ile HSRT veriminde gelişme olacağı değerlendirilmiştir.

**Anahtar kelimeler:** Aerodinamik özellikler, Faz açısı, Rüzgâr türbini, Hesaplamalı akışkanlar dinamiği, Sürüklenme kuvveti

\*Yazışılan Yazar

İntihal Kontrol: Evet – Turnitin

Şikayet: [fujece@firat.edu.tr](mailto:fujece@firat.edu.tr)

Telif Hakkı ve Lisans: Dergide yayın yapan yazarlar, CC BY-NC 4.0 kapsamında lisanslanan çalışmalarının telif hakkını saklı tutar



## Investigation of The Effect of Phase Angle on The Aerodynamic Performance of Three-Bladed Helical Savonius Wind Turbines Using Computational Fluid Dynamics Method

Mernuş GÜL<sup>1</sup> , Muhammed Safa KAMER<sup>2</sup> , Erdem ALIÇ<sup>3\*</sup> 

<sup>1</sup>Turkish Aerospace Industries, Ankara, Turkey.

<sup>2</sup>Department of Mechanical Engineering, Faculty of Engineering and Architecture, Kahramanmaraş Sutcu Imam University, Kahramanmaraş, Turkey.

<sup>3</sup>Andırın Vocational High School Department, Kahramanmaraş Sutcu Imam University, Kahramanmaraş, Turkey.

<sup>1</sup> [mernusdertlii@gmail.com](mailto:mernusdertlii@gmail.com), <sup>2</sup> [msafakamer@ksu.edu.tr](mailto:msafakamer@ksu.edu.tr), <sup>3</sup> [alic@ksu.edu.tr](mailto:alic@ksu.edu.tr)

Received: 03.01.2024

Accepted: 12.02.2024

Revision: 09.02.2024

doi: 10.62520/fujece.1414345

Research Article

Citation: M. Gül, M. S. Kamer and E. Aliç, "Investigation of the effect of phase angle on the aerodynamic performance of three-bladed helical savonius wind turbines using computational fluid dynamics method", *Firat Univ. Jour. of Exper. and Comp. Eng.*, vol. 3, no 1, pp. 53-64, February 2024.

### Abstract

In this study, the effect of the phase angle of the semicircular blades between the stages on the aerodynamic performance of the three-blade, double-stage helical Savonius wind turbines (HSWT), which are vertical axis wind turbines, was examined by the computational fluid dynamics (CFD) method. In the Savonius wind turbine system, the drag force effect provides the most significant contribution to aerodynamic performance. Performance improvements that can affect drag force can provide significant advantages. For this purpose, three-bladed double-stage helical Savonius rotors with eccentricity  $L/H=1/2$  and phase angles of the semicircular blades between the stages  $\Theta=0^\circ, 45^\circ$  and  $90^\circ$  were designed. Solidworks R2018 is used for designs and ANSYS-Fluent 18.1 programs are used for analysis. The turbine with  $L/H=1/2$  and  $\Theta=90^\circ$  was produced on a 3D printer and tested experimentally. Experiments were carried out in the T-490 air tunnel. The results obtained were used as a reference for numerical analysis and the ideal turbine model was tried to be determined. 10 different air velocities ranging between 3.83-20.35 m/s were used in the numerical analysis. As a result, an 11.64% increase in the drag force was observed by changing the phase angle from  $0^\circ$  to  $45^\circ$  in HSWT 1/2s. By changing the phase angle from  $0^\circ$  to  $45^\circ$  in HSWT 1/2s, a 10.77% rise in the drag coefficient was observed. It has been evaluated that the HSWT efficiency improved with the increment in drag force.

**Keywords:** Aerodynamic properties, Computational fluids Dynamics, Drag force, Numerical analysis, Phase angle, Wind turbine

\*Corresponding author

## 1. Introduction

Nowadays, interest in sustainable and renewable energy sources has increased with the awareness of the decrease and limitation of underground resources that cause global warming and environmental pollution [1]. Savonius wind turbines are machines that use the kinetic energy of the wind to produce electricity and obtain mechanical power. Horizontal-axis wind turbines, which have a wide usage rate in the wind turbine group, are becoming increasingly common. There are many types of wind turbines. In the classification made according to rotor axes, they are classified as horizontal axis wind turbines and vertical axis wind turbines [2].

Vertical axis SWTs were first invented by Sigurd Savonius in 1924 and were patented in 1929 [3]. It is very easy to construct due to its simple structure. SWTs consist of two half-cylindrical blades placed between two horizontal disks and their centers shifted symmetrically to each other. Winds coming at a certain velocity create a positive moment on the inside of the cylinder and a negative moment on the outside of the cylinder. The magnitudes of these moments differ from each other. Since the moment of the inner part is greater than the moment of the outer part, rotational movement is achieved [4]. Reupke and Probert [5], to increase the operating efficiency of the SWT, replaced the curved parts of the turbine blades with a row of hinged blades. They obtained less flow resistance in the vanes that opened automatically under the influence of wind pressure. They determined that the blades automatically closed again when coming to the initial position and that at very low tip velocity rates, higher moments were obtained from the corrected segmented blade impellers compared to the classical SWTs.

Wenehenubun et al. [28] conducted an experimental study on the performance of SWTs regarding the number of blades. They compared the power coefficients, blade tip velocity ratios, and torques of one, two, three, four, and five-bladed Savonius rotors at certain wind speeds. Şahin [6] placed 6 and 8 guide plates around the classical SWT to improve wind turbine performance. The performance and velocity ratio of the SWT by changing the number, length, and position of the guide plate, were examined by taking into account the torque and momentum coefficients. An average of 30% increase in the power coefficient of the newly designed SWT was determined compared to the classical turbine. Liang et al. [7] systematically examined the radius ratio and coupling angle of a Combined Type (Savonius + Darrieus) rotor with low initial conditions but aiming for high aerodynamic performance. They investigated the effects of these two parameters on startup performance and efficiency with a computational fluid dynamics approach. They have conducted many numerical studies using the Reynolds-averaged Navier-Stokes equations and the  $k-\epsilon$  turbulence model to obtain the static torque. Kothe et al. [8] numerically and experimentally examined the aerodynamic performance of the helical Savonius rotor model consisting of a  $180^\circ$  bent blade and the two-stage Savonius rotor model. As a result of the studies, static torque, dynamic torque, and power coefficients were compared. Although the helical Savonius rotor has a more complex manufacturing process than the two-stage SWT, it offers stable torque and a higher power coefficient. When  $\lambda = 0.65$ , the maximum power coefficient of the rotor was obtained in both cases. Saad et al. [9] investigated single, two, three-, and four-stage Savonius rotors with helical blades to increase the performance of vertical axis wind turbines and compared them with a single-stage Savonius rotor with aspect ratios ranging from 1 to 4. To determine performance parameters such as torque, power, and thrust coefficients, they developed a three-dimensional flow model using the Reynolds-averaged Navier-Stokes equations and the  $k-\omega$  turbulence model. As a result of this study, they showed that the new design of the multistage rotor with helical blades significantly increased the output power. Evran and Yıldır [10] evaluated the drag and lift coefficient performances of NACA-4415 and NACA-0009 airfoils at constant wind velocity and various angles of attack. They determined the drag and lift coefficients of the airfoils in the ANSYS-Fluent environment. They adopted attack angles and airfoil types as control factors. In conclusion; By using the NACA4415 airfoil instead of the NACA0009 airfoil; They achieved a higher lift coefficient and lower drag coefficient. ANSYS program is one of the computer-aided engineering programs where analysis and simulations are made in engineering studies. Thanks to this program, effective studies such as mechanics, structural analysis, computational fluid dynamics and heat transfer can be carried out. In this study, flow and aerodynamic performance analysis was carried out by ANSYS-Fluent 18.1.

It has been observed in the literature that the effect of the position of the plate providing the stage to the Savonius turbine to the origin and the phase angle of the semicircular blades between the stages in Savonius turbines on the aerodynamic performance has not been investigated in helical Savonius turbines. In this study, unlike the literature, the effect of the plate's position providing the stage and the phase angle of the semicircular blades between the stages on the aerodynamic performance of the three-bladed, double-stage helical Savonius turbine has been a numerical investigation. The novelty of this study is to investigate the performance improvement of 3-blade HSWT by changing the phase angle. For this purpose, the aerodynamic analysis (lift and drag forces and lift and drag coefficients) of the HSWT were examined numerically.

## 2. Material and Method

In this study, a research CFD investigation was conducted on the three-bladed double-stage HSWT, which is a vertical axis wind turbine model. In particular, the effect of the phase angle of the semicircular blades between the stages on the aerodynamic performance was examined. The eccentricity of the model examined is  $L/H=1/2$  and the phase angle is  $\Theta = 0^\circ, 45^\circ, \text{ and } 90^\circ$ , respectively. The rotor length of HSWT is ( $H$ ) = 110 mm, rotor diameter ( $D$ ) = 46 mm, and shaft diameter ( $d$ ) = 5 mm. The designs for the effect of the phase angle on the turbine in geometries with eccentricity  $L/H=1/2$  are given in Figure 1.

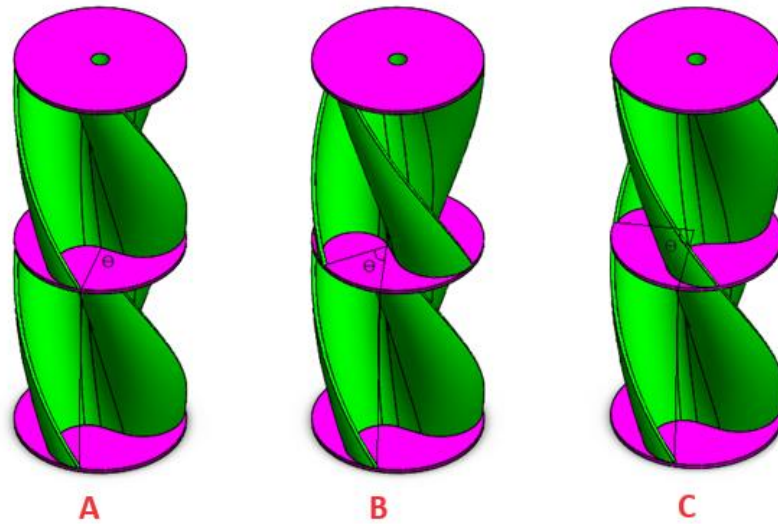


**Figure 1.** Design of the different phase angle HSWTs a)  $\Theta = 0^\circ$ , b)  $\Theta = 45^\circ$ , c)  $\Theta = 90^\circ$

The production of the HSWT, which was designed in the Solidworks environment, with an eccentricity of  $L/H = 1/2$ , was carried out with an Ultimaker Extended 2 3D printer. PLA filament is used in the solid model produced for experimental studies. Considering the surface roughness and manufacturing time of the wind turbine produced; A layer thickness of 0.1 mm was determined and a 0.40 mm nozzle tip was used.

In this study, experimental studies were carried out on a wind turbine with  $L/H = 1/2$  to determine the initial and boundary conditions in numerical studies. Fifty experiments were carried out with this experimental turbine at ten different air velocities, and these processes were repeated three times. Then, air velocity ( $V_s$ ), number of revolutions ( $n$ ), and drag force ( $F_d$ ) were measured by taking average values. Reynolds number ( $Re$ ), drag coefficient ( $C_d$ ), and blade tip velocity ratio ( $\lambda$ ) were calculated. The air tunnel used in the experiment is an open-air tunnel. The T-490 air tunnel is designed to conduct experiments in the fields of aerodynamics and fluid mechanics. The Savonius rotor produced by the 3D printer was placed in the test area of the experimental setup. Experiments were carried out for the turbine with  $L/H = 1/2$  at 10 different air velocities in the air tunnel, and the air tunnel test area during the experiment is shown in Figure 2.



**Figure 2.** Air tunnel test area during the experiment

Savonius rotors work with the effect of drag force. The drag force  $F_d$  is given in Eq. 1 and the drag coefficient  $C_d$  is given in Eq. 2. In these equations,  $V_s$  is the wind velocity,  $A_p$  is the projection area,  $\rho$  is the density of the air and  $C$  is the aerodynamic coefficient [11,12].

$$F_d = \frac{1}{2} \cdot A_p \cdot C_d \cdot \rho \cdot V_s^2 \quad (1)$$

$$C_d = \frac{F_d}{\frac{1}{2} \cdot A_p \cdot \rho \cdot V_s^2} \quad (2)$$

The Reynolds number is used to determine the characteristics of different flow regimes, such as laminar flow or turbulent flow. The flow regime depends on the ratio of inertial forces to viscous forces in the fluid [13]. Reynolds number ( $Re$ ) given in Eq. 3 [14].

$$Re = \frac{\rho \cdot V_s \cdot d}{\mu} \quad (3)$$

After carrying out many experiments, one of the methods developed to determine the error rates of the experiments is the "Uncertainty Analysis" method [15,16]. The uncertainty of the drag coefficient  $C_d$  in this study was calculated using Eq. 4 and Eq. 5.

$$C_d = f(F_d, V_s, A_p, \rho) \quad (4)$$

$$W_{C_d} = \left[ \left( \frac{\partial C_d}{\partial F_d} \cdot W_{F_d} \right)^2 + \left( \frac{\partial C_d}{\partial V_s} \cdot W_{V_s} \right)^2 + \left( \frac{\partial C_d}{\partial A_p} \cdot W_{A_p} \right)^2 + \left( \frac{\partial C_d}{\partial \rho} \cdot W_{\rho} \right)^2 \right]^{1/2} \quad (5)$$

When the studies investigating the aerodynamic performance of SWTs are examined; In many studies, it has been determined that only the test area of the air tunnel is modeled. Similarly, in this study; Considering the analysis times and the working capacity of the workstation, the flow volume created when the wind turbine model was placed in the test chamber was modeled and the airflow was defined as linear. When the wind turbine model was placed in the 200mm x 200mm x 500mm test chamber of the air tunnel, the resulting flow volume obtained as CAD data through the SOLIDWORKS program, and a network structure defined for this geometry in the ANSYS-Fluent program. By comparing the experiments and analysis results, problems that may arise from the experimental setup or analysis investigated and the most suitable mesh for the analysis obtained. The CAD drawing and mesh of the air tunnel (test zone) are depicted in Figure 3.

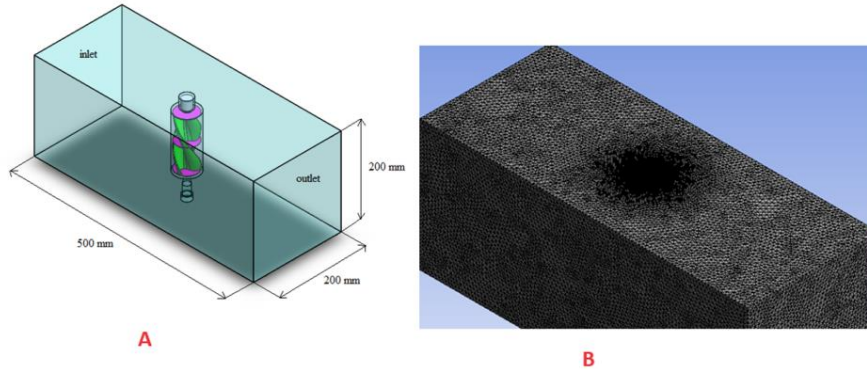


**Figure 3.** Air tunnel test domain a) Solid model b) Mesh model

The following values were chosen as initial and boundary conditions in the numerical analysis; Air was chosen as the fluid in the analysis carried out in the ANSYS-Fluent program. 'Velocity-inlet' is defined as the entrance section of the air to the test area (air tunnel). Air velocities are  $V_s=3.83$  m/s, 6.83 m/s, 8.47 m/s, 10.15 m/s, 11.67 m/s, 13.26 m/s, 15.28 m/s, 16.76 m/s, 18.76 m/s and 20.35 m/s. In numerical studies, the  $k-\epsilon$  realizable turbulence model is used as the turbulence model. Analysis was performed steady state. 'Pressure outlet' is defined as the section where the air exits the test area. Except for the parts defined as velocity-inlet and pressure-outlet, the outer regions of the test region are defined as 'wall'. For the continuity equation, a convergence condition of up to  $10^{-4}$  was used [17]. Some grid specifications are given in Table 1.

**Table 1.** Grid specifications

Body Sizing - Domain	Face Sizing - Wall	Face Sizing - Other	Body Sizing - Rotary	Face Sizing - Turbine	Skewness (max.)	Growth Rate
5mm	5mm	1mm	3mm	0.5mm	0.88	1.05

When the studies on improving the aerodynamic performance of SWT were examined in the literature, it determined that the  $k-\epsilon$  realizable turbulence model was widely used and this turbulence model gave better results. Due to the success of the  $k-\epsilon$  realizable turbulence model in HSWT flow analysis,  $k-\epsilon$  realizable was chosen as the turbulence model in this study. The transport equations valid for turbulent kinetic energy ( $k$ ) and loss rate ( $\epsilon$ ) are written as given in Equation 6 and Equation 7, respectively.

Turbulence Kinetic Energy ( $k$ ) equation in Eq.6 ;

$$\frac{\partial}{\partial t}(\rho k) + \frac{\partial}{\partial x_j}(\rho k u_j) = \frac{\partial}{\partial x_j} \left[ \left( \mu + \frac{\mu_t}{\sigma_k} \right) \frac{\partial k}{\partial x_j} \right] + G_k + G_b - \rho \epsilon - Y_M + S_k \quad (6)$$

Loss Rate ( $\epsilon$ ) equation in Eq.7 ;

$$\frac{\partial}{\partial t}(\rho \epsilon) + \frac{\partial}{\partial x_j}(\rho \epsilon u_j) = \frac{\partial}{\partial x_j} \left[ \left( \mu + \frac{\mu_t}{\sigma_\epsilon} \right) \frac{\partial \epsilon}{\partial x_j} \right] + \rho C_{1\epsilon} S_\epsilon - \rho C_{2\epsilon} \frac{\epsilon^2}{k + \sqrt{\nu \epsilon}} + C_{1\epsilon} \frac{\epsilon}{k} C_{3\epsilon} G_b + S_\epsilon \quad (7)$$

Turbulence viscosity equation in Eq.8;

$$C_1 = \max \left[ 0.43; \frac{\eta}{\eta + 5} \right], \quad \eta = S \frac{k}{\epsilon}, \quad S = \sqrt{2S_{ij}S_{ij}} \quad (8)$$

The constant values used in the turbulence model of this study are as follows;

$$C_{1\epsilon} = 1.44, \quad C_{2\epsilon} = 1.9, \quad \sigma_k = 1.0, \quad \sigma_\epsilon = 1.2$$

### 3. Result and Discussion

In this study, the effect of the phase angle between the stages of the HSWT on the aerodynamic performance was examined numerically. The drag force and drag coefficient of double-stage helical Savonius wind turbines (HSWT 1/2) with eccentricity  $L/H=1/2$  were investigated at different phase angles ( $\Theta=0^\circ, 45^\circ$ , and  $90^\circ$ ), and ten different air velocities. First, the grid independence study of the 3D-designed digital model was carried out. Second, experimental studies were carried out on HSWT ( $L/H=1/2$ )  $90^\circ$  to serve as a reference for numerical analysis. Moreover, the last, the experimental results were compared with all other numerical analysis results.

For mesh independence analysis, analysis was carried out with four different numbers of elements. In the analysis, the number of personnel starts from approximately 13 million and goes up to 17.5 million. Figure 4 shows the mesh independence study. Since the analysis, results were very close to each other after the number of elements was 14 million, the mesh model with the number of elements 14 million was chosen. Another reason for choosing the model with 14 million elements is that it reduces the analysis time. The results given hereafter are the same as the mesh model with 14097168 elements.

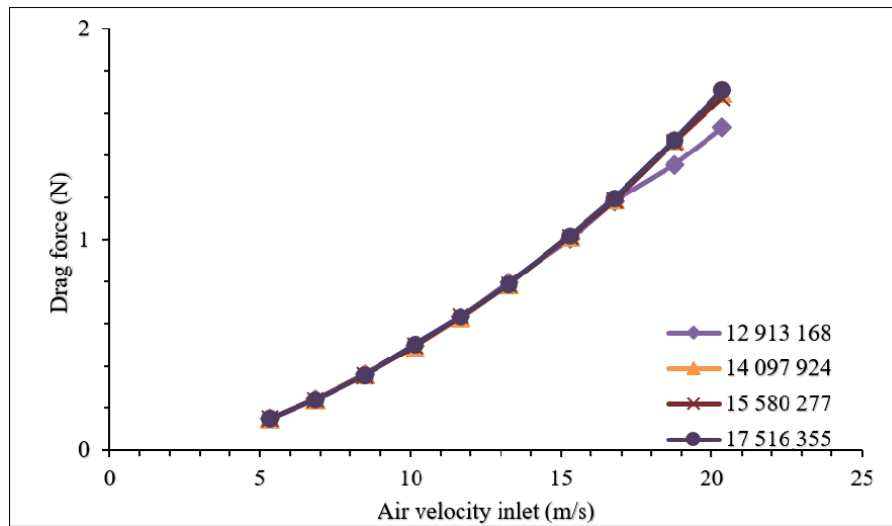


Figure 4. Domain mesh independency

ANSYS program is one of the computer-aided engineering programs where analysis and simulations are made in engineering studies. Thanks to this program, effective studies such as mechanics, structural analysis, computational fluid dynamics, and heat transfer were carried out. ANSYS is one of the most used CAE (computer-aided engineering) programs in Turkey and uses the finite element method (FEA) [18]. In the literature, the ANSYS-Fluent program is frequently used in the analysis of wind turbines [19, 20].

Experiments were carried out on HSWT1/2  $90^\circ$  to verify the numerical results in this study. The experimental results and the numerical analysis results are shown in Figure 5. The effect of air velocity on the drag force was examined for numerical analysis and comparison with experimental results. According to Figure 5, as the air velocity increases, the error rate of the numerical analysis also increases. Here, at the highest velocity of 20.35m/s, the maximum error rate does not exceed 15%. When 3D WT studies in the literature were examined, this error rate was considered acceptable [21–23].

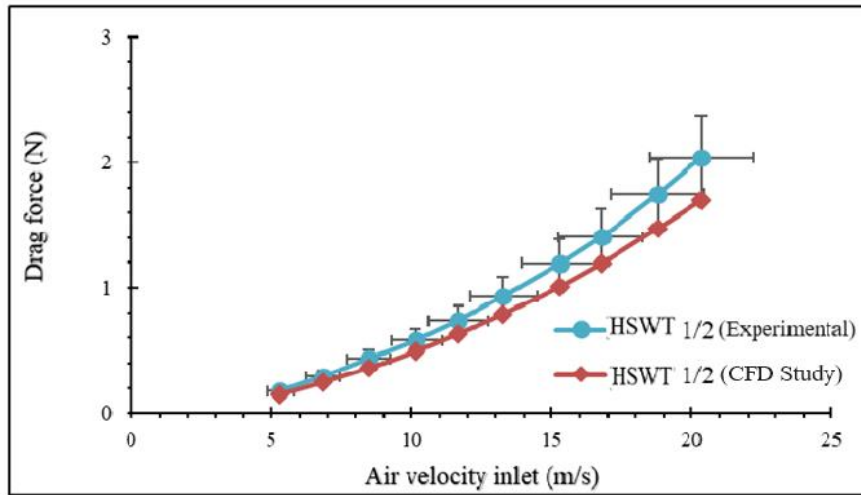


Figure 5. Domain mesh independency

In Savonius wind turbines, drag force directly affects aerodynamic performance. Many researchers have stated that as the drag force increases, the torque or power generation also increases [24–26]. Utomo et al. In their experimental studies, they stated that by adding a fin to the SWT, they obtained a drag force that increased the efficiency [27]. The effect of the phase angle between the stages of three different wind turbines on the aerodynamic performance was examined numerically. The effect of air velocity on the drag force (N) at different phase angles ( $\Theta$ ) of double-stage helical Savonius wind turbines (HSWT 1/2) with eccentricity  $L/H=1/2$  is given in Figure 6.

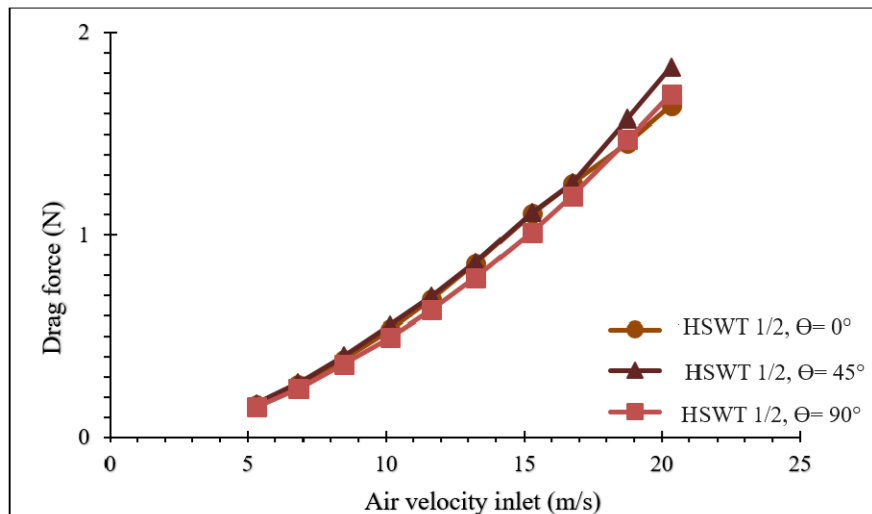


Figure 6. Effect of air velocity on drag force in HSWT 1/2s

According to Fig. 6, the drag force increased as the air velocity increased for all three geometries. When compared according to phase angles, the drag force of HSWT 1/2,  $\Theta=45^\circ$  was higher than the others. As a result, for the highest air velocity (20.35 m/s) in HSWT 1/2s, An increase of 11.64% in the drag force was observed by increasing the phase angle from  $0^\circ$  to  $45^\circ$ . In HSWT 1/2s, by increasing the phase angle from  $45^\circ$  to  $90^\circ$ , a 7.24% decrease in the drag force was observed. The effect of the Reynolds number on the drag coefficient in double-stage helical Savonius wind turbines (HSWT 1/2) with eccentricity  $L/H=1/2$  is given in Figure 7.

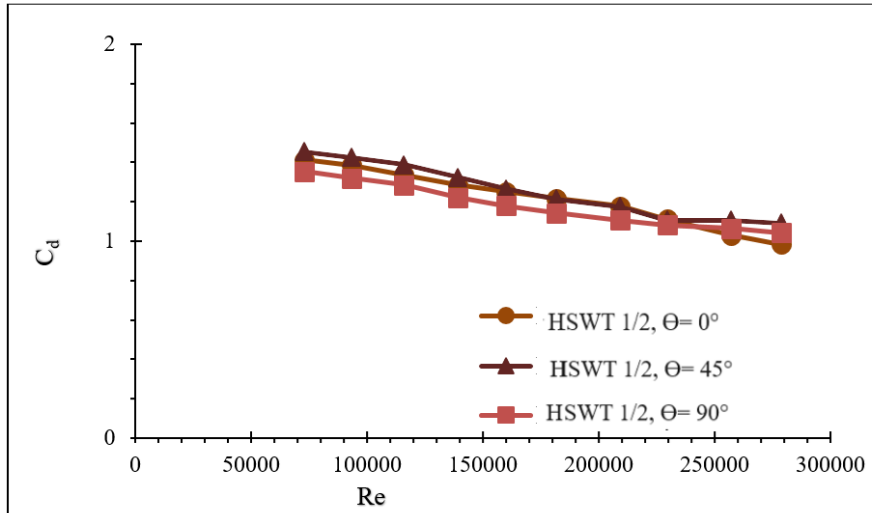


Figure 7. Effect of Reynolds number on drag coefficient in HSWT 1/2s

Wenehenubu et al. [28] studied the SWT performance related to the number of blades. They stated that the drag force of the four-bladed SWT was higher than that of the two- and three-bladed SWTs. For this reason, they stated that the four-blade SWT has produced more torque. In this study, it was tried to determine the HSWT model with the highest drag force at three different phase angles. When compared according to phase angles; It was observed that the drag coefficient of HSWT 1/2,  $\Theta=45^\circ$  was higher than the others. As a result, for the highest air velocity (20.35 m/s); In HSWT1/2s, by increasing the phase angle from  $0^\circ$  to  $45^\circ$ , a 10.77% increase in the drag coefficient was observed. In HSWT 1/2s, by increasing the phase angle from  $45^\circ$  to  $90^\circ$ , a 4.29% decrease in the drag coefficient was observed. At maximum air velocity (20.35 m/s), according to numerical results, HSWT 1/2 gives the best result,  $\Theta=45^\circ$ ; the velocity distribution in the origin section of the test area of the air tunnel is depicted in Figure 8.

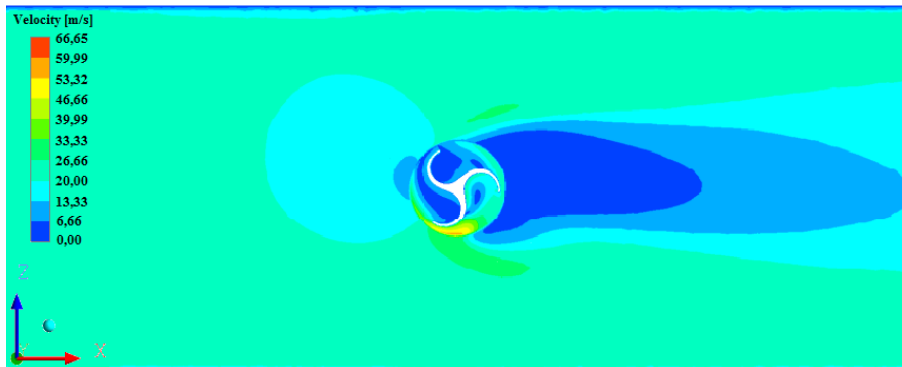
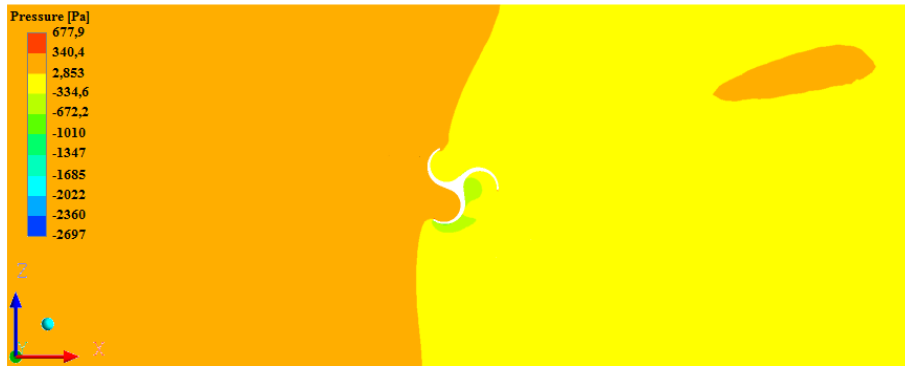


Figure 8. Velocity contour distribution created by HSWT 1/2  $\Theta=45^\circ$  in the test region (origin section)

According to Figure 8, it observed that the air velocity decreased slightly in front of the turbine, and behind the turbine, the air velocity decreased considerably and almost stopped. At maximum air velocity (20.35 m/s), HSWT 1/2  $\Theta=45^\circ$ , the pressure distribution in the origin section of the test area of the air tunnel is shown in Figure 9.



**Figure 9.** Pressure distribution created by HSWT 1/2  $\Theta=45^\circ$  in the test area (origin section)

Figure 10 shows that the velocity vectors progress linearly from the inlet part. The velocity vectors increase immediately around the turbine. Especially, high-velocity distribution arrows are seen in the flow region breaking away from HSWT 1/2,  $f = 45^\circ$ . Low-velocity distribution arrows are seen just behind the turbine. High-velocity distribution arrows are seen in the area breaking away from the lower and upper plates. The arrows scattered on the edges and behind the turbine become linear again towards the outlet section.

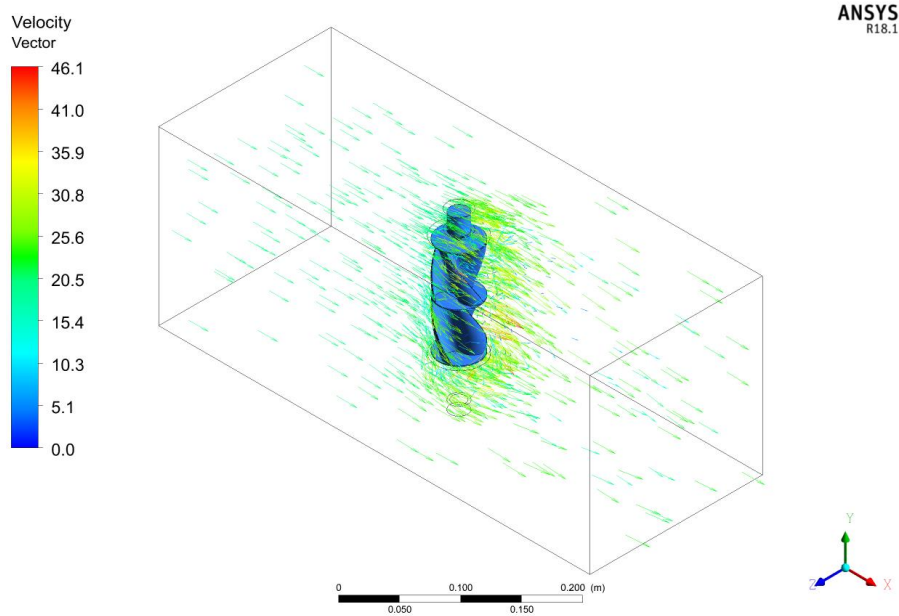


**Figure 10.** Velocity distribution created by HSWT 1/2  $\Theta=45^\circ$  in the test area

The optimum wind turbine geometry was tried to be obtained by examining the drag and lift forces, drag and lift coefficients, as well as the effects on the power coefficient and speed of the 3-blade HSWT at different air velocities. With this, the HSWT model with high energy efficiency has been introduced. As a result, electrical energy will be produced with less loss. It is evaluated that electrical energy produced more and at a cheaper cost will minimize the use of fossil fuels.

#### 4. Conclusion

In this study, the aerodynamic performance of the phase angle of the semicircular blades between the stages of a three-bladed double-stage HSWT was investigated by the CFD method. The power obtained from wind turbines is determined by the lift and drag forces they have at certain wind velocities. For HSWTs to be more efficient, a good drag force must be obtained from the existing drag force.

- In HSWT 1/2s, it was observed that there was an increase of 11.64% in the drag force by changing the phase angle from 0° to 45°.
- In HSWT 1/2s, it was observed that there was a 10.77% increase in the drag coefficient by changing the phase angle from 0° to 45°.
- In HSWT 1/2s, it was observed that there was a 7.24% decrease in the drag force by changing the phase angle from 45° to 90°.

In this study, the good performance model among the HSWTs examined was determined as HSWT 1/2  $\Theta = 45^\circ$ . The drag force and drag coefficient of this model are raiser than other models. In the future, new generation wind turbines will develop by combining different types of wind turbines into the ideal model determined in this study.

## **5. Acknowledgement**

This study was supported by the KSU Scientific Research Unit (BAP Project No: 2021/2-3YLS).

## **6. Author Contribution Statement**

Mernuş GÜL: Formation of the idea, design, numerical analysis, and literature review, M. Safa KAMER: Formation of the idea, numerical analysis, and project manager, Erdem ALIÇ: supervised the whole research work and reviewed the writing – original draft, project researcher, All authors have approved the final version.

## **7. Ethics Committee Approval and Statement of Conflict of Interest**

There is no need to obtain ethics committee permission for the article prepared. There is no conflict of interest with any person/institution in the prepared article.

## **8. List of Abbreviations**

A: Area, m<sup>2</sup>  
Cd: Drag coefficient,-  
CFD: Computational fluids Dynamics  
Fd: Drag force, N  
HSWT: Helical Savonius wind turbine  
k: Turbulent kinetic energy, J/kg  
Re: Reynolds number  
SWT: Savonius wind turbine  
Vs: airflow velocity, m/s  
WT: Wind turbine  
 $\Theta$ : Phase angle  
 $\rho$ : Air density, kg/m<sup>3</sup>  
3D: Three dimension

## 9. References

- [1] K. K. Jaiswal, C. R. Chowdhury, D. Yadav, R. Verma, S. Dutta, K. S. Jaiswal, SangmeshB and K. S. K. Karuppasamy, “Renewable and sustainable clean energy development and impact on social, economic, and environmental health”, *Ener. Nex.*, vol. 7, pp. 100118, April 2022.
- [2] M. Pourhoseinian, S. Sharifian and N. Asasian-Kolur, “Unsteady-state numerical analysis of advanced Savonius wind turbine”, *Energy Sources, Part A Recover. Util. Environ. Eff.*, vol. 00, no. 00, pp. 1–16, 2021.
- [3] D. Afungchui, B. Kamoun, A. Helali and A. Ben Djemaa, “The unsteady pressure field and the aerodynamic performances of a Savonius rotor based on the discrete vortex method,” *Renew. Energy*, vol. 35, no. 1, pp. 307–313, 2010.
- [4] T. Ogawa, “Theoretical study on the flow about savonius rotor,” *J. Fluids Eng. Trans. ASME*, vol. 106, no. 1, pp. 85–91, 1984.
- [5] P. Reupke and S. D. Probert, “Slatted-blade Savonius wind-rotors,” *Appl. Energy*, vol. 40, no. 1, pp. 65–75, 1991.
- [6] İ. Şahin, “Bir savonius rüzgar türbininin performansının sayısal incelenmesi ve iyileştirilmesi, Gazi Üniversitesi,” *Fen Bilim. Enstitüsü Enerj. Sist. Mühendisliği, Yüksek Lisans Tezi*, 2015.
- [7] X. Liang, S. Fu, B. Ou, C. Wu, C. Y. H. Chao and K. Pi, “A computational study of the effects of the radius ratio and attachment angle on the performance of a Darrieus-Savonius combined wind turbine”, *Renew. Energy*, vol. 113, pp. 329–334, 2017.
- [8] L. B. Kothe, S. V. Möller and A. P. Petry, “Numerical and experimental study of a helical Savonius wind turbine and a comparison with a two-stage Savonius turbine”, *Renew. Energy*, vol. 148, pp. 627–638, 2020.
- [9] A. S. Saad, A. Elwardany, I. I. El-Sharkawy, S. Ookawara and M. Ahmed, “Performance evaluation of a novel vertical axis wind turbine using twisted blades in multi-stage Savonius rotors”, *Energy Convers. Manag.*, vol. 235, no. February, p. 114013, 2021.
- [10] S. Evran and S. Z. Yildir, “Numerical and statistical aerodynamic performance analysis of NACA0009 and NACA4415 airfoils”, *J. Polytech.*, vol. 0900, pp. 0–2, 2023.
- [11] B. Deda Altan and G. S. Gultekin, “Investigation of performance enhancements of savonius wind turbines through additional designs,” *Processes*, vol. 11, no. 5, 2023.
- [12] M. Basumatary, A. Biswas and R. D. Misra, “CFD study of a combined lift and drag-based novel Savonius vertical axis water turbine”, *J. Mar. Sci. Technol.*, vol. 28, no. 1, pp. 27–43, 2023.
- [13] Y. A. Cengel and A. J. Ghajar, “Heat and mass transfer (a practical approach, SI version)”, McGraw-Hill Education, 2011.
- [14] Y. A. Çengel and J. M. Cimbala, “Fluid Mechanics: Fundamentals and Applications, Forth Edition”, New York: McGraw-Hill Education, 2018.
- [15] T. S. Rengma and P. M. V. Subbarao, “Optimization of semicircular blade profile of Savonius hydrokinetic turbine using artificial neural network”, *Renew. Energy*, vol. 200, no. September, pp. 658–673, 2022.
- [16] M. Basumatary, A. Biswas and R. D. Misra, “Experimental verification of improved performance of Savonius turbine with a combined lift and drag based blade profile for ultra-low head river application”, *Sustain. Energy Technol. Assessments*, vol. 44, no. December 2020, p. 100999, 2021.
- [17] K. R. Abdelaziz, M. A. A. Nawar, A. Ramadan, Y. A. Attai and M. H. Mohamed, “Performance investigation of a Savonius rotor by varying the blade arc angles”, *Ocean Eng.*, vol. 260, no. July, p. 112054, 2022.
- [18] A. Fluent, “ANSYS fluent theory guide 15.0,” ANSYS, Canonsburg, PA, 2013.
- [19] A. Hesami, A. H. Nikseresht and M. H. Mohamed, “Feasibility study of twin-rotor Savonius wind turbine incorporated with a wind-lens”, *Ocean Eng.*, vol. 247, no. January, p. 110654, 2022.
- [20] H. E. Tanürün, İ. Ata, M. E. Canlı and A. Acir, “Farklı açıklık oranlarındaki NACA-0018 rüzgâr türbini kanat modeli performansının sayısal ve deneysel incelenmesi”, *Politek. Derg.*, vol. 23, no. 2, pp. 371–381, 2020.
- [21] D. H. Didane, M. N. A. Bajuri, M. I. Boukhari and B. Manshoor, “Performance investigation of vertical axis wind turbine with savonius rotor using computational fluid dynamics (CFD)”, *CFD Lett.*, vol. 14, no. 8, pp. 116–124, 2022.

- [22] H. A. Hassan Saeed, A. M. Nagib Elmekawy and S. Z. Kassab, “Numerical study of improving Savonius turbine power coefficient by various blade shapes”, *Alexandria Eng. J.*, vol. 58, no. 2, pp. 429–441, 2019.
- [23] M. S. Abdullah, M. H. H. Ishak and F. Ismail, “Numerical study of the 3D Savonius turbine under stationary conditions”, *Eng. Fail. Anal.*, vol. 136, no. February, p. 106199, 2022.
- [24] M. H. M. Al Ghriyah, “An experimental study on improvement of a savonius rotor performance with multiple halves blades”, Near East University, 2017.
- [25] M. M. Kamal and R. P. Saini, “A numerical investigation on the influence of savonius blade helicity on the performance characteristics of hybrid cross-flow hydrokinetic turbine”, *Renew. Energy*, vol. 190, pp. 788–804, 2022.
- [26] M. B. Salleh, N. M. Kamaruddin and Z. Mohamed-Kassim, “The effects of deflector longitudinal position and height on the power performance of a conventional Savonius turbine”, *Energy Convers. Manag.*, vol. 226, no. August, p. 113584, 2020.
- [27] I. S. Utomo, D. D. D. P. Tjahjana and S. Hadi, “Experimental studies of Savonius wind turbines with variations sizes and fin numbers towards performance”, *AIP Conf. Proc.*, vol. 1931, 2018.
- [28] F. Wenehenubun, A. Saputra and H. Sutanto, “An experimental study on the performance of Savonius wind turbines related with the number of blades”, *Energy Procedia*, vol. 68, pp. 297–304, 2015.



## Susurluk Havzası Akımlarının Trend Analiz Yöntemleri Kullanılarak Değerlendirilmesi

Ramazan ACAR<sup>1\*</sup>

<sup>1</sup>İnşaat Mühendisliği, Mühendislik Fakültesi, Munzur Üniversitesi, Tunceli, Türkiye.  
[ramazanacar@munzur.edu.tr](mailto:ramazanacar@munzur.edu.tr)

Geliş Tarihi: 17.01.2024  
Kabul Tarihi: 11.02.2024

Düzeltilme Tarihi: 31.01.2024

doi: 10.62520/fujece.1421090  
Araştırma Makalesi

Alıntı: R. Acar, "Susurluk havzası akımlarının trend analiz yöntemleri kullanılarak değerlendirilmesi", Fırat Univ. Jour.of Exper. and Comp. Eng., vol. 3, no 1, pp. 65-74, Şubat 2024.

### Öz

Yıllık ortalama akım verilerinin trend analizi, daha iyi su kaynakları yönetimi, planlanması ve işletilmesi için çok önemlidir. Bu çalışmada, Susurluk Havzası üzerinde bulunan M. Kemal Paşa, Orhaneli ve Simav akım gözlem istasyonlarından alınan yıllık ortalama akım verileri Mann-Kendall, Spearman Rho ve Şen'in Yenilikçi trend yöntemleri ile test edilmiş ve istasyonlara ait eğilimler belirlenmeye çalışılmıştır ve bu yöntemlerin performansları değerlendirilmiştir. Ayrıca yıllık ortalama akım verileri regresyon analizine tabi tutulmuş ve denklem takımları elde edilmiştir. Her istasyon için azalış-artış miktarları yıllık ve 100 yıllık değişimleri m<sup>3</sup>/s cinsinden tespit edilmiştir. Sonuçlar irdelendiğinde sadece Şen'in Yenilikçi trend yöntemi analizlerinde 3 istasyon için de genel anlamda azalan bir trend tespit edilmiştir. Mann-Kendall ve Spearman Rho yöntemleri analizlerinde ise 3 istasyonda da herhangi bir trend tespit edilememiştir. Ayrıca 3 istasyona ait verilerin 100 yıllık değişim yüzdesi değerleri belirlenmiştir. Bu değerlere göre istasyonların akım değerlerinde gelecekte ciddi bir düşüş olacağı sonucuna varılmıştır.

**Anahtar kelimeler:** Akım, Trend, Mann-Kendall, Spearman's rho, Şen yenilikçi Trend testi

\*Yazışılan yazar



## Evaluation of Susurluk Basin Flows Using Trend Analysis Methods

Ramazan ACAR <sup>1\*</sup> 

<sup>1</sup>Department of Civil Engineering, Faculty of Engineering, Munzur University, Tunceli, Turkey.

<sup>1</sup>[ramazanacar@munzur.edu.tr](mailto:ramazanacar@munzur.edu.tr)

Received: 17.01.2024

Accepted: 11.02.2024

Revision: 31.01.2024

doi: 10.62520/fujece.1421090

Research Article

Citation: R. Acar, "Evaluation of susurluk basin flows using trend analysis methods", Firat Univ. Jour. of Exper. and Comp. Eng., vol. 3, no 1, pp. 65-74, February 2024.

### Abstract

Trend analysis of annual average flow data is very important for better water resources management, planning and operation. In this study, annual average flow data from M. Kemal Paşa, Orhaneli and Simav flow observation stations located in Susurluk Basin were tested with Mann-Kendall, Spearman Rho and Şen's Innovative trend methods and the trends of the stations were tried to be determined and the performances of these methods were evaluated. In addition, annual average flow data were submitted to regression analysis, yielding equation sets. For each station, the annual and 100-year changes in m<sup>3</sup>/s were determined. Analyzing the results, only Şen's Innovative Trend Method analysis found a general decreasing trend for all 3 stations. In the analyses of Mann-Kendall and Spearman's Rho methods, no trend was detected in all 3 stations. In addition, 100-year percentage change values of the data of 3 stations were determined. According to these values, it is concluded that there will be a significant decrease in the flow values of the stations in the future.

**Keywords:** Flow, Trend, Mann-Kendall, Spearman's rho, ITA

---

\*Corresponding author

Plagiarism Checks: Yes – Turnitin

Complaints: [fujece@firat.edu.tr](mailto:fujece@firat.edu.tr)

Copyright & License: Authors publishing with the journal retain the copyright to their work licensed under the CC BY-NC 4.0

## 1. Introduction

Climate dynamics have a substantial impact on hydrological regimes in river basins around the world. Supply in the watersheds have substantial consequences on ecosystems, agriculture, forestry, fisheries, industry, and risk management [1]. With global warming and extreme weather events becoming more frequent, water resources are facing serious challenges. Global climate change is reducing water resources in many regions, and water scarcity is becoming more serious over time, especially in regions that are both arid and ecologically sensitive. It is of great importance to constantly monitor the water flow and take the necessary precautions to prevent these situations from occurring and to prevent water resources from decreasing [2].

Observational and historical hydroclimatological data are commonly utilized to plan and develop water resource projects [3]. As a result, identifying trends in streamflow in a watershed can help us understand the influence of climatic variability and change in the region. Trend analysis can also suggest future research requirements and directions, as well as assist decision makers in future planning [4].

Many approaches and studies have been devised and conducted in the literature to determine trends in hydrometeorological data (flow, precipitation, temperature, relative humidity, and so on). Examples of trend analysis methods often used in the literature include the Mann-Kendall (MK) test [5-6], Spearman Rho (SR) test [7], Şen Innovative Trend Analysis (ITA) [8-9], and Innovative Polygon Trend Analysis (IPTA) [10].

Gümüş and Yenigün made trend analyses of the annual average flows of 4 stations they selected from the Lower Euphrates Basin. They used the non-parametric MK test, one of the trend analysis methods. In addition, they used the non-parametric MK Order Correlation test to determine the starting year of the trend at the stations where trend detection was made. In conclusion; they detected a decreasing trend in half of the preferred stations. They determined the starting years of the decreasing trend as 1973-1985 [11]. In their study, Gumus and his colleagues determined the trends of monthly average and annual flow values of 16 stream measurement stations in the Tigris Basin. They used the Mann-Kendall test, Şen's Slope Method and Innovative Trend Analysis (ITA) method to determine trends. As a result, they stated that the trend directions of MK and ITA methods are generally similar [12]. Wang and his colleagues examined the flow processes of seven major rivers in terms of trend and stability at 7 stations in Western Europe. In the results of their analysis with the MK test, they found that there was no trend in the annual average flow values [13]. Ali and Abubaker used the MK test, Şen's Slope Estimator, and the Innovative Trend Method to analyze Yangtze River flow trends throughout seasonal and annual time periods. As a result, they detected a significant increasing trend only in the source region of the Yangtze River and a statistically non-significant decreasing trend in all study areas [14]. Summary information about the studies mentioned above and the current study are presented in Table 1.

**Table 1.** Summary of past studies

Study	Examined Stations	Method	Data Used	Data Examination Interval
Gümüş and Yenigün (2006)	Lower Euphrates Basin (Turkey)	Non-parametric MK test, Non-parametric MK Order Correlation test	Flow	Annual
Gumus et al. (2022)	Tigris Basin (Turkey)	MK, Sen's Slope Estimator, Innovative trend analysis	Flow	Annual-Monthly
Wang et al. (2005)	Western Europe	MK, Seasonal Kendall test	Flow	Annual
Ali and Abubaker (2019)	Yangtze River (Western China)	MK, Sen's Slope Estimator, Innovative trend analysis	Flow	Seasonal-Annual
This Study	Susurluk Basin (Turkey)	MK, SR, Innovative trend analysis	Flow	Annual

In this study, Mann-Kendall (MK), Spearman Rho (SR) and Sen's Innovative Trend Analysis (ITA) methods, which are nonparametric statistical trend analysis methods, were used to investigate the future trends of annual average flow data obtained from the General Directorate of State Hydraulic Works (DSİ) of Susurluk

Basin. One program (software) was created in Matlab program in order to obtain the results of trend analysis of annual average flow data more quickly using MK test and SR test methods. The 3 methods used in trend analysis were compared with each other in terms of performance. In addition, annual average flow data were applied to the regression method separately for all 3 stations and equation sets were obtained. According to the slope value of these equation sets, the annual and 100-year decrease or increase amounts were determined in  $m^3/s$ .

## 2. Material and Method

### 2.1. Study area and data used

Susurluk Basin was chosen as the study area. It is located in the west of Turkey and between the coordinates  $39^{\circ}$ -  $40^{\circ}$ N and  $27^{\circ}$ -  $30^{\circ}$ E. It covers approximately 3.11% of Turkey's surface area and has an area of approximately 24349.09  $km^2$  [15]. M. Kemal Paşa numbered 302, Orhaneli numbered 311 and Simav current observation stations numbered 316, located within the basin borders, were selected to be used in the study (Figure 1). Annual average flow data for these 3 stations were obtained from the General Directorate of State Hydraulic Works. Statistical analysis values of these data were given in Table 2.

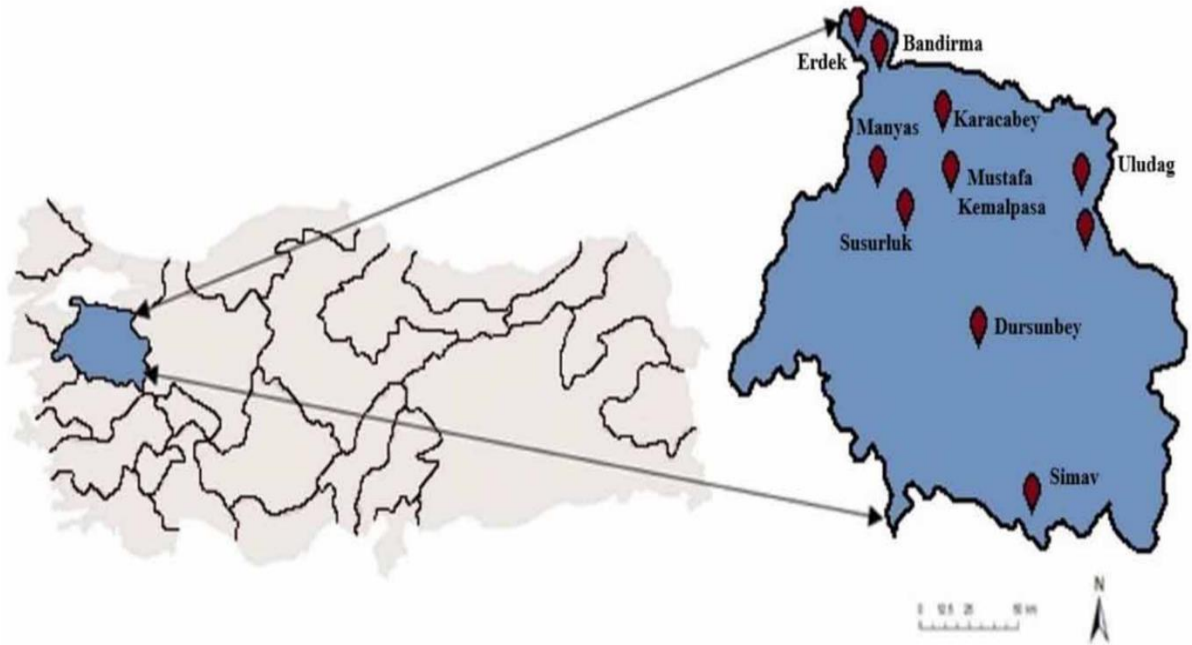


**Figure 1.** Susurluk Basin Location Map [16]

**Table 2.** Statistical analysis results of annual average flow data of stations

Station	Year	Coordinates	Number of Data	Minimum	Maximum	Average	Standard Deviation
Simav	1980-2011	$39^{\circ} 59' 10''$ N $28^{\circ} 10' 34''$ E	32	9.23	76.57	37.36	17.59
Orhaneli	1980-2015	$39^{\circ} 37' 31''$ N $29^{\circ} 27' 52''$ E	36	2.04	13.69	5.34	2.96
M Kemal Paşa	1980-2015	$39^{\circ} 57' 41''$ N $28^{\circ} 30' 58''$ E	36	10.16	84.78	43.25	18.51

## 2.2. Methods used in the study

### 2.2.1. Mann-Kendall trend test

The MK test [5-6] is a rank-based nonparametric test that is insensitive to outliers. This test does not require that the data adhere to normal distribution assumptions [17-18]. Here's how the MK test statistic is calculated:

$$S = \sum_{i=1}^{n-1} \sum_{j=i+1}^n \text{sign}(x_j - x_i), \text{sign}(x_j - x_i) = \begin{cases} +1 & (x_j - x_i) > 0 \\ 0 & (x_j - x_i) = 0 \\ -1 & (x_j - x_i) < 0 \end{cases} \quad (1)$$

A positive S value indicates an uptrend, whilst a negative S value indicates a downtrend. The variance value is calculated to get the Z value. The variance (S) is calculated as follows:

$$\text{Var}(S) = \frac{n(n-1)(2n+5) - \sum_{i=1}^m t_i(t_i-1)(2t_i+5)}{18} \quad (2)$$

Equation 3 calculates the normal Z test statistic for a connected group (m) with a sample size of n>10.

$$Z = \frac{S \pm 1}{\text{Var}(S)^{1/2}} \quad (3)$$

In this equation, if S>0, S-1 is used, if S<0, S+1 is used, and if S=0, Z = 0. The positive value of Z indicates an increasing trend. Otherwise, it shows a downward trend [19].

### 2.2.2. Spearman's Rho trend test

The SR test [7-20] is another method of finding linear and nonlinear trends. It is a popular way to determine if there are patterns [21]. It is a quick and simple test for detecting whether a linear trend exists. As a result, it has become one of the most widely used trend analysis approaches for spotting current trends [22]. The null hypothesis (H<sub>0</sub>) for this test asserts that all data in the time series are independent and uniformly distributed. The alternative hypothesis (H<sub>1</sub>) holds that trends are either increasing or declining [23]. Equations 4 and 5 describe the test statistic R<sub>sp</sub> and the standardized test statistic Z<sub>SR</sub>, respectively.

$$R_{sp} = 1 - \frac{6 \sum_{i=1}^n (D_i - i)^2}{n(n^2 - 1)} \quad (4)$$

$$Z_{SR} = R_{sp} \sqrt{\frac{(n-2)}{(1-R_{sp}^2)}} \quad (5)$$

Here, D<sub>i</sub> is the observation order, and i is the chronological sequence number. N denotes the total length of the time series. Positive Z values indicate a growing trend across the hydrological time series, whilst negative Z values indicate diminishing trends. In normal distributions, if the Z value is above the significance level for Z<sub>α/2</sub> (α = 0.05), the null hypothesis (H<sub>0</sub>) is rejected and the trend is accepted [24].

### 2.2.3. Şen trend test

The ITA approach was initially proposed by Şen [8]. The ITA's primary advantage over the MK test and other procedures is that it makes no assumptions (serial correlation, non-normality, sample size). First, the time series is divided into two equal parts and sorted in ascending order. The first and second sections of the time series are then plotted using the X and Y axes, respectively. Figure 2 illustrates the innovative method in Cartesian coordinates. When data is collected along the 1:1 ideal straight line (45° line), it is discovered that the time series has an increasing trend. If the data falls within the bottom triangular area of the ideal

straight line, the time series shows a downward trend. As a result, the ITA method can identify low, medium, and high value trends in any hydro-meteorological or hydroclimatic time series [25-26-27].

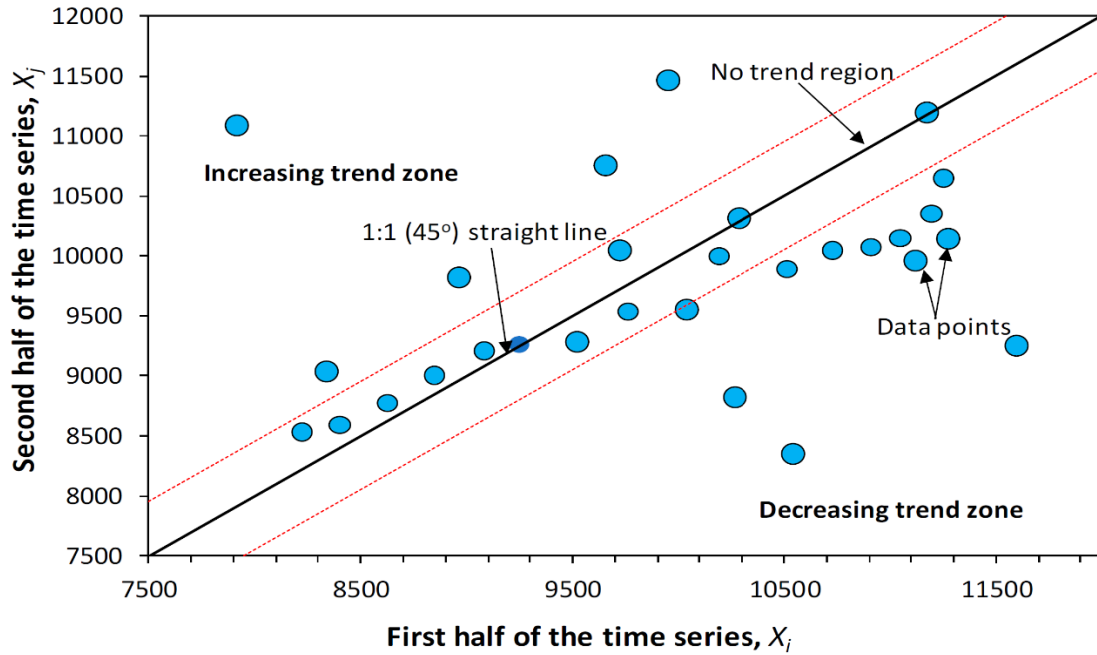


Figure 2. ITA method scatter result graph [28]

### 2.2.4. Regression analysis method

This method is based on the solution of the graph created by writing two different variables (dependent variable and independent variable) on separate axes. A line that best expresses the created graph should be selected. Then, the slope of the line needs to be determined [29]. This approach can be utilized for both linear and non-linear situations. There must be one dependent variable and at least one independent variable in this procedure (Equation 6) [30].

$$Y = \beta_0 + \beta_1 * X \quad (6)$$

Here  $\beta_0$  represents a constant value.  $\beta_1$  represents the slope of the line. If this equation is used for trend analysis,  $\beta_1$  represents the increase or decrease values [31-32].

### 3. Findings and Discussions

In the study, the annual average flow values of M. Kemal Paşa, number 302, Orhaneli, number 311, and Simav stations, number 311, of the Susurluk Basin located in the west of Turkey, were analyzed by ITA, SR test and MK between the years 1980-2015, 1980-2015 and 1980-2011, respectively. Test methods were applied and trends were determined. A software was created using MATLAB program for SR and MK methods analyses. Additionally, flow data was applied to the regression method. Furthermore, the slope and first-order equations of the trend changes were found, as well as the changes in the flow data throughout the required years. The study's findings were summarized using tables and graphs.

Table 3 shows the annual average flow data trend analysis results for stations 302, 311, and 316. As a result, the statistical analyses of the MK test and the SR test are identical. Based on the results of the two methods, the absolute value of Z for all three stations is less than the  $Z_{\alpha/2} = 1.96$  value of the standard normal distribution, which corresponds to the selected  $\alpha = 0.05$  level, indicating that "H0 = no trend" and concluding that there is no trend in the time series examined.

In the ITA method, it can be said that there was a trend of decreasing by 5% for low value flow data, increasing by 5% for average value flow data and increasing by 10% for high value flow data at station number 302. At station number 311, it was observed that there was no trend for low values, an increasing trend of 5% for medium values, and a decreasing trend of 10% for high values. At station number 316, a decreasing trend of 5% was observed at low and medium values, and a decreasing trend of over 10% was observed at high values. The graphs drawn for the ITA method are shown in Figure 3. In addition, annual average flow values for 3 stations were applied to regression analysis and first-order equation sets were determined to determine the slopes of trend changes. Then, the changes in annual average flow values for the given water year intervals at all 3 stations were calculated in terms of (m<sup>3</sup>/s) (Figure 4).

**Table 3.** Results of annual average flow data of stations

Station	Mann-Kendall		Spearman Rho		Annual Change (m <sup>3</sup> /s)	100 Years Change (%)
	Z	Trend Z (0.95)	Z	Trend Z (0.95)		
Simav	-0.8595	↔	-0.8889	↔	-0.3888	-40.39
Orhaneli	-0.5857	↔	-0.6097	↔	-0.0348	-24.45
M. Kemal Paşa	-1.4847	↔	-1.7197	↔	-0.7099	-60.48

Indicators: (↔) no trend

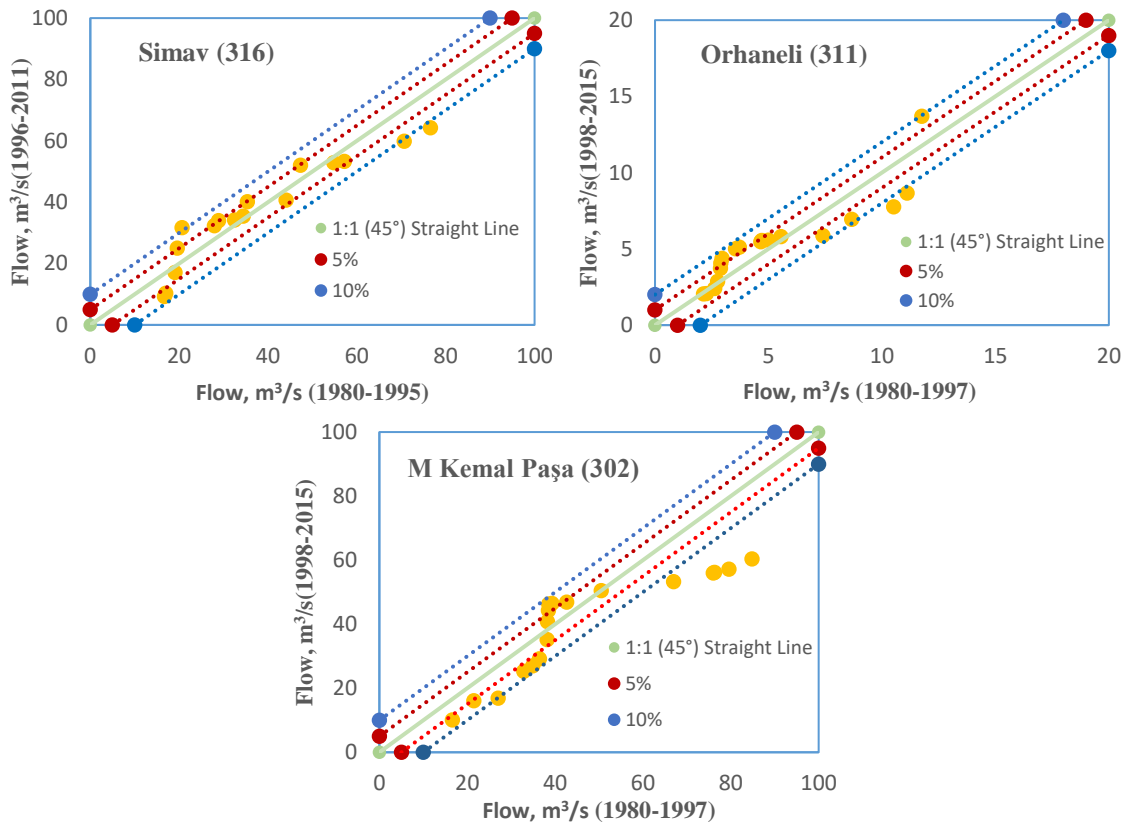


**Figure 3.** Trend graphs of annual average flow data of stations

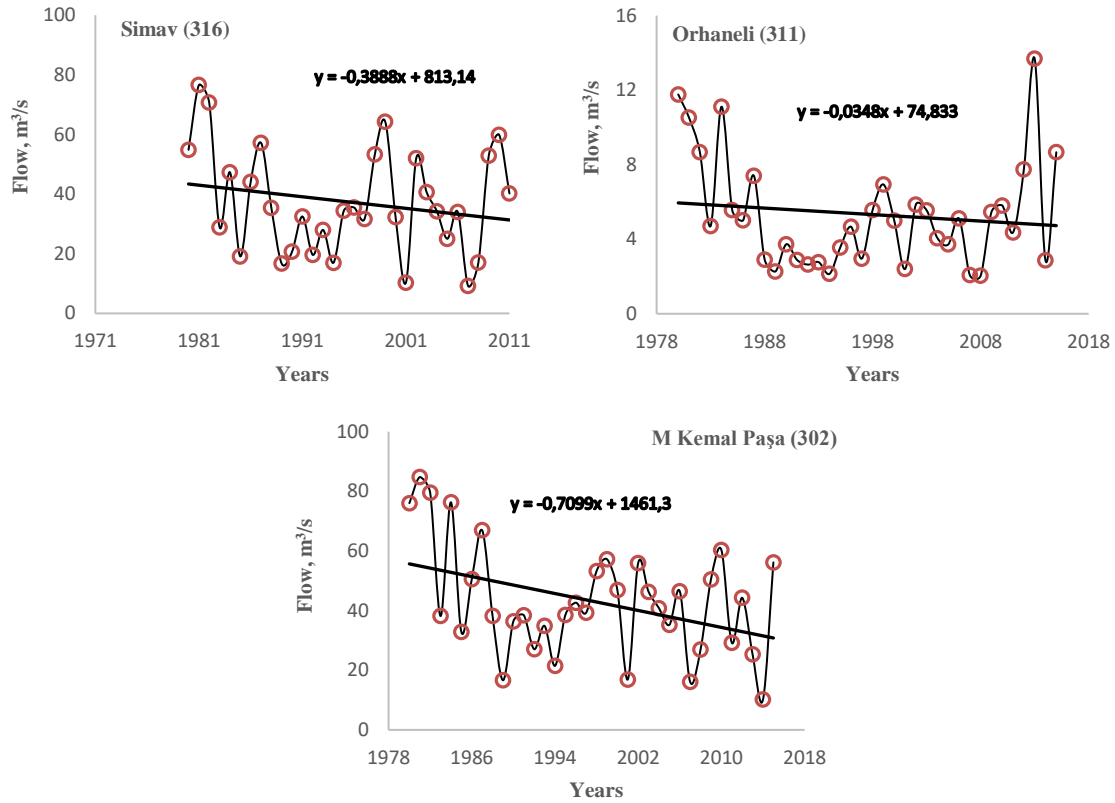


Figure 4. Annual average flow trend change of three stations

#### 4. Results

In this study, the Susurluk Basin located in the west of Turkey was studied. Annual average flow data of M. Kemal Pasha numbered 302, Orhaneli numbered 311 and Simav stations numbered 316 in this basin were examined and trends were determined using MK, SR and ITA methods. Furthermore, annual average flow data were subjected to regression testing, and annual variations were calculated. Furthermore, the outcomes of the MK, SR, and ITA approaches, which differ from one another, were compared.

- As a result of the analysis, a general decreasing trend was detected in all 3 stations for annual average flow data using the ITA method.
- The MK and SR test statistical methods revealed no trend for all 3 stations. Furthermore, it was found that the MK and SR test statistical approaches produced equivalent results for all 3 stations.
- The trend slope direction and annual change values of the stations in the trend change graphs given in Figure 4 also confirm the results of the ITA method.
- According to the 100-year change percentage values of the 3 stations, it was concluded that the current values of the region where stations 302, 311 and 316 are located will also decrease significantly, but this reliability rate is statistically outside the 95% confidence interval.
- The results indicate that there may be a water shortage in this basin in the future. Therefore, necessary precautions should be taken to use water resources consciously.

#### 5. Author Contribution Statement

Ramazan ACAR contributed to the formation of the idea and literature review in the study, evaluation of the results obtained, obtaining the data used and examining the results, checking the article for spelling and content.

## 6. Ethics Committee Approval and Conflict of Interest Declaration

The authors declare that they have no known competing financial interests or personal relationships that could have appeared to influence the work reported in this paper.

## 7. References

- [1] M. Zaghloul, E. Ghaderpour, H. Dastour, B. Farjad, A. Gupta, H Eum and Q. Hassan, "Long term trend analysis of river flow and climate in northern Canada", *Hydr.*, vol. 9, no. 11, pp. 197, 2022.
- [2] C. Zang and J. Liu, "Trend analysis for the flows of green and blue water in the Heihe River basin, northwestern China", *Jour. of Hydr.*, vol. 502, pp. 27-36, 2013.
- [3] E. Kahya and S. Kalaycı, "Trend analysis of streamflow in Turkey", *Jour. of Hydr.*, vol. 289 no. 1-4, pp. 128-144, 2004.
- [4] M. Gautam and K. Acharya, "Streamflow trends in Nepal", *Hydr. Sci. Jour.*, vol. 57 no. 2, pp. 344-357, 2012.
- [5] H. Mann, "Nonparametric tests against trend", *Econometrica: Jour. of the Econ. Soc.*, pp. 245-259, 1945.
- [6] M. Kendall, "Rank correlation methods", 1975.
- [7] E. Lehmann and H. D'Abbrera, "Nonparametrics: statistical methods based on ranks", Holden-day, 1975.
- [8] Z. Şen, "Innovative trend analysis methodology", *Jour.of Hydr. Eng.*, 17(9), 1042-1046, 2012.
- [9] Z. Şen, "Trend identification simulation and application", *Jour.of Hydr. Eng.*, vol. 19 no. 3, pp. 635-642, 2014.
- [10] Z. Şen, E. Şişman and I. Dabanli, "Innovative polygon trend analysis (IPTA) and applications", *Jour. of Hydr.*, vol. 575, pp. 202-210, 2019.
- [11] V. Gümüş and K. Yenigün, "Aşağı Fırat Havzası akımlarının trend analizi ile değerlendirilmesi", *Yedinci Uluslararası İnşaat Mühendisliğinde Gelişmeler Kongresi*, 11, 13, 2006.
- [12] V. Gumus, Y. Avsaroglu and O. Simsek, "Streamflow trends in the Tigris river basin using Mann–Kendall and innovative trend analysis methods", *Jour. of Ear. Sys. Sci.*, vol. 13, no.1, pp. 34, 2022.
- [13] W. Wang, P. Van Gelder and J. Vrijiling, "Trend and Stationarity Analysis for Streamflow Processes of Rivers in Western Europe in the 20th Century", In *Proceedings: IWA International Conference on Water Economics, Statistics, and Finance Rethymno, Greece*, 810, 2005.
- [14] R. Ali and S. Abubaker, "Trend analysis using Mann-Kendall, Sen's slope estimator test and innovative trend analysis method in Yangtze River basin, China", *Int. Jour. of Eng. & Tech.*, vol. 8 no.2, pp. 110-119, 2019.
- [15] C. Yerdelen, "Susurluk havzası yıllık akımlarının trend analizi ve değişim noktasının araştırılması" *Dokuz Eylül Üni. Müh.Fak. Fen ve Müh.Dergisi*, vol. 15, no. 44, pp. 77-87, 2013.
- [16] G. Ceribas and A. Ceyhunlu, "Analysis of total monthly precipitation of Susurluk Basin in Turkey using innovative polygon trend analysis method", *Jour. of Water and Clim. Chan.*, vol. 12, no. 5, pp. 1532-1543, 2021.
- [17] M. Ashraf, I. Ahmad, N. Khan, F. Zhang, A. Bilal and J. Guo, "Streamflow variations in monthly, seasonal, annual and extreme values using Mann-Kendall, Spearman's Rho and innovative trend analysis", *Water Res. Manag.*, vol. 35, pp. 243-261, 2021.
- [18] A. Gadedjisso-Tossou, K. Adjegan and A. Kablan, "Rainfall and temperature trend analysis by Mann–Kendall test and significance for Rainfed Cereal Yields in Northern Togo", *Sci*, vol. 3, no. 1, pp. 17, 2021.
- [19] F. Aditya, E. Gusmayanti and J. Sudrajat, "Rainfall Trend Analysis Using Mann-Kendall and Sen's Slope Estimator Test in West Kalimantan" In *IOP Conference Series: Earth and Environmental Science*, vol. 893, no.1, pp. 012006, 2021.
- [20] C. Spearman, "The proof and measurement of association between two things", *Oamerican J*, 1904.
- [21] M. Rahman, L. Yunsheng and N. Sultana, "Analysis and prediction of rainfall trends over Bangladesh using Mann–Kendall, Spearman's rho tests and ARIMA model" *Meteorology and Atmospheric Physics*, vol. 129, no. 4, pp. 409-424, 2017.

- [22] R. Ergüven, “Küresel iklim değişikliğinin yukarı firat havzası hidrometeorolojik verileri üzerine etkisi”, Master's Thesis, Fırat University Graduate School of Natural and Applied Sciences, Elazığ, 2022.
- [23] M. Shadmani, S. Marofi and M. Roknian, “Trend analysis in reference evapotranspiration using Mann-Kendall and Spearman’s Rho tests in arid regions of Iran”, *Water Res.Manag.*, vol. 26, pp. 211-224, 2012.
- [24] I. Ahmad, D. Tang, T. Wang, M. Wang and B. Wagan, “Precipitation trends over time using Mann-Kendall and spearman’s rho tests in swat river basin, Pakistan”, *Adv. in Meteor.*, 2015.
- [25] T. Caloiero, “Evaluation of rainfall trends in the South Island of New Zealand through the innovative trend analysis (ITA)”, *Theor. and Appl. Clim.*, vol. 139 no.1-2, pp. 493-504, 2020.
- [26] K. Saplıoğlu and Y. Güçlü, "Combination of wilcoxon test and scatter diagram for trend analysis of hydrological data", *Jour. of Hydr.*, vol. 612, pp. 128132, 2022.
- [27] K. Saplıoğlu and E. Çoban, “Karadeniz bölgesi yağış serilerinin trend analizi”, VII. Ulusal Hidroloji Kongresi Bildirileri, Isparta, Turkey, 500, 512, 2013.
- [28] R. Ali, A. Kuriqi, S. Abubaker and O. Kisi, "Long-term trends and seasonality detection of the observed flow in Yangtze River using Mann-Kendall and Sen’s innovative trend method", *Water*, vol. 11, no. 9, pp. 1855, 2019.
- [29] E. Çoban, “Investigation of the effects of global warming in the büyük menderes river basin with the innovative sen test”, Available at SSRN, 4659255, 2023.
- [30] R. Acar and K. Saplıoğlu, “Etkili girdi parametrelerinin çoklu regresyon ile belirlendiği su sertliğinin anfis yöntemi ile tahmin edilmesi”, *Afyon Kocatepe Üni. Fen ve Müh. Bil. Derg.*, vol. 22, pp. 1413-1424, 2022.
- [31] A. Aksakal and A. Gündoğay, "Determination of Column Curvature Ductility by Multiple Regression Analysis", In *Ist-International Congress on Modern Sciences Tashkent, Uzbekistan*, 395, 403, 2022.
- [32] S. Barlas, T. K. Öztürk, F. Şenel and K. Saplıoğlu, "Using Multiple Regression Models To Identify Missing Flow Data", *Conference: Tashkent 1st International Congress on Modern Sciences*, 1(1), 372-381, 2022.